

Cooling design and thermal analysis for dual-stator 6-slot 4-pole flux-switching permanent magnet machine

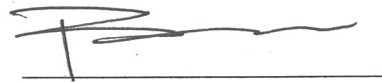
by
Mingda Liu

A thesis submitted in partial fulfillment of the
requirement for the degree of:

Master of Science
(Electrical and Computer Engineering)

At the
University of Wisconsin-Madison
August 2017

Approved by



Prof. Bulent Sarlioglu

Date

08.15.2017

Abstract

This research report focusses on the thermal management of the electrical machine, which is another important aspect of the machine design. The machine components are often influenced by the variation of temperature, especially for permanent magnet machines. Researchers and engineers have spent many efforts in predicting the temperature distribution and variation in the machine as well as controlling the temperature rise.

The first part of this report recapitulates the commonly used thermal analysis methods, including lumped-parameter thermal network (LPTN), finite element analysis (FEA) and computational fluid dynamics (CFD). The most challenging part for LPTN is the modeling of the machine. Thermal resistance equations for different geometry and different nature of heat transfer (conduction, convection or contact) are given. Example of LPTN is given to illustrate the usage of this method. FEA and CFD tools are more widely used today because of the development in computing capability. Commonly used FEA and CFD tools are introduced, advantages of these numerical tools over the LPTN are presented.

Cooling technologies for electric machines are presented in the second part of this report. Depending on the power rating and the size of the machine, simple cooling such as air cooling as well as advanced high-performance cooling like direct winding cooling are reviewed. The passive cooling has a more reliable structure because of its simplicity, whereas the advanced active cooling has more component. There is a balance between the simplicity, efficiency and cooling requirement. New cooling technologies with simple structure, working principle and high performance are desirable.

After the literature review for thermal analysis method and cooling technology, a case study is conducted for a dual-stator 6-slot 4-pole flux-switching permanent (FSPM) machine. A water jacket integrated housing is used to cool the machine. Since most of the heat source of FSPM machine is on the stator side, therefore, a water jacket could do a good job in removing the heat. Thermal analysis is done based on the cooling design mentioned previously. LPTN and FEA are done and compared. Both steady state and transient temperature distribution are predicted by FEA. The flow characteristic of the coolant in the water jacket is also presented. A prototype machine has been built, the manufacturing design is presented at the end.

Acknowledgement

First of all, I would like to address my thanks to my advisor, Prof. Bulent Sarlioglu for offering me the opportunity to work on this project. As my advisor, he helped me not only with technical support but also time-management skills, which beneficial beyond the academy life.

Secondly, I would like to thank the colleagues in our research group. During my two years' study, they generously provided many advices and help. It's hard to name all the members, I would like to thank especially Dr. Yingjie Li who graduated one year after I started the research. He helped me establish the fundamental knowledge about the FSPM machine that I worked on, and educated me on the experiment setup. And most importantly, without him, this project won't even exist. Dheeraj and Ju also helped me a lot on the finite element analysis setup, their help speeds up my learning curve for the simulation software.

I would also like to thank the WEMPEC family. It is very comfortable to work in this friendly and collaborative community. WEMPEC administrator Helene did an excellent job of the management of events and room etc. Senior PhD student Baoyun (Paul) who sit next to me in the office also gave me much help in the research, helping me have a better understanding of electrical machine and drive.

I would like to thank the national science foundation (NSF) for funding this project under GOALI award 1507609.

Finally, I would like to thank my family, who supported me during my Master study. Their emotional support is indispensable.

Thank you all.

Table of Contents

Abstract	i
Acknowledgement.....	iii
List of figures	vi
List of tables	viii
Nomenclatures.....	ix
Introduction	1
1. Research overview	1
2. Research contribution	1
3. Chapter overview	2
Chapter 1 Commonly Used Methods of Thermal Analysis of Electric Machines	4
1. Lumped-Parameter Thermal Network (LPTN)	5
2. Finite Element Analysis (FEA).....	14
3. Computational Fluid Dynamics (CFD).....	16
Chapter 2 State of art of machine cooling technology	17
1. Air/Gas Cooling.....	18
2. Liquid-Cooling.....	23
3. End-winding cooling technologies	25
Chapter 3 Cooling design and thermal analysis for a high-speed dual stator 6/4 FSPM machine.....	39

1. Sizing and Loss Distribution in The Novel 6/4 Dual-Stator FSPM Machine.....	40
2. Stator Heat Extraction System Topology	41
3. LPTN and FEA Model Parameter Derivation for Novel 6/4 FSPM Machine.....	42
Chapter 4 prototype machine design and manufacture	57
1. stator design	57
2. rotor design	59
3. winding specification	61
4. Bearing	61
5. water jacket integrated housing	62
6. end cap fin design	64
7. thermal sensor placement.....	65
Chapter 4 Conclusion and Proposed future work.....	67
1. Research conclusion.....	67
2. Future work.....	68
Reference.....	69
Annex 1 Manufacture Print	75

List of figures

Fig.1.1. Natural convection in fluid due to temperature difference	8
Fig.1.2. Geometry for natural convection example.....	9
Fig.1.3. Randomly distributed gap in a microscopic view of contact surface	11
Fig.1.4. Winding model for calculating equivalent heat transfer coefficient.....	13
Fig.1.5(a). FEA thermal simulation with Infolytica-ThermNet	14
Fig.1.5(b). FEA thermal simulation with FLUX.....	15
Fig.1.6. Computational fluid dynamics simulation with ANSYS Fluent.....	16
Fig.2.1. Electric machine housing fin design examples	19
Fig.2.2. Dependency between heat transfer coefficient and air velocity	19
Fig.2.3. Different fan blade shaped being investigated.....	20
Fig.2.4. External air blower for forced air-cooling	21
Fig.2.5. Electric field driven piezoelectric blade fan cooling	21
Fig.2.6. Scheme and installation of a Hydrogen cooled turbine generator	23
Fig.2.7. Nissan Leaf electric motor CFD simulation	24
Fig.2.8. Comparison of SRM with concentrated winding and toroidal winding	26
Fig.2.9. Slot area view: comparison among different winding types.....	28
Fig.2.10. Potting material on end-winding.....	30
Fig.2.11. Graphite sheet acting as heat pipes between windings	32
Fig.2.12. Oil-spray cooling	33
Fig.2.13. Direct Winding Heat Exchanger placed between windings.....	34
Fig.2.14. Direct slot cooling with in-slot cooling channel.....	35
Fig.2.15. Laminated winding with forced air cooling.....	36
Fig.2.16. End winding cooling with magnetic fluid.....	37

Fig.3.1. 3D model of novel 6/4 FSPM machine.....	40
Fig.3.2. Cut view of the proposed dual-stator 6/4 FSPM machine with water jacket housing.	42
Fig.3.3. LPTN in x-y plane	44
Fig.3.4. LPTN in x-z plane.....	45
Fig.3.5. Equivalent rotor representation.....	46
Fig.3.6. Section view of winding model	48
Fig.3.7. 3D structure of the dual-stator 6/4 FSPM machine	51
Fig.3.8. Heat transfer and heat source conditions	51
Fig.3.9. Thermal circuit for convective heat transfer	52
Fig.3.10. Meshes for the thermal simulation of machine	52
Fig.3.11. Temperature contour from steady state thermal simulation	53
Fig.3.12 Temperature variation during machine start up	54
Fig.3.13 Spiral cooling channel in the water jacket	55

List of tables

Table-1.1 Thermal resistance modeling for common geometry	6
Table-1.2 Typical contact heat transfer coefficient for different interface	11
Table-2.1. Thermal and Mechanical properties of different gases for cooling	22
Table-2.2. Thermal and Mechanical properties of common liquid coolant	23
Table-2.3 Electrical and thermal properties of various impregnation material.....	29
Table-2.4 Electrical and thermal properties of New Potting Material	30
Table-2.5 Slot Liner Properties Considering Interface Gap Between Components.....	31
Table-3.2 Loss Distribution in Novel 6/4 FSPM Machine	41
Table-3.1 Basic Design Parameters of Novel 6/4 FSPM Machine	41
Table-3.3 Interface Gap for Commonly Seen Contact Surface.....	48
Table-3.4 Heat source inside the machine	49
Table-3.5 Thermal resistance for the LTPN model of 6/4 FSPM machine	49
Table-3.6 Temperatures Calculated from LPTN and FEA	53

Nomenclatures

<i>EM</i>	Electromagnetic
<i>PM</i>	Permanent magnet
<i>FSPM</i>	Flux-switching permanent magnet
<i>IPM</i>	Interior permanent magnet
<i>SPM</i>	Surface permanent magnet
<i>LTPN</i>	Lumped-parameter thermal network
<i>FEA</i>	Finite element analysis
<i>CFD</i>	Computational fluid dynamic
<i>R_{cond}</i>	Thermal resistance for conduction heat transfer
<i>R_{conv}</i>	Thermal resistance for convection heat transfer
<i>R_{cont}</i>	Thermal resistance for contact surface
<i>Ra</i>	Rayleigh number
<i>Pr</i>	Prandtl number
<i>Nu</i>	Nusselt number
<i>c_p</i>	Specific heat of material
<i>k</i>	Thermal conductivity
<i>μ</i>	Dynamic viscosity of fluid
<i>h</i>	Heat transfer coefficient

K_f	slot filling factor
A_{slot}	Stator slot area
L_{core}	Stator core length
EV	Electric Vehicle
$FSCW$	Fractional slot concentrated winding
AFM	Axial flux machine
SRM	Switch reluctance machine
$SbTCM$	Silicon-based thermally conductive material
AlN	Aluminum nitride
DWC	Direct winding cooling
$DWHX$	Direct winding heat exchanger
$TSFF$	Temperature sensitive ferrofluid

Introduction

1. Research overview

Electrical machine design has always been considered belonging to electrical engineering, since the majority of the designing work is related to electromagnetic (EM) analysis, and a lot of work has been done in this area. Thanks to these efforts, nowadays the electrical machines could reach an efficiency as high as more than 90% in ideal condition [1][2][3]. However, to guarantee the machine performance or further increase the power/torque density, mechanical conditions and limitations of the machine should be taken care of. For example, the mechanical stress of the moving parts and the thermal behavior. For most of the time, mechanical conditions are results of the EM operation, i.e. the rotation speed affects the stress, losses determine the machine temperature. In return, the mechanical conditions also influence the EM performance, e.g. the winding resistance usually increases with temperature, the most permanent magnet is subject to partially demagnetized under high temperature. This research will discuss the thermal management of a Permanent Magnet (PM) machine with high power density. To have a better understanding of the thermal management of electric machines, a review on the thermal analysis methods and cooling technologies are made in the first two chapter. Then a case study on a novel high-speed dual-stator flux-switching permanent magnet (FSPM) machine is conducted, with thermal network, finite element analysis and experimental test.

2. Research contribution

This research focuses on the thermal management issue of a high-speed FSPM machine. This type of PM machine has its windings and the PM located on the stator [4][5][6], therefore, it is inherently easier for cooling (for the critical components such as permanent magnet and the

armature winding), comparing to other types of PM machines such as Interior Permanent Magnet (IPM) machine and Surface Permanent Magnet (SPM) machine. Besides, the rotor structure of this type of machine is simple and robust, which makes it suitable for high-speed application [7][8].

As mentioned previously, thermal management is critical for machines with high power density. However, the thermal analysis and cooling management of FSPM machine are not as well developed as the other type of PM machine. One of the reason could be that IPM and SPM have been commercially used in industrial application such as Electrical Vehicles [9]–[12], but FSPM is still a relative novel machine topology. This report will discuss the thermal analysis of the FSPM machine and present a few novel cooling technologies for the machine. The use of the proposed cooling scheme is proven to be sufficient for the high-speed application by the prototype machine. The knowledge gathered in the first two chapters also helps to develop more advanced cooling technologies for electric machines in the future.

3. Chapter overview

Chapter 1 presents a review of the thermal analysis for electrical machines. Analytical method with lumped parameter thermal network, numerical method such as finite element method and computational fluid dynamic. For certain model parameters, empirical methods are also presented and compared.

Chapter 2 shows the state of art of cooling technologies for electrical machines. Passive cooling and active cooling are reviewed. The strength and weakness of each type of cooling technologies are discussed.

Chapter 3 gives the thermal analysis of a novel high-speed FSPM machine with a designed water jacket integrated housing. Steady state thermal behavior is predicted by both analytical and numerical method, transient behavior is simulated by the numerical method. Prototype machine are presented in this chapter as well.

Chapter 5 summarizes this research's work and results. Future work related to this research is also suggested.

Chapter 1 Commonly Used Methods of Thermal Analysis of Electric Machines

One important aspect of electric machine design is thermal management. In the past, the electromagnetic design has been paid more attention than thermal design because of low power density. The efficiency of machine could be largely increased by more appropriate electromagnetic design. Machines could be mostly cooled by passive design such as cooling fin. Fan cool and water jacket cooling are enough for high performance machine at the time.

Thermal management is usually done by limiting the current density in the winding according to manufacturer manual [13]. With the increase in power density of electric machines, thermal design is receiving more and more attention. Electrical machine thermal analysis can be divided into two basic types: analytical lumped-circuit and numerical methods. The analytical approach has the advantage of being very fast in the calculation, however, the developer of the network model must invest effort in defining a circuit that accurately models the main heat transfer paths, and the result is usually relatively coarse compared to numerical approaches. With a complex machine geometry, this method is either inaccurate or has a large circuit. The main strength of numerical analysis is that any device geometry can be modeled in 3D, which could capture the three dimensional heat transfer and the heat source distribution. Therefore, it is inherently more accurate than the analytical method. However, it is very demanding in terms of model setup and computational time.

In this chapter, commonly used thermal analysis methods such as lumped-parameter thermal network (LPTN), finite element analysis (FEA) and computational fluid dynamics (CFD). Examples are given for illustration.

1. Lumped-Parameter Thermal Network (LPTN)

Before the advent of modern computational machine and software, LPTN is used because of its simplicity in the calculation which enables human beings to calculate by hand. Even today the LPTN still exist because it gives the result rapidly. The disadvantages of LPTN is that the accuracy of the results strongly depends on how good the model is. If one wants to have an accurate result, he needs to divide the machine into smaller parts, then the time required for calculation arises.

A. Establishing thermal network

Generally speaking, the heat transfer network is similar to an electrical circuit. The analogous relation between the parameters of the two systems is as follow:

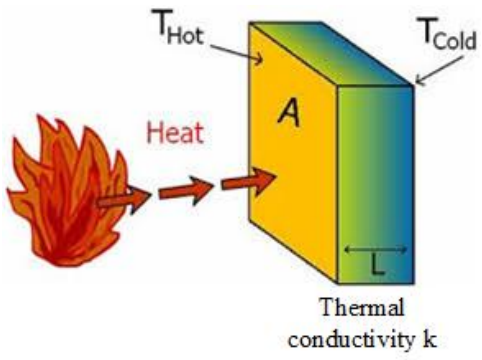
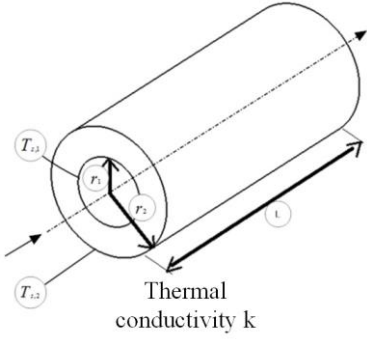
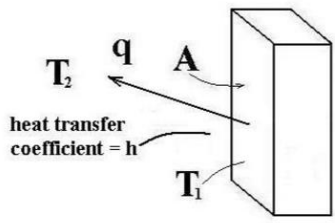
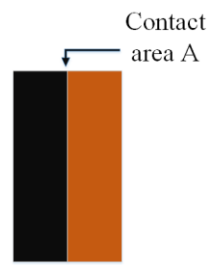
- Temperature difference [K] vs Voltage difference [V]
- Heat flux [W] vs Current [A]
- Thermal resistance [K/W] vs Electric resistance [Ω]

Therefore, the modeling of thermal network consists of the determination of different thermal resistance due to the conduction, convection and radiation in the network. Following the conduction path of the heat in electrical machines, various thermal resistances can be defined.

The following thermal resistance is usually considered based on previous experience:

- Resistance due to conduction heat transfer within stator/rotor lamination and winding
- Resistance due to convection heat transfer between stator/rotor/winding and air inside machine housing
- Resistance due to contact heat transfer between adjacent parts

Table-1.1 Thermal resistance modeling for common geometry

 $R_{cond} = \frac{L}{kA}$	 $R_{cond} = \frac{\ln(r2 / r1)}{2\pi Lk}$
<p>Conduction thermal resistance in rectangular volume</p>	<p>Conduction thermal resistance in cylindrical volume</p>
 $q = h A (T_1 - T_2)$ $R_{conv} = \frac{1}{hA}$	 $R_{cont} = \frac{1}{h_{contact} A}$
<p>Convection thermal resistance</p>	<p>Contact thermal resistance</p>

The modeling of different types of thermal resistance is presented in most heat transfer textbook, recapitulated here in Table 1.1. The value of the thermal resistance depends on the machine/coolant material properties and the machine geometry. Notice that some parameters in the equations above are empirical, because some thermal characteristics are highly related to the

manufacturing process. For example, the smoothness of the stator lamination and the inner housing surface greatly affect the contact thermal resistance.

The thermal resistance is the most critical part in a thermal network. In addition to the thermal resistance, the heat source is usually modeled by a current source, or to be accurate, a heat flux source, in the unit of [W]. In the steady state, the thermal network is made up of the thermal resistance and heat flux source. As a matter of fact, all the machine components have certain heat capacity, which will affect the temperature transient response. Similar to the electric capacitor, thermal capacitor could also be placed in the thermal network.

The nomenclature of thermal inductance could be found in the literature, it involves in the change of heat flux and the surrounded fluid flow behavior. This topic is beyond the thermal analysis of electric machine, therefore, we are not going to include this in our discussion.

B. Thermal network parameters derivation

As mentioned in the previous section, some of the parameters are straight forward such as the thermal conductivity in conduction resistance model. However, for convection and contact thermal resistance model, the heat transfer coefficient is not simply given in the datasheet.

1) *Heat transfer coefficient for natural convection*

The heat transfer coefficient is in the domain of mass and energy transport, fluid mechanics expertise is required. Luckily, this topic has been investigated deeply in the literature. In microscopic view, the convection heat transfer is caused by molecular movement, which could be divided into two categories: natural convection and forced convection.

Natural convection is driven by the fluid internal stress. The temperature difference in the fluid will cause a density gradient, and an internal stress is created due to gravity, which induces the fluid flow. This process is illustrated in Fig. 1.1.

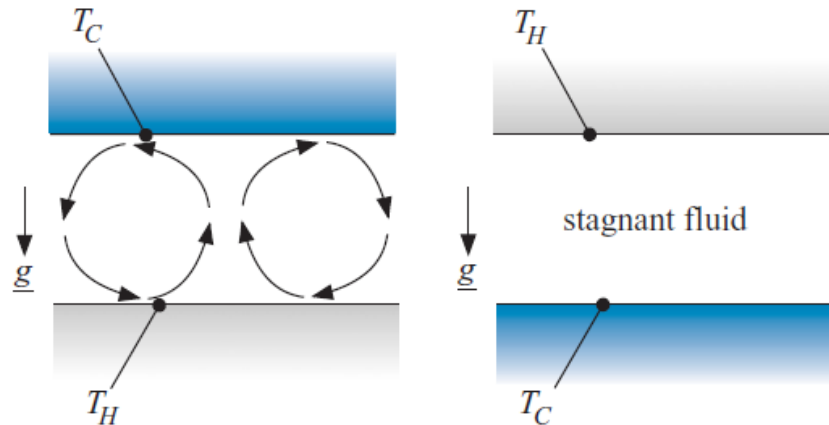


Fig.1.1. Natural convection in fluid due to temperature difference [14]

Of course, the stress needs to be large enough to overcome the viscous dragging force of the fluid. Fluid engineers have come up with a dimensionless number Rayleigh number (Ra) to characterize natural convection, given in equation 1-1

$$Ra = \frac{g\beta}{\nu\alpha}(T_s - T_\infty)x^3 \quad (1-1)$$

where β is the thermal expansion coefficient, ν is the kinetic viscosity, α is the thermal diffusivity, g is the gravity acceleration, T_s and T_∞ are the surface temperature and surrounding temperature, x is the characteristic length.

The convection phenomena depend on many fluid parameters, Prandtl number (Pr) assemble them together (equation 1-2) and is used to simplify the expression.

$$Pr = \frac{c_p\mu}{k} \quad (1-2)$$

where c_p is the fluid specific heat, μ is the dynamic viscosity and k is the fluid thermal conductivity.

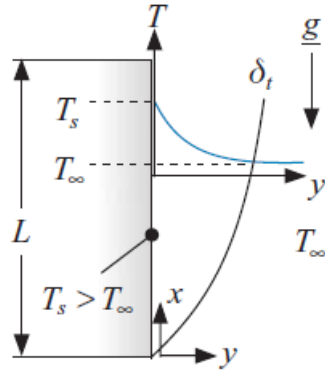


Fig.1.2. Geometry for natural convection example

Heat transfer efficient could be then calculated using these dimensionless numbers, based on empirical equations. These empirical equations are derived from experimental results done by engineers, and vary for different geometry. As an example, for a vertical heated plate (Fig. 1.2), the heat transfer coefficient h could be calculated by the following equations [14]:

$$Nu = \frac{hL}{k} \quad (1-3)$$

$$Nu = (Nu_{lam}^6 + Nu_{turb}^6)^{1/6} \quad (1-4)$$

$$Nu_{lam} = \frac{2}{\ln(1 + \frac{2}{C_{lam} Ra^{0.25}})} \quad (1-5)$$

$$C_{lam} = \frac{0.671}{[1 + (\frac{0.492}{Pr})^{9/16}]^{4/9}} \quad (1-6)$$

$$Nu_{turb} = \frac{C_{turb} Ra^{1/3}}{1 + (1.4 \times 10^9) \frac{Pr}{Ra}} \quad (1-7)$$

$$C_{lam} = \frac{0.13 Pr^{0.22}}{(1 + 0.61 Pr^{0.81})^{0.42}} \quad (1-8)$$

where Nu is another dimensionless number called Nusselt number. Equations for other geometry could be found in the literature and textbooks.

2) *Heat transfer coefficient for forced convection*

Force convection usually happens in a closed channel, similar to natural convection, forced convection heat transfer coefficient is also determined by empirical equations. In this case, Reynold number is used to determine the status of the flow, whether it is laminar flow or turbulent flow:

$$\text{Re} = \frac{\rho D_h u}{\mu} \quad (1-8)$$

$$D_h = \frac{4A_c}{\text{Perimeter}} \quad (1-9)$$

where u is the mean flow velocity, A_c is the channel section area.

If Re is smaller than a critical Reynold number (typically 2700), then the flow would be laminar. Laminar is mostly preferred, since it causes a lower pressure drop. And the Nusselt number for forced convection with laminar flow is

$$\text{Nu} = 1.86 \times (\text{Re Pr})^{1/3} \left(\frac{D}{L}\right)^{1/3} \left(\frac{\mu_b}{\mu_w}\right)^{0.14} \quad (1-10)$$

where μ_b and μ_w are the fluid viscosity at bulk temperature and tube wall surface temperature. Then the heat transfer coefficient could be calculated with equation 1-3.

3) *Contact heat transfer coefficient*

Contact heat transfer is another parameter in the thermal network which is strongly depended on the manufacturing process. As shown in Fig.1.3, the randomness of airgap between the two contact surfaces makes the heat transfer behavior hard to predict precisely.

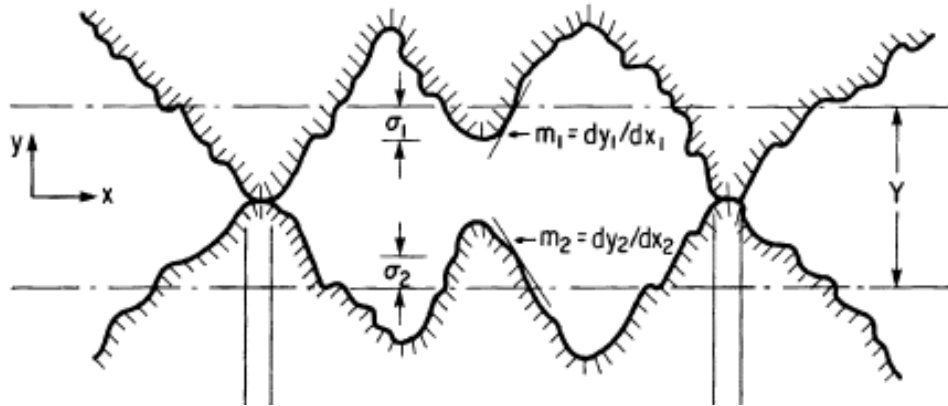


Fig.1.3. Randomly distributed gap in a microscopic view of contact surface [15]

For decades, engineers have been trying to get an accurate estimation of contact heat transfer coefficient. There are mainly two methods, by experiments and by geometry. Reference [15], [16] derive an approximate expression for the heat transfer coefficient base on an equivalent gap. Whereas [17], [18] use experiments to give empirical values. It is interesting to see that experimental approach is used more often by later researchers, whereas early researchers prefer geometric derivation. Table-1.2 gives the typical contact heat transfer coefficient for the various interface.

Table-1.2 Typical contact heat transfer coefficient for different interface [86]

	Interfacial Conductance [W/m ² /C]	Effective Interface Gap [mm]
Ceramic-Ceramic	500-3000	0.0087 – 0.0052
Ceramic-Metal	1500-8500	0.0031 – 0.0173
Graphite-Metal	3000-6000	0.0043 – 0.0087
Stainless-Stainless	1700-3700	0.0070 – 0.0153
Aluminum-Aluminum	2200-12000	0.0022 – 0.0012
Stainless-Aluminum	3000-4500	0.0058 – 0.0087
Iron-Aluminum	4000-40000	0.0006 – 0.0060
Copper-Copper	10000-25000	0.0010 – 0.0026

4) *Thermal capacitance model*

As mentioned previously, thermal capacitance affects the transient behavior of the temperature response. For example, the loss generated by the winding need to first heat up the winding itself to create enough temperature difference for the conduction and convection heat transfer. Similar to the thermal resistance, capacitance is also influenced by the material properties and the mass of the component. The common heat capacity related property for a given material is its specific heat, which has a unit of [J/kg K], whereas the thermal capacity has unit of [J/K], therefore, these two quantities are related by the mass of the material. In the thermal network, the thermal capacity is usually put in parallel with the thermal resistance. At steady state, it only holds up the temperature difference between its two terminals, and has no influence on the temperature distribution. Machines with large thermal capacity are less vulnerable to the short-time overload, the heating of components takes more time. In contrary, small machines might reach a very high temperature and damage the insulation.

An example of the usage of the thermal capacitance is given later in this chapter.

c. Equivalent component modeling

For part like machine windings, which is made up of many coils turns, each wire is composite of copper or aluminum, varnish for insulation. And there is random space between coils. These variants make it impossible to model the windings as a whole volume. There is a large difference between the thermal conductivity of axial direction and that of radial direction. And these two values are both a fraction of the bulk conductor material.

Many researchers have been trying to create an equivalent winding model. In reference [19], an empirical factor is used for the axial and radial thermal conductivity. As mentioned previously, the heat transfer in windings is largely affected by the manufacturing process.

Therefore, this approach is not very accurate. Many researchers and engineers use experimental results to interpolate curves for thermal properties of winding [20]–[23], given in equation (1-11). This is a more rigorous method, but it seems to not having taken the thermal conductivity of insulation material as a variable.

$$k_{cu-ir} = 0.2425[(1 - K_f)A_{slot}L_{core}]^{-0.4269} \quad (1-11)$$

where K_f is the slot filling factor, A_{slot} and L_{core} are the slot area and core length respectively.

Other researchers derive the equivalent thermal conductivity base on winding geometry [24]–[27], as shown in Fig. 1.4, winding is decomposed into several layers to get an equivalent thermal conductivity. This method is used for the thermal analysis of the dual-stator 6/4 FSPM machine, which will be presented in detail in chapter 3.

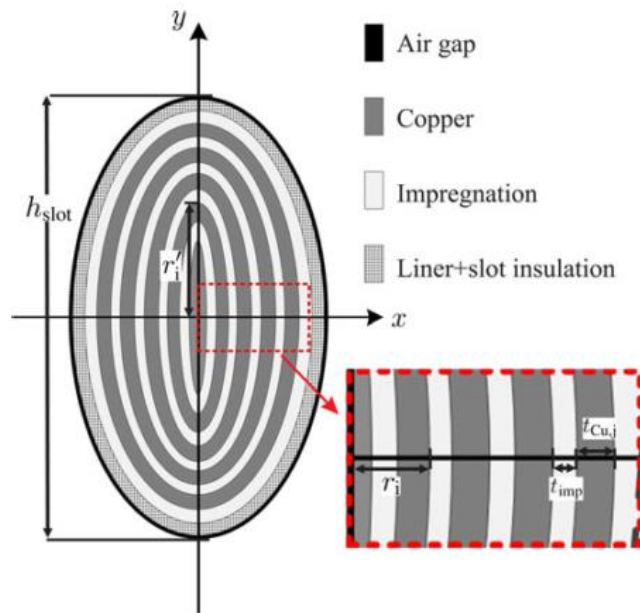


Fig.1.4. Winding model for calculating equivalent heat transfer coefficient [26]

2. Finite Element Analysis (FEA)

A. Finite element analysis overview

For an actual machine design, the geometry could be much more complex than rectangular volume or cylindrical tube described previously. The thermal network modeling becomes inaccurate or too complicated in this case. Nowadays, with increasing computing capability of computers, finite element method is an alternative solution. Based on the geometry entered by 3D modeling tools, local differential equations are established automatically, steady state or transient solution could be derived with boundary conditions specified by the user.

There are many commercial software packages doing FEA thermal analysis, such as FLUX, Infolytica-ThermNet, JMAG-Designer, ANSYS etc. The procedure is almost identical, user first needs to input the geometry, then set up the boundary condition and mesh size. Fig.1.5 gives an example of thermal simulation from two software. In chapter 3, another detailed FEA study on a novel dual-stator FSPM machine will be given.

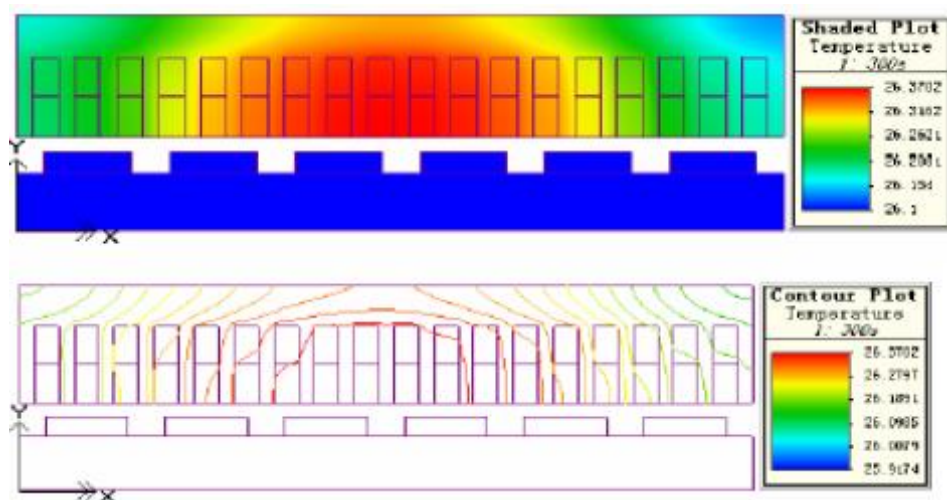


Fig.1.5(a). FEA thermal simulation with Infolytica-ThermNet [28]

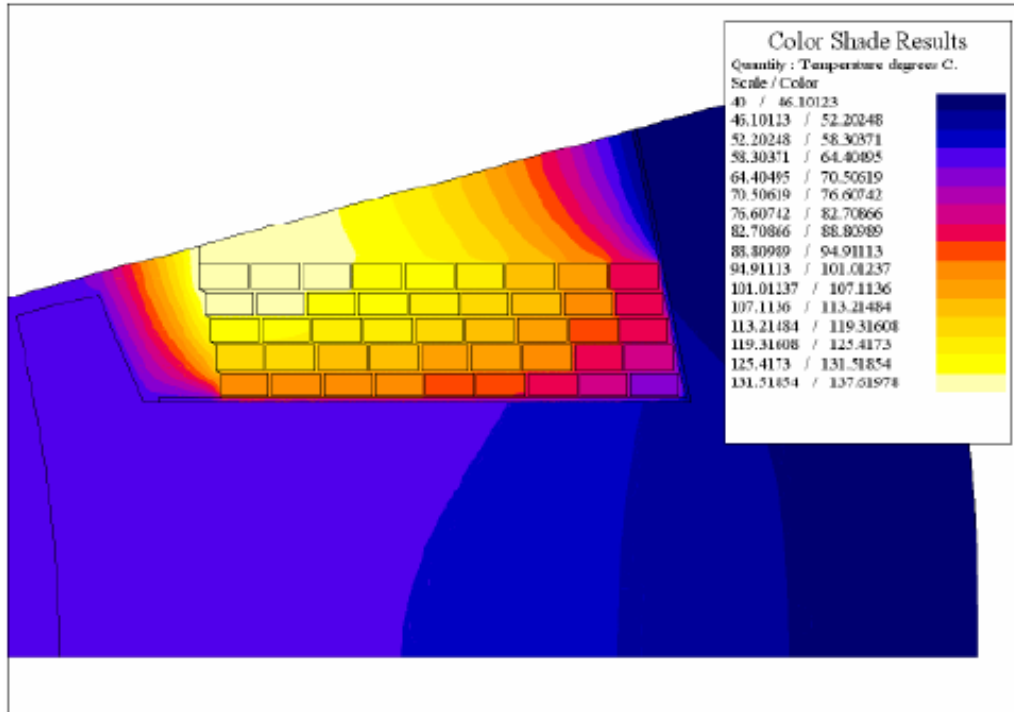


Fig.1.5(b). FEA thermal simulation with FLUX[29]

The FEA could provide detailed information like temperature contour and heat flux in a specific point. The disadvantage of FEA is its time-consuming computing time, but with the rapid development of CPU capability and parallel computation technology, the FEA speed could be comparable to the LPTN.

Due to the nature of FEA, it is good at conduction heat transfer, but for convective heat transfer, the user needs to enter the heat transfer coefficient which is coming from the empirical equations in the previous section. To have a more accurate result, computational fluid dynamic need to be used to get local heat transfer coefficient.

Another advantage of FEA is that the thermal simulation could be coupled with electromagnetic simulation. For electric machine design, this is an important advantage, since the temperature strongly affects the machine component properties.

3. Computational Fluid Dynamics (CFD)

Knowledge in fluid dynamic provide engineers with tools to analytically estimate the heat transfer coefficient for simple geometry. However, it is hard to study the transfer properties for complex geometry, where CFD is more reasonable to employ. As mentioned in the previous section, CFD is needed for accurate convection heat transfer coefficient for complex parts. Same as FEA, CFD also needs geometry and boundary conditions entered in the software. In addition, CFD simulation helps the engineer to have a better view of flows in the machine. For high-speed machine, windage loss is not negligible. Same as the thermal FEA simulation, CFD could also be coupled with the electromagnet simulation. Actually, the electromagnetic, thermal and fluid dynamic simulation could be coupled together, which makes the numerical method more powerful since it's closer to the reality.

A widely used commercial CFD code is ANSYS Fluent, Fig. 1.6 gives an example of CFD simulation result done by ANSYS Fluent. More information could be found online. Note that there is other possible choice of CFD software as well.

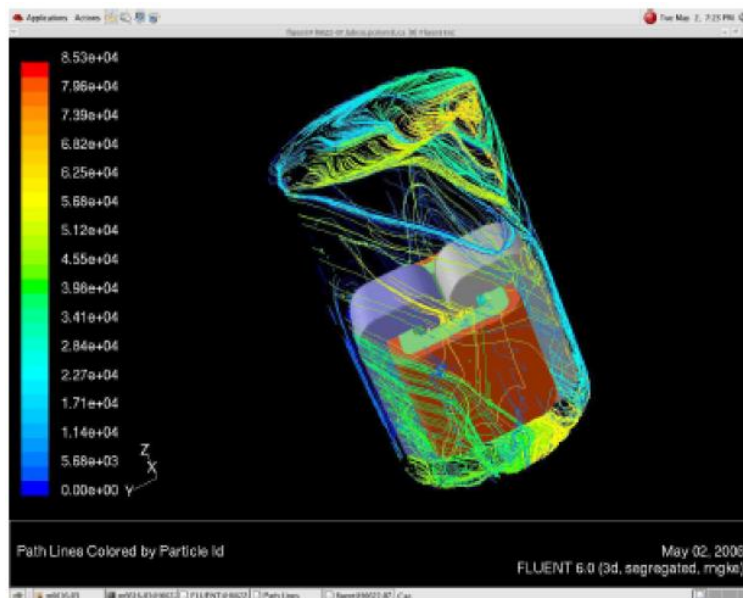


Fig.1.6. Computational fluid dynamics simulation with ANSYS Fluent [30]

Chapter 2 State of art of machine cooling technology

The cooling design has always come together with the electrical machine design, since the thermal behavior influences the performance, especially for high-performance machines and harsh condition application. In the old days when electrical machines are large and relatively low power, the cooling requirement could be accomplished mostly by air-cooling. And even for today, air-cooling is still widely used because of its simple design. The first section of this chapter presents the commonly used air-cooling design for electrical machines. And as an extension, other gas cooling technology like hydrogen-cooling will be mentioned.

For high power density electrical machines, simple air-cooling might not be sufficient to maintain the operation temperature, or the working condition demand sealed enclosure, which might impede the air-cooling. In these cases, liquid-cooling could be applied. Normally, liquid has a larger heat capacity and a higher heat transfer coefficient under the similar condition comparing to gas. Therefore, liquid-cooling could provide better cooling capability than air-cooling. However, liquid generally has a higher viscosity and density than gas, a liquid-cooling system usually consumes more energy than the air-cooling system. Therefore, the efficiency of the overall system will be drawn down. In the second section, different liquid cooling technology will be presented and compared.

Air-cooling and liquid-cooling could be regarded as traditional cooling technology, since they have been applied for many decades. Recently, high power density electrical machines have been studied intensively to replace traditional combustion engine. Especially the development of Electrical Vehicle (EV) has driven the research in high-performance electrical machine. Besides the electromagnetic (EM) performance, thermal management is also becoming a limitation.

Researchers came up with new technologies to cool the machine, increasing the cooling capability as well as improving the efficiency. The third section of this chapter will introduce the existing novel cooling technologies.

1. Air/Gas Cooling

A. Natural air-cooling

When Michael Faraday and Peter Barlow first invented a rotating device powered by electromagnetism [31], they probably didn't think of how to cool it. One reason for this might be the power rating of device at that time is relatively low. The heat generated could be easily dissipated through the surrounding air governed by the convective heat transfer equation below:

$$P = \Delta T \cdot hS \quad (2-1)$$

where P is the heat dissipated in [W], ΔT is the temperature difference between the machine surface and the surrounding air in [K], S is the contact surface area between the machine and the air in [m²], h is the heat transfer coefficient in [W/m²K]. From equation (2-1) we see that the cooling capability of natural air-cooling method depends on the surface area of the machine and the heat transfer coefficient.

The heat transfer coefficient of air is mainly a function of relative speed, in this part we discuss natural air-cooling, so the air velocity is set to be 0, the speed influence will be discussed in next part (forced air-cooling). At standstill, air has a heat transfer coefficient of approximately 5-10 [W/m²K].

One way to dissipate more heat with natural air is increasing the surface area. Many machines employ fins at the outer surface for better cooling. Fig. 2.1 shows different fins design for electrical machines.

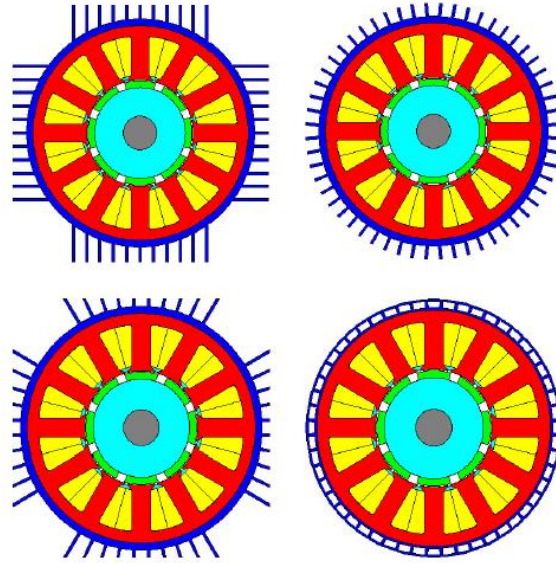


Fig.2.1. Electric machine housing fin design examples [32]

To keep the cooling effect, we need to maintain the temperature difference between the air and the machine surface. Therefore, nature air-cooling is usually used on machines located in a relatively open area.

B. Forced air-cooling

As mentioned before, the heat transfer coefficient of air is dependent on the relative speed, Fig. 2.2 shows the dependency of air heat transfer coefficient and the speed, from work of many researchers around the world [33].

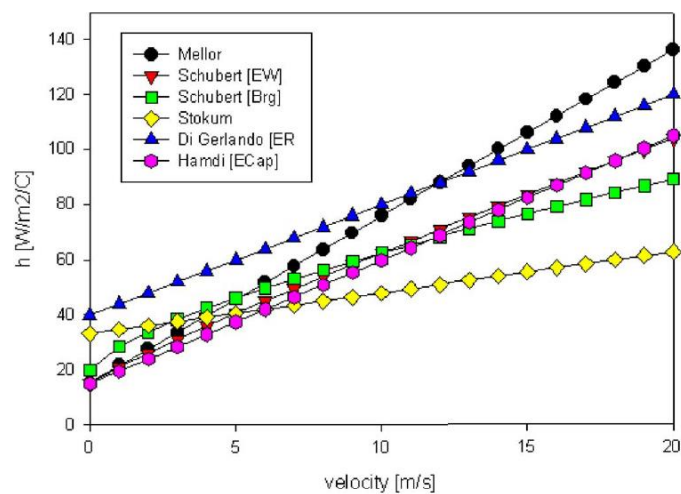


Fig.2.2. Dependency between heat transfer coefficient and air velocity [33]

Researchers have summarized an empirical equation (equation 2-2) for the relation between heat transfer coefficient and speed.

$$h = \text{Pr}^3 \text{Re}^{\frac{2}{3}} \quad (2-2)$$

Shaft-mounted fan is usually used for driving airflow through the machine. The fan will consume certain shaft torque and its rotation speed will depend on the machine speed. The windage loss of the fan is proportional to the cubical of rotating speed. Therefore, this method is not quite suitable for high-speed application.

The fan blade design is the critical point, Computational Fluid Dynamic (CFD) is widely used for this purpose. For example in [34], different types of blade shape are investigated and compared, as shown in Fig. 2.3.

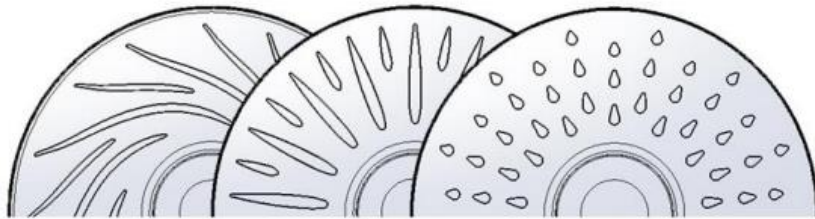


Fig.2.3. Different fan blade shaped being investigated [34]

Because of the simple structure and robust operation, shaft-mounted fan is widely used in the low-cost application. One of the disadvantages of the fan-cool method is that it exposes the inner parts of the machine to the ambient, tiny particles inhaled into the gap could damage the machine.

In order to have an airflow which doesn't depend on machine speed, researchers have proposed to use external blowers to provide the pressure [35], the topology is shown in Fig.2.4. By decoupling the cooling fan and the shaft, cooling can be controlled in a closed loop by sensing the machine temperature. However, the drawback is obvious, it increases the complexity of the system and will harm the reliability.

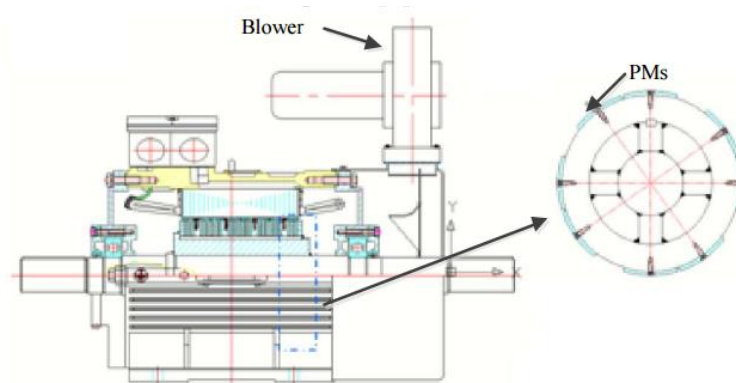


Fig.2.4. External air blower for forced air-cooling [35]

Besides conventional rotating fan, [36] has proposed an electric field driven piezoelectric fan, shown in Fig.2.5. The fan blade is fabricated by bonding of a piezoelectric patch to a lightweight cantilever beam. By applying an alternating current, the piezoelectric patch will vibrate and the movement is amplified by the cantilever beam, thus generating air flow.

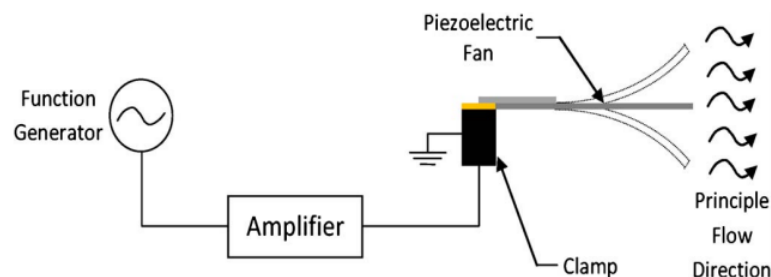


Fig.2.5. Electric field driven piezoelectric blade fan cooling [36]

The main advantage of this technology is its small size and low noise, which makes it suitable for aerospace application.

C. Other gas-cooling

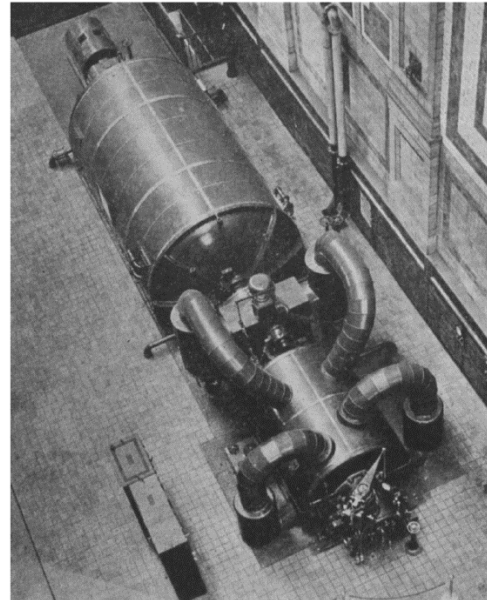
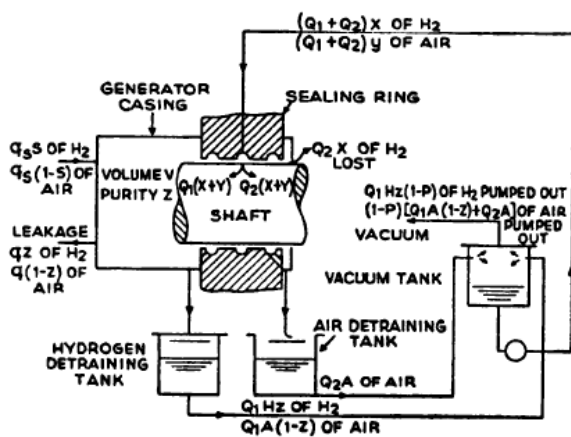
Air has a thermal conductivity of 0.026 [W/mK] at 25 °C, which is relatively low, to increase the cooling efficiency, gas with higher conductivity could be used. The most commonly used cooling gas is Hydrogen because of its low price, and Helium for the steady chemical

Table-2.1. Thermal and Mechanical properties of different gases for cooling

	Temperature [C]	Conductivity [W/mK]	Density [kg/m ³]	Specific Heat [J/kg K]	Kinetic Viscosity [m ² /s]
Helium	93	0.169	0.133	5.2e3	173.6e-6
Helium	204	0.197	0.102	5.2e3	259.3e-6
Hydrogen	77	0.206	0.07	14.4e3	141.9e-6
Hydrogen	127	0.228	0.061	14.5e3	177.1e-6
Air	80	0.03	1.0	1.01	20.94e-6
Air	140	0.034	0.854	1.01	27.55e-6

properties. Another benefit is that, compared to air, Hydrogen and Helium have a lower density. Therefore, the required driving force is lower. Table 2.1 gives the thermal and mechanical properties of different gases used for cooling at different temperatures. However, because these gases are not the major component of the atmosphere, a total enclosed fluid loop is required, which increase the cost of maintenance. Besides, the sealing could be another challenge, the liquid-film type of sealing is the most commonly used method.

Since the coolant fluid is enclosed, it requires additional heat exchanger to reject the heat in the coolant. Therefore, the entire system could be bulky, so this approach is usually used in large electrical machines such as hydraulic power generators [37] or large turbine generators [38]. Fig.2.6. shows the scheme and actual installation of a Hydrogen cooled turbine generator.



(a)

(b)

Fig.2.6. Scheme and installation of a Hydrogen cooled turbine generator [38]

2. Liquid-Cooling

Generally speaking, liquid usually has higher thermal conductivity and thermal capacity than gas. For high power density machines where gas-cooling is not sufficient, liquid cooling

Table-2.2. Thermal and Mechanical properties of common liquid coolant [90]

Fluid	Conductivity [W/m K]	Specific Heat [kJ/kg K]	Density [kg/m ³]	Kinetic Viscosity [m ² /s]
Brayco Micronic	0.1344	1.897	835	1.35e-5
Dynalene HF-LO	0.1126	2.019	778	3.2e-6
EGW 50/50	0.37	3.0	1088	7.81e-6
PGW 50/50	0.35	3.5	1050	1.9e-5
Engine Oil	0.147	1.796	899	4.28e-3
Silicone KF96	0.15	1.5	1000	8e-5
Skydrol 500-4	0.1317	1.75	1000	3.5e-5
Water	0.56	4.217	1000	1.78e-6

could be applied. On the other hand, liquid is normally more viscous than gas. Therefore, it needs more energy to drive. A trade-off is made between the cooling capability and the device

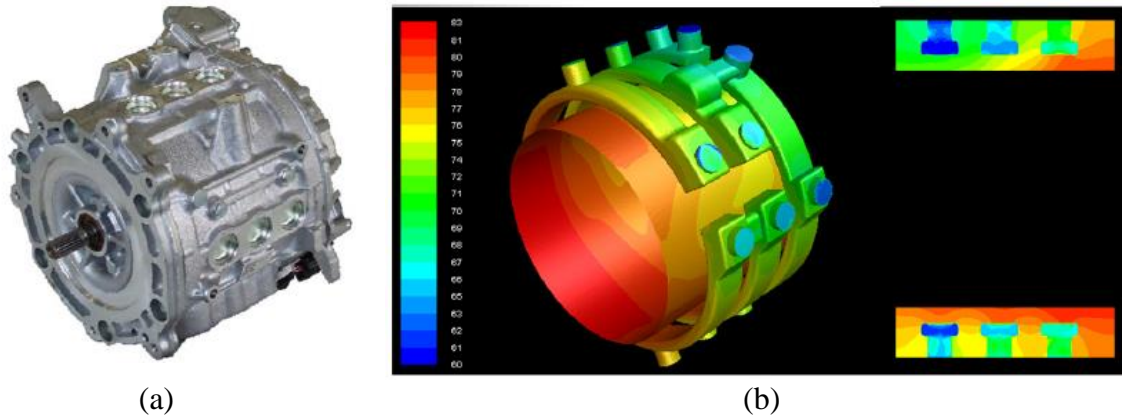


Fig.2.7. Nissan Leaf electric motor CFD simulation (a) 3D structure of Nissan-Leaf electric motor (b) Computational Fluid Dynamic of the cooling system [91][90]

overall efficiency. The thermal conductivity and viscosity are the main metrics for selecting the liquid coolant. Table-2.2 gives the commonly used liquid coolants' thermal properties.

As a more aggressive cooling approach, liquid cooling has been used in many applications, in this section, water jacket will be explained in detail. Other liquid cooling technologies are being presented in the section of End-winding cooling technologies.

Water jacket cooling has been widely used for high-performance electrical machines and electronic devices, mostly because of its low price. Besides, the non-toxic fluid property makes it easier for maintenance. Usually, the water jacket not only takes the responsibility of heat dissipation but also mechanical support and protection. Fig.2.7. shows the Nissan-Leaf electric motor with water jacket cooling and its CFD simulation.

The performance of water jacket mainly depends on the flow rate (mass or volume) of the coolant running through the channel and the cooling channel design. It is obvious that higher flow rate will lead to better cooling capability, but comes with higher drive power consumption. For thermal engineer, it is meaningful to design the cooling duct to achieve higher heat dissipation with given flow rate.

3. End-winding cooling technologies

With the rapid development of electric vehicles (EV), electrical machines with high torque density and small size are gaining more and more attention [39], [40], [41], new designs with different topologies such as IPM [42], SPM [43] and FSPM [44] are emerging rapidly. Most literature was focusing on electromagnetic design. Besides the electromagnetic design, another challenge for high-torque machine design is thermal management, since with the increase of torque density, current in the windings is grumping up. The peak current due to the frequent acceleration of EV also makes thermal management challenging. The reduction of machine size leads to even a higher power density, and the room left for cooling shrinks. Without efficient cooling method, the machine only works in the simulation.

Many papers on thermal analysis show that windings are usually the hot spot inside a machine [45][46]. The difficulty in winding cooling is that it is buried inside the machine and because of the impregnation material coated outside the wire and limited slot-filling factor, the heat is difficult to be transferred to the outside. Furthermore, In EV applications, for the safety consideration, the electrical machine is usually enclosed in the housing, which makes the heat exchange more challenging. Traditional ways of high power machine cooling such as water-jacket liquid cooling might not be enough for the future's high torque machines because the windings heat could not be removed efficiently.

A. Different Winding topologies for easy cooling

1) *Thermal Performance Comparison among Concentrated Wining, Distributed Winding and Toroidal Winding*

Generally, AC machine windings could be divided into two categories, either overlapping or non-overlapping. The overlapping windings could be further classified into distributed and

concentrated windings depending on the slot/pole number relation. The distributed windings have the advantage of lower harmonic distortion in the electromagnetic aspect. From the sense of thermal management, Joule loss is more evenly distributed in the stator, and therefore, the overheat won't focus on some specific part of the machine. However, the distributed windings usually have longer end-windings and incur higher Joule loss, which will degrade the thermal performance.

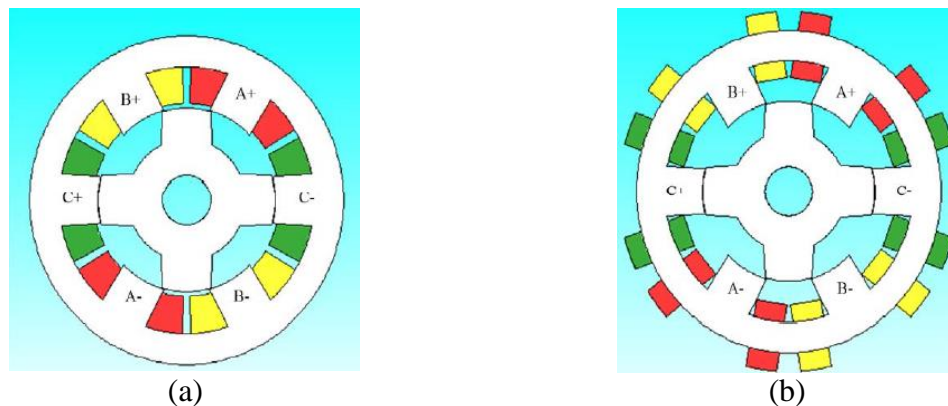


Fig.2.8. Comparison of SRM with concentrated winding and toroidal winding
(a) Conventional wound SRM (b) Toroidal wound SRM [49]

The non-overlapping windings, also referred as Fraction Slot Concentrated Winding (FSCW), has the advantages of a higher slot-filling factor, better flux-weakening capability and shorter ending-winding [47]. Since there is no overlapping among the windings, FSCW could be pre-formed, comparing to random wound windings, preformed windings' internal thermal conductivity is much higher, because of the smaller air gap. Use of highly thermal conductive impregnation and potting material could further increase the heat dissipation.

All concentrated winding, distributed winding and FSCW have the copper wound around the stator teeth. An alternative winding topology is called toroidal winding, where the winding is wound on the stator yoke. This type of winding is usually used in Axial Flux

Machines (AFM) [48]. Fig.2.8.(a) [49] shows the winding structure of a Switch Reluctance Machine (SRM), and Fig.2.8.(b) gives a toroidal winding version of SRM. This winding topology offers better cooling capability because the winding has a larger exposure surface [50], and the outer part of the winding has a close contact with the outer case, which significantly reduces the thermal resistance between the windings and the heat sink. Note that for concentrated/distributed winding, the heat from the windings needs to travel through the insulation layer and the stator yoke to reach the heat sink. Besides, toroidal winding is easier to wound, which leads to a higher filling factor[51]. However, for conventional radial flux machine, toroidal winding usually leads to low torque, the trade-off is made between the easy cooling and torque density.

2) *Hairpin Winding*

Round conductor windings will inevitably leave unused space in the slot, for a given machine volume and power level, low slot-filling factor causes high current density. For this reason, hairpin winding has been used [52], so that the slot area could be more effectively used. Fig. 2.9 gives a comparison among hairpin, round wire and Litz-wire winding. Lower current density will lead to lower copper loss and ease the cooling of the machine. However, the hairpin winding installation is more complex since the winding needs to be pre-formed and inserted into the stator slot.

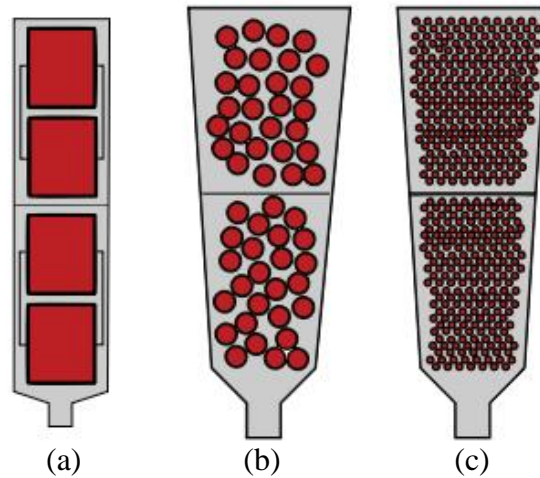


Fig.2.9. Slot area view: comparison among different winding types
 (a) hairpin winding (b) round wire and (c) Litz-wire winding [92]

B. Enhanced Indirect Winding Cooling

Besides considerable Joule loss from the winding, another reason that leads to winding's overheat is that there is no effective way to bring the heat out of the buried windings. Winding wires are usually coated with impregnation material for electrical insulation. And materials with good electrical insulating property usually have degraded thermal conductivity. For random wound windings, numerous air gaps exist between the adjacent turns, the air exist between the wires makes the heat dissipation even worse since air has a very low thermal conductivity (0.026 [W/mK]). Slot liner used for separate stator core and different sets of windings also impede the heat transfer. Therefore, reducing the thermal resistance between the windings and the heat sink will largely increase the winding thermal behavior. This could be done by using insulation material with higher thermal conductivity.

1) *Alternative Impregnation Material with High Thermal Conductivity*

Varnish has been used as impregnation material for years because it can be easily applied to the windings and it has good electrical properties. Although varnish has a poor thermal

Table-2.3 Electrical and thermal properties of various impregnation material [54]

Material	Varnish	Epoxyite	SbTCM
Thermal conductivity [W/mk]	≈ 0.25	≈ 0.85	3.2
Dielectric strength [kV/mm]	≈ 80	≈ 20	≈ 10
Volume resistivity [Ω .cm]	$\geq 10^{15}$	$\geq 10^{14}$	$\geq 10^{14}$
Viscosity [Pa.s]	-	3.5	25
Price (P.U)	1	≈ 2.0	≈ 4.0

conductivity (~ 0.25 [W/mK]), it is still widely used in most of the low power density machines because of the easy manufacturing process and the low price[53]. Epoxy is being used recently as an alternative to varnish on some high-performance electrical machines because it provides higher thermal properties (~ 0.85 [W/mK]).

With further increase in power density, more effective heat transfer material is needed. In [54], a silicon-based thermally conductive material (SbTCM) with a thermal conductivity of 3.2 [W/mk] is presented and three prototype machines with impregnation of varnish, epoxy and SbTCM were manufactured to prove the good thermal behavior of this material. Table-2.3 gives the electrical and thermal properties of the three impregnations material. We can tell from the table that the better thermal property comes with the price of sacrificing electrical properties and higher cost.

In [55], a multi-component composite which combines the advantage of individual component is introduced. This composite is based on Epoxy with nano/micro fillers with high thermal conductivity such as Silica (SiO_2). The overall thermal conductivity could reach 1.5

[W/mK] with a filling factor of 1%. The experiment results also indicate that the composite has better dielectric capability comparing to the pure epoxy resin.

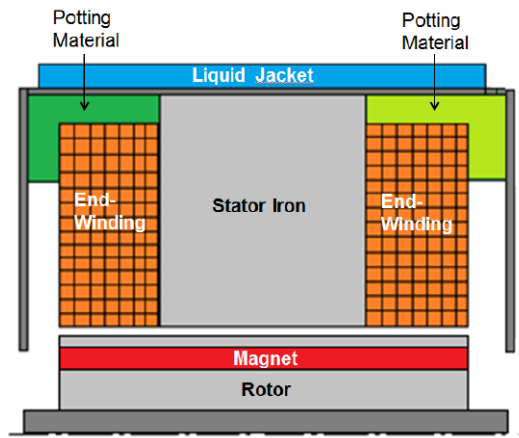


Fig.2.10. Potting material on end-winding[56]

2) Potting Material between Windings and Housing

Table-2.4 Electrical and thermal properties of New Potting Material[56][57]

Material	Thermal conductivity [W/mK]	Heat Capacity [J/kg K]	Specific Density [kg/m ³]	Temperature Limit [K]	Dielectric Strength [kV/m]	Volume Resistivity [Ω m]
Ceramacast 675N	100	740	3260	1200	1.2e4	10e11
Epoxy 2315	58	1000	1800	185	1.9e4	10e14
Alumina Filled Epoxy	20-25	-	-	-	-	10e15
AlN Filled Epoxy	3.8	-	2470	143	-	10e16
Silicone	2.0	-	1960	250	-	10e16

A better impregnation material facilitates the heat conduction through the windings, potting material can be used to fill the air gap between the winding and the outer components to further enhance the heat transfer between the windings and the stator/housing [56]. Fig. 2.10 illustrate the placement of the potting material. The placement of potting material also helps to increase the mechanical stability of windings under vibration, thus benefits the reliability. In the early years,

Bitumen has been used for coil potting, later polyester and silicones material are used for their higher thermal conductivity [57]. In recent years, more novel materials with higher thermal conductivity have been investigated and used as a potting material, such as special ceramic material [56] and Aluminum Nitride (AlN) composite [58]. Aluminum Oxide such as Alumina has also been used as filler to epoxy resin to increase the thermal conductivity [59].

Same as the impregnation material, potting materials also need to have a satisfactory electrical as well as mechanical properties for the machines to work properly. Besides, the designer needs to pay attention to the melting temperature of the material, it should be away from the operating temperature of the machine to maintain sufficient structural strength. Different possible potting materials and their properties are recapitulated in Table-2.4.

3) Slot Liner Selection

Table-2.5 Slot Liner Properties Considering Interface Gap Between Components [60]

Slot Liner	Nomex 410 (Dupont)	ThermaVolt (3M)	CeQUIN I (3M)
Thickness [mm]	0.25	0.25	0.25
Dielectric breakdown voltage [kV]	0.249	0.366	0.270
Thermal conductivity @ 180 C [W/mK]	0.139	0.230	0.195
Tensile strength [kN/m]*	29.6/16.1	9.3/6.0	2.1/0.7
Insulation class	R (220C)	R (220C)	R (220C)
Equivalent thermal conductivity [W/mK]	0.046	0.067	0.053

*Fibre machine direction of paper/across fiber direction of paper

Besides wire impregnation and winding potting, slot liner placed between windings and stator slots also plays an important role in the thermal resistance of the heat path. Note that the slot liner might interact with the impregnation material and alter the overall thermal property of the stator winding region, i.e. the slot liner will absorb some of the impregnation material, especially when the working temperature increases. In [60], several stator-winding samples have been made and tested to evaluate the heat transfer from the winding body to the machine

periphery. The actual thermal performance depends not only on the slot liner/impregnation material properties, but also the manufacturing process. The interface between different component largely determines the overall performance. This influence could be captured as contact resistance in the Lumped-parameter thermal network (LPTN) for thermal analysis.

Table-2.5 shows the experimental results from [60], the electrical and thermal properties of different commercially available slot liner as well as their equivalent thermal conductivity taking the contact resistance into consideration.

4) Graphite Heat Pipe in Windings

Recently with the development of carbon material, graphite sheet is widely used in various applications. [61] inserts thin graphite sheet of 100 μm into the winding pack to conduct the heat to the outer heat sink. The graphite sheet has a thermal conductivity of 700 [W/mK] which is even higher than copper. This technology is brought up here just as a reference, because this is an ultra-high-speed motor application instead of EV application. The fragile thin graphite sheet is not suitable for machine subject to vibration.

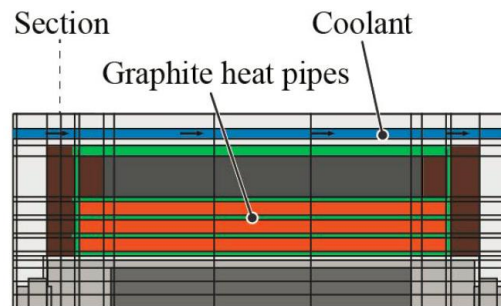


Fig.2.11. Graphite sheet acting as heat pipes between windings [61]

c. Direct Winding Cooling

Methods recapitulated in the previous sections help in reducing the thermal resistance between the windings and the outer part, and facilitate the heat transfer. A more efficient way to

cool the windings is removing the heat away directly from the coils, and this approach is usually called Direct Winding Cooling (DWC). With the increasing demand for more effective ways to remove the heat, different direct winding cooling topologies have been proposed. As the name has suggested, for DWC, coolant will be in direct contact with some sort. Therefore, the choice of coolant is more critical, it needs to be at least non-conductive and non-corrosive. For most cases, oil-based coolant is chosen.

1) *Oil-spray Cooling*

Oil spray cooling has been applied to high-performance power unit for aircraft for a long time [62], and recently to Electric vehicle (EV) motors. The cooling system injects coolant directly on the windings to remove heat directly. A reservoir is placed at the bottom of the housing, collecting and cooling the dropped coolant. A pump is placed at the side and circulates the coolant from the reservoir to the nozzle again. Oil-spray cooling turns out to be an extremely efficient way to dissipate heat, and many literatures focus on this cooling technology with Computational Fluid Dynamic analysis and experiment, predicting the flow of coolant [63]. Fig.2.12 gives an example of oil spraying cooling with nozzles.

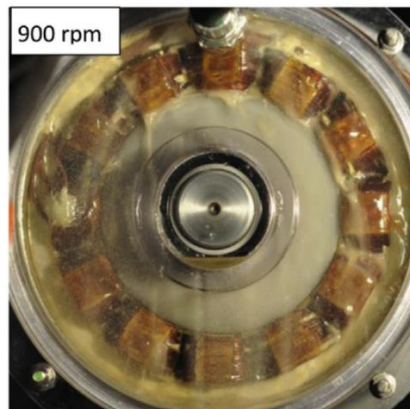


Fig.2.12. Oil-spray cooling [63]

Although this is an effective way of cooling, its drawback is obvious: it needs extra nozzles inside the housing which will increase the size of the system and degrade the power density. And for high-speed machines, the coolant flow needs to be well controlled to prevent it from hitting the rotating parts.

For a large electric machine, two-phase oil spraying could be applied [64]. The phase change of coolant further increases the cooling capability. An extra condenser needs to be installed. Therefore, this method is more practical for machines such as the hydraulic power generator.[65]

2) *In-slot Cooling Channel between Windings*

In [66] a Direct Winding Heat Exchanger (DWHX) is introduced for a high torque density machine. It consists of micro-features channel placed between the windings, shown in Fig. 2.13. The micro-features on the tunnel brings a heat transfer coefficient as high as 10 000 [W/m²K] between the coolant and the winding. The terminal of each channel is connected to an insulating bulkhead to reduce eddy current induced.

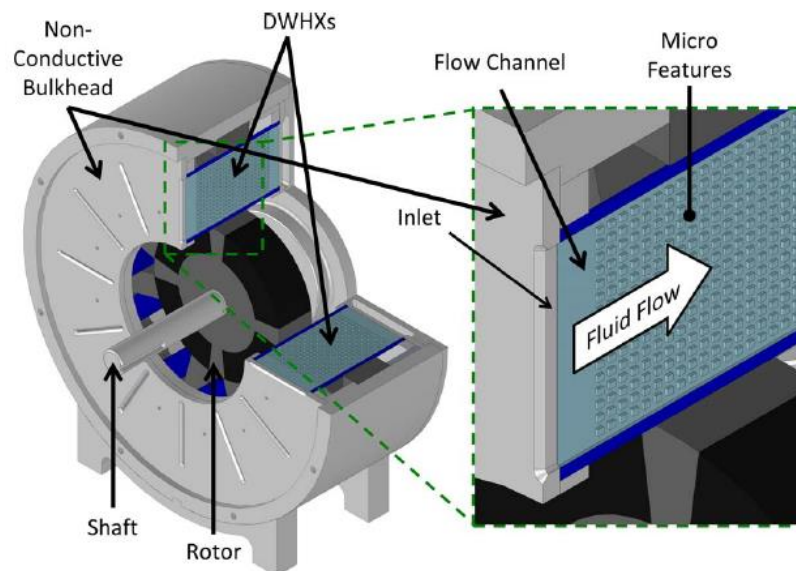


Fig.2.13. Direct Winding Heat Exchanger placed between windings [66]

The channel's material needs to be chosen carefully to avoid short-circuit between phase. In [66] another layer of insulating material was applied between the channel and the winding. Besides, the cooling channel has a tiny hydraulic diameter from 0.1mm to 0.5 mm. This in turns requires significant pumping power to achieve certain flow rate. Therefore, the overall system might be bulky due to the large pumping power source.

Other types of in-slot cooling channel have been proposed, in [67], flat conductor is used, and cooling channel is inserted in the space between windings to remove the heat directly (Fig. 2.13(a)). As mentioned in the previous section, the use of rectangular wire could help to increase the slot filling factor thus decrease the copper loss. A similar concept has been introduced in [68], where the cooling channel is embedded in a Litz wire, shown in Fig. 2.14(b). Similar as the DWHX, this system also needs large pumping force to drive the coolant, and it can only remove the heat from the windings of the machine. Heat in stator/rotor due to the core loss still need to be dissipated through another heat path.

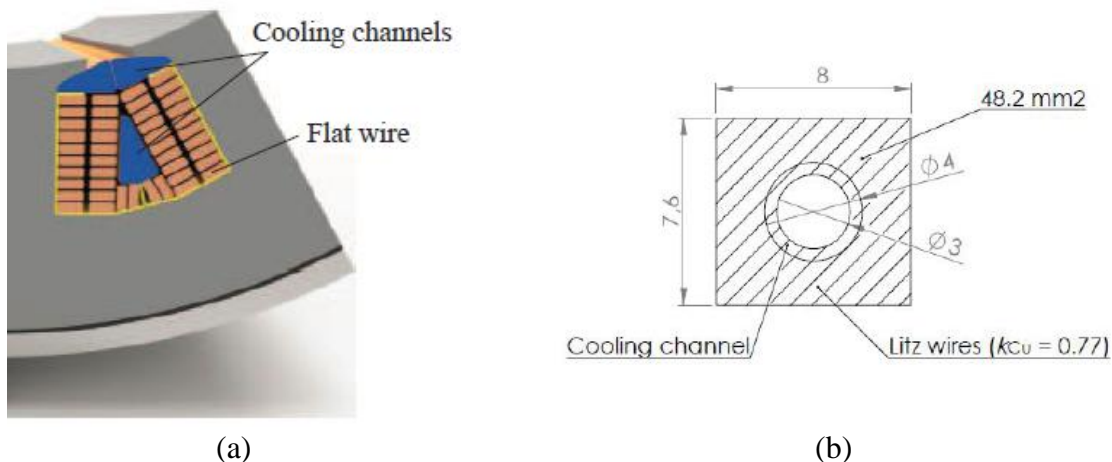


Fig.2.14. Direct slot cooling with in-slot cooling channel
 (a) Channels between flat copper wire (b) Direct winding cooling channel embedded in Litz wire [67][68]

3) *Laminated Windings with Forced Convection Cooling*

The in-slot cooling channel mentioned above still requires an extra fluid guide to run the coolant, which adds thermal resistance between the heat source and the sink. In [69], a laminated winding (Fig. 2.15) is presented. Flat conductors are specially placed to enable cooling air flowing directly through the windings. However, this requires precise manufacture to maintain the space of air channel, and the fabrication process is much more complex than conventional windings. The unsupported winding structure makes this machine more vulnerable to vibration. In this design, the windings are directly exposed to air. Therefore, there is a risk of contamination. And due to the moderate heat transfer coefficient of air, the cooling capability is limited.

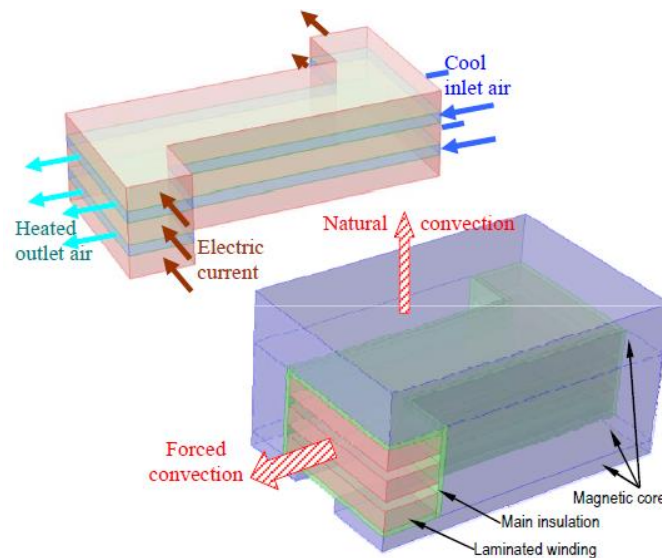


Fig.2.15. Laminated winding with forced air cooling [69]

However, this approach could be used in the hydrogen-cooled machine where the machine is enclosed in a sealed housing, filtered hydrogen is used as coolant flow through the windings. Hydrogen has a higher thermal conductivity than air (0.182 [W/mK]).

4) Direct Cooling with Magnetic Fluid/Ferro-Fluid

Most of the technologies presented previously requires additional driving force to circulate the coolant, which reduces the system's overall efficiency (although not much, the pumping power is usually smaller than 1% of the output power) and more importantly increases the volume of the system. Self-driven cooling system using temperature sensitive ferro-fluid (TSFF) has been largely investigated for electronic circuit cooling [70], [71].

Ref. [72] applied this technology to electric machine cooling. It encloses the TSFF at the end-winding region of the machine, as shown in Fig. 2.16. As the magnetic fluid used is temperature-sensitive, the fluid close to the end winding will be first heated up and lose its magnetic properties, then the cool fluid will be attracted towards the magnet, which drives the flow of fluid. It is using the waste heat to be the driving force. Therefore, no extra pumping power is needed. Besides, cooling with magnetic fluid is "self-regulated", which means the flow rate depends on the temperature difference between the hot and cold fluid.



Fig.2.16. End winding cooling with magnetic fluid [72]

Note that a dissipater still needs to be designed and added to the system to reject the heat in the fluid. The TSFF only helps to bring the heat inside the machine to a more convenient place to dissipate. This is a relatively new cooling technology for electric machine, and few reference could be found. The interaction between the TSFF and the varying magnetic field of machine

need to be taken care of. Thermal and electromagnetic properties of TSFF also need to be investigated.

Chapter 3 Cooling design and thermal analysis for a high-speed dual stator 6/4 FSPM machine

After having reviewed the commonly used thermal analysis methods and state of the art of the cooling technologies, in this chapter, a specific design and thermal analysis of a high-speed dual-stator 6/4 FSPM machine with water jacket integrated housing is presented.

Flux-switching permanent magnet (FSPM) machines have been investigated over decades for its high-power density. Different typologies have been proposed and investigated since first proposed in 1955 [73]. This machine has armature windings and permanent magnets in the stator, and the rotor has only stack laminations which make its structure simple, robust, and suitable for the high-speed application. Three of the main heat sources are the copper losses at armature windings, core losses, and permanent magnet eddy current losses. One needs to pay special attention to the stator side, since all these three heat sources are located there, and the magnets are vulnerable to demagnetization under high temperature. There is a limited thermal analysis done on FSPM machine in the past few years [74], [75]. However, the anisotropic thermal conductivity is neglected in the analysis. Reference [76] discussed moderate speed operation without showing results under high-speed conditions.

The majority of research on FSPM machine focus on 12-slot/10-pole (12/10) topology [77], [78]. However, having 10 rotor poles for very high-speed conditions requires formidably high switching frequency, which is very hard to achieve with a silicon-based inverter. In addition, the high fundamental frequency of the 10-pole machine results in more high-frequency losses, excessive generated heats, and cooling challenges. A novel structure of dual-stator 6/4 topology is proposed to make the 4-pole FSPM machine feasible for operation [79]. This proposed novel dual-stator 6/4 topology is particularly amenable for high-speed operation due to

the required lowest fundamental frequency and switching frequency for a three-phase operation. Fig. 3.1. shows the 3-D model of this dual-stator 6/4 FSPM machine.

1. Sizing and Loss Distribution in The Novel 6/4 Dual-Stator FSPM Machine

The sizing of a machine is vital for its thermal design. Table-3.1 presents the geometry information and the power rating of the machine under study. This is a very compact design for the given power rating, which shows that the power density is relatively high.

As has been mentioned previously, the loss of this machine is mostly located at the stator side. The rotor is simple and robust, only have iron loss inside, which is also minimized with lamination. Table-3.2 resumes the loss from different parts. These losses will be used later in the thermal network as a heat source.

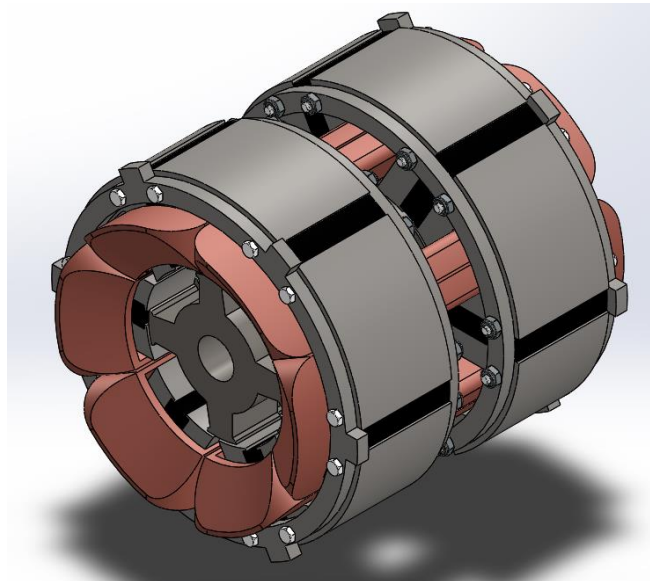


Fig.3.1. 3D model of novel 6/4 FSPM machine.

Table-3.1 Basic Design Parameters of Novel 6/4 FSPM Machine[79]

Parameters	Value
Stator outer radius [mm]	65
Total rotor length [mm]	110
Rotor outer diameter [mm]	30
Total stator length [mm]	80
Magnet Thickness [mm]	9
Rated power [kW]	10
Rated current [A]	68
Rated speed [rpm]	15000
Total active mass [kg]	7.453

Table-3.2 Loss Distribution in Novel 6/4 FSPM Machine

Copper loss (winding) [W]	126
Stator part 1 iron loss [W]	56
Stator part 2 iron loss [W]	112
Rotor iron loss [W]	84
Magnet eddy current loss [W]	129
Windage loss [W]	36
Total loss [W]	543

2. Stator Heat Extraction System Topology

One commonly used cooling approach is shaft-mounted fan. But at high-speed operation, a mounted fan on the rotor will no longer be a good idea, since that will create lots of windage loss, and the cooling performance will be highly dependent on the rotor speed. In addition, for a compact machine stator design, the air flowing through the stator side is very limited. Therefore, cooling method like water jacket is preferable.

Fig.3.2. shows the water jacket applied to this machine. Besides the water jacket attached to the stator iron, the end caps also have fins to enhance the natural convection. Openings are presented on the end caps, to facilitate the air flowing through the rotor, as well as the

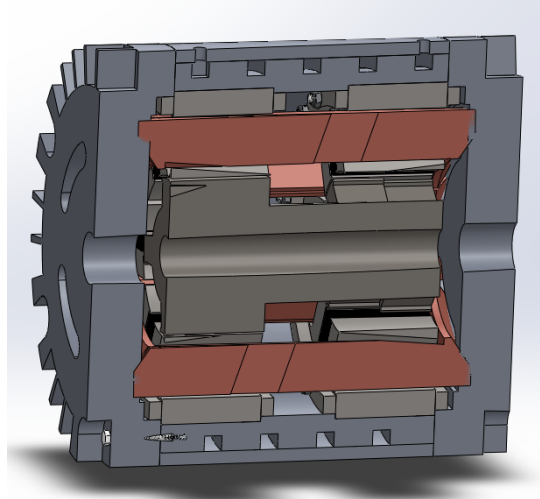


Fig.3.2. Cut view of the proposed dual-stator 6/4 FSPM machine with water jacket housing. measurement of the rotor and end windings temperature.

To calculate the coolant flow in the water jacket, over-design principle is employed, i.e. we assume that all the heat from the machine will be taken away by the water jacket. The temperature rise between the inlet and outlet of water jacket is assumed to be 5 degrees. The necessary volume flow rate needed is calculated using equation (1) and (2), where Q is the heat need to be dissipated by the water jacket.

$$rate_{mass} = Q / (Cp_{water} \Delta T) \quad (3-1)$$

$$rate_{vol} = rate_{mass} / \rho_{water} \quad (3-2)$$

Where Cp_{water} is the specific heat and ρ_{water} is the density. The section area of the water channel is 42mm^2 , then the flow velocity can then be derived.

3. LPTN and FEA Model Parameter Derivation for Novel 6/4 FSPM Machine

Thermal analysis is usually carried out with two approaches, analytical method using the thermal network and numerical method using FEA. The thermal network is beneficial for its

short calculation time, and the quasi-instant results enable designers to work with fast iterations. However, engineers need to spend more time on setting up the appropriate thermal model for the machine. Whereas finite element analysis has better accuracy and is geometry-based, and engineers only need to draw the geometry of the machine and define the boundary condition. However, finite element analysis is very time-consuming, which is more appropriate for design verification. In this section, both approaches are employed, and their results are compared.

1) *Lumped-Parameter Thermal Network (LPTN)*

The thermal network is similar to an electrical circuit, where one can analogize heat source to current source, heat flow to current flow, temperature reference to voltage reference, heat insulation to electrical resistance. The critical component in a thermal network is the thermal resistance. Depending on the heat transfer mode, it can be put into three main categories: conduction, convection and radiation heat transfer. Many literatures have covered the derivation of these three kinds of thermal resistance [80][81]. Below are the equations used for calculating different types of thermal resistances. Radiation is not considered here since it is negligible compared to the other ways of heat transfer.

$$\text{conduction (rectangular shape)} \quad R = L/Ak \quad (3-3)$$

$$\text{conduction (cylindrical shape)} \quad R = \frac{\ln(\frac{r1}{r2})}{\alpha k L} \quad (3-4)$$

$$\text{convection} \quad R = 1/hA \quad (3-5)$$

In equation (3)(4)(5), L represents the conduction path length, A represents section area of the path, k means thermal conductivity, h is the heat transfer coefficient, and α is the angle in rad.

Based on the 3D geometry of the machine, a thermal network could be generated with varies thermal resistances and heat sources. We are interested in the steady state thermal behavior, so the thermal capacitance is not modeled. The Lumped Parameter Thermal Network

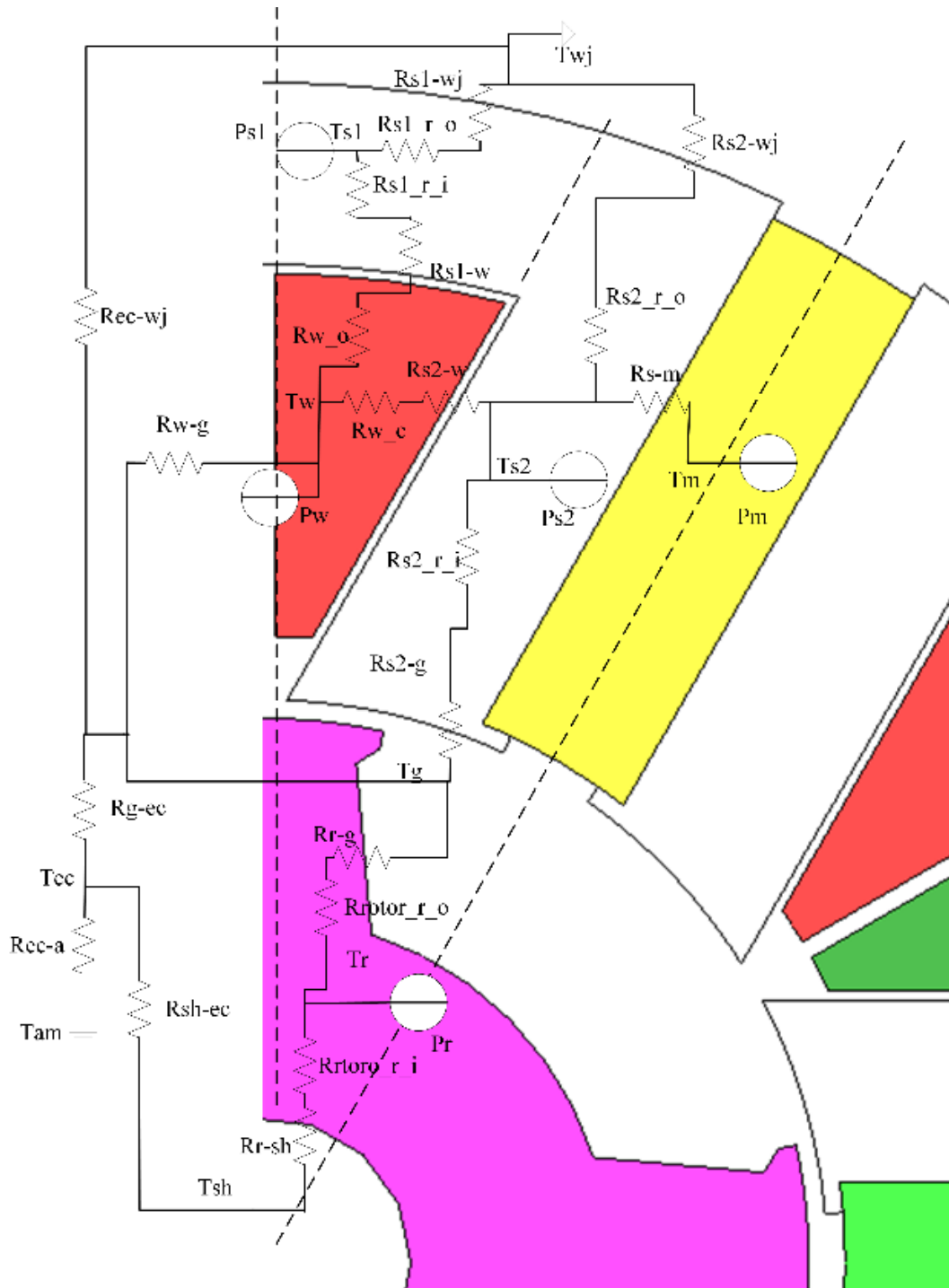


Fig.3.3. LPTN in x-y plane

in x-y plane and x-z plane are shown in Fig. 3.3. and Fig. 3.4. Note that they are complementary to each other, together they form the complete thermal network of the machine. In the next few

subsections, some critical thermal resistance models are presented that are not simply conduction heat transfer.

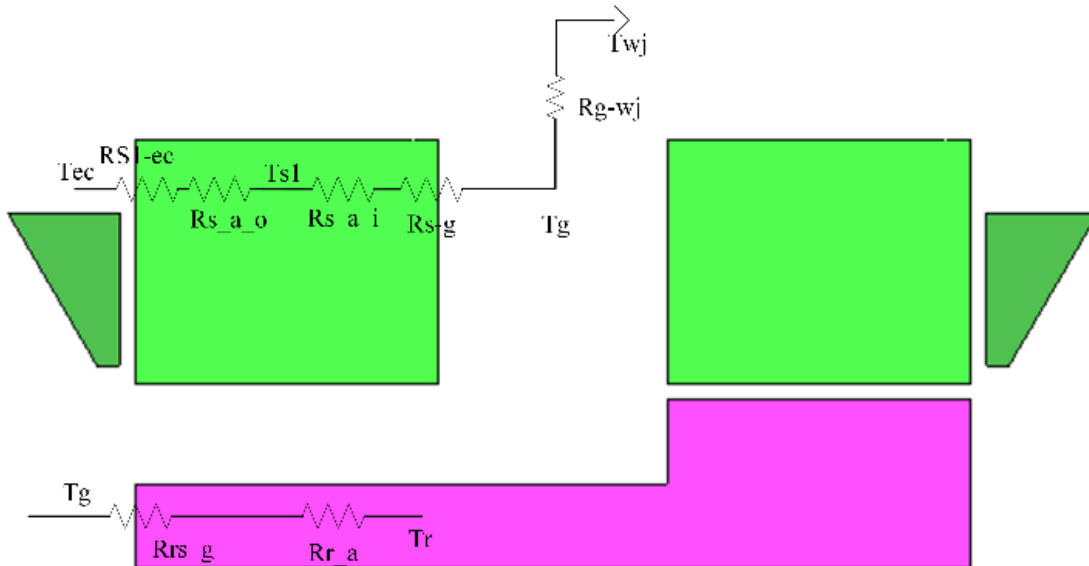


Fig.3.4. LPTN in x-z plane

1) Anisotropic Thermal Conductivity in Stator/Rotor Lamination

Nowadays, to reduce eddy current, laminated steel is used in the stator and rotor iron. However, the insulation in between each steel layer degrades the heat transfer. This results in an anisotropic property of the thermal conductivity. An equivalent thermal conductivity along the lamination direction could be calculated with equation (6). The conductivity vertical to the lamination direction can be calculated with equation (7), where K is the lamination factor.

$$k_{eq,vertical} = k_{iron}K + k_{insul}(1 - K) \quad (3-6)$$

$$k_{eq,parallel} = k_{iron}K \quad (3-7)$$

The stator of FSPM machine is C-shape, to simplify the thermal model, we divide it into two sub-parts, as shown in Fig. 3.3, the heat is assumed to be generated uniformly in the stator. Each sub-part has its heat source.

2) Equivalent Rotor Modeling

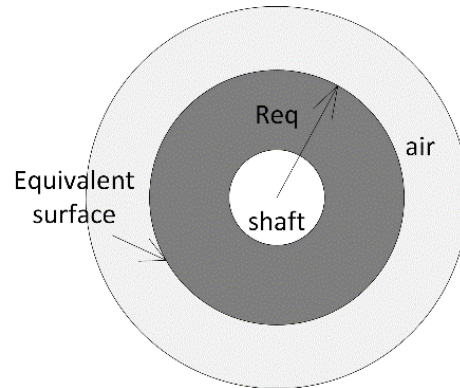


Fig.3.5. Equivalent rotor representation.

The shape of the rotor is not uniform circumferentially, and the pole number are different from the stator slot number, which makes it difficult to form the partial thermal network model. Since the heat generation of the rotor can be considered as uniform, and the heat dissipation is mostly through convection on the rotor surface, we could model the rotor into a cylinder shape as shown in Fig. 3.5. rad_{eq} is set in such a way that the equivalent surface is the same as the area that is in contact with the air in the real rotor ($S_{rotor-air}$). In equation (8), L_{stack} is the length of the rotor.

$$rad_{eq} = \frac{S_{rotor-air}}{2\pi L_{stack}} \quad (3-8)$$

3) Winding Equivalent Thermal Resistance Model

The coil has always been a difficult component to model since it is sometimes not regularly placed and has insulation coating. The thermal conductivity along the wires can be easily calculated using equation (3-9), K_{fill} represents the filling factor.

$$k_{eq} = k_{cu} K_{fill} \quad (3-9)$$

The winding thermal model has also been largely discussed in the literature. Some use empirical correlation equation [82][83], some benefit from the use of FEA tools [84]. The model

is done in [85] is based on approximate wire placement in the slot area. In the author's opinion, this method is more general and is easy to be extended to other designs.

A section view of winding coil is shown in Fig.3.6, area factors are first calculated for different parts as equation (3-10). Then an equivalent conductivity vertical to the alinement of the wires could be calculated:

$$\phi_{cu} = \frac{A_{cu}}{A_{total}}, \phi_{insul} = \frac{A_{insul}}{A_{total}}, \phi_{air} = \frac{A_{air}}{A_{total}} \quad (3-10)$$

$$k'_2 = \frac{\phi_{insul}k_{insul} + \phi_{air}k_{air}}{\phi_{insul} + \phi_{air}} \quad (3-11)$$

$$\bar{k}_x = 2\sqrt{3} \left\{ \int_0^{1-F} \frac{k_1 k'_2}{(k_1 - k'_2) \sqrt{F^2 - y^2} + \sqrt{3} k_1} dy + \int_{1-F}^{1/2} \frac{k_1 k'_2}{(k_1 - k'_2) (\sqrt{3} - \sqrt{F^2 - y^2} - \sqrt{F^2 - (y-1)^2}) + \sqrt{3} k'_2} dy \right\} \quad (3-12)$$

$$\bar{k}_y = \frac{2}{\sqrt{3}} \left\{ \int_0^{\sqrt{3}-F} \frac{k_1 k'_2}{(k_1 - k'_2) \sqrt{F^2 - x^2} + k_1} dx + \int_{\sqrt{3}-F}^{\sqrt{3}/2} \frac{k_1 k'_2}{(k_1 - k'_2) \left(1 - \sqrt{F^2 - x^2} - \sqrt{F^2 - (x - \sqrt{3})^2} \right) + k'_2} dx \right\} \quad (3-13)$$

$$\bar{k} = (\bar{k}_x + \bar{k}_y) / 2 \quad (3-14)$$

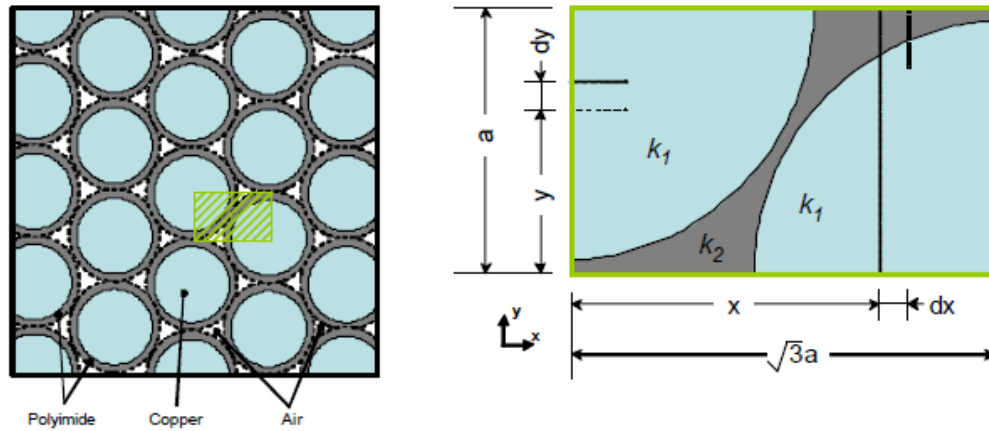


Fig.3.6. Section view of winding model [85]

4) Contact Resistance Between Surface

Due to manufacturing limit, the surface of the machine parts cannot be perfectly flat, the gaps between surface impede the heat transfer. The most commonly used method to capture this resistance is using average air gap [86], and this layer is treated as air to calculate the equivalent thermal resistance. A table of effective interface gap of common contact surface is provided in Table-3.3 [87]. Another estimation method could be found in [88]. But it is highly depended on the parameters such as the radius of contact spot, which is hard to get an accurate value due to its microscopic nature. Here the look-up table method is used since it is based on empirical results and is easy to calculate.

Table-3.3 Interface Gap for Commonly Seen Contact Surface [87]

Contact surface	Effective interface gap [μm]
Stainless - Stainless	7 - 15.3
Aluminum - Aluminum	1.2 - 2.2
Stainless - Aluminum	5.8 - 8.7
Iron - Aluminum	0.6 - 6
Copper - Copper	1 - 2.6

Table-3.4 Heat source inside the machine

Copper loss (winding) [W]	126
Stator part 1 iron loss [W]	56
Stator part 2 iron loss [W]	112
Rotor iron loss [W]	84
Magnet eddy current loss [W]	129
Windage loss [W]	36
Total loss [W]	543

5) *Lumped-parameter thermal network results*

With the critical thermal components discussed above, Table-3.4 gives the value of the heat source in the machine. Table-3.5 shows the value of thermal resistance of different machine

Table-3.5 Thermal resistance for the LTPN model of 6/4 FSPM machine

	Re	Location of	[K/
Conduction	Rs	Outer side of	5.9
	Rs	Inner side of	6.4
	Rs	Outer side of	0.4
	Rs	Inner side of	0.4
	Rr	Outer side of	0.2
	Rr	Inner side of	0.1
	Rs	Outer side of	2.3
	Rs	Inner side of	2.3
	Rr	Rotor axial	4.2
Convection	Rs	Stator side and	5.7
	Rrs	Rotor side and	5.2
	Rw	Windings and	1.1
	Rs	Stator part 2 and	17.
	Rr-	Rotor and inner	7.7
	Rg	Inner airgap and	6.9
	Re	End cap and	6.9
	Rg	Air gap and	9.8
Contact	Rs	Stator part 1 and	1.3
	Rs	Stator part 2 and	2.5
	Rs	Stator part 1 and	1.8
	Rs	Stator part 2 and	1.0
	Rs	Stator part 2 and	8.1
	Rs	Shaft and end	0.6
	Rr-	Rotor and shaft	4.5

components. One can use LT-Spice to solve the equivalent circuit. The results are put in Table-3.5, together with the results from FEA.

D. Finite Element Analysis Verification

LPTN model is built with many assumptions but provides quick results. To have a more accurate result, FEA should be implemented.

There are many software available for the FEA, their setup process is similar one to another, in this report, JMAG-designer is used to do the FEA simulation. This software is also used for the electromagnetic design, and from that the losses are put into the thermal model. Therefore, we don't need to map the losses from the electromagnetic simulation to the thermal simulation. JMAG has its limit in thermal simulation, such as it doesn't include CFD, which is useful to get the convection heat transfer between the rotor/stator and the air, as well as between the water jacket channel and the cooling water. The CFD simulation is done in ANSYS-Fluent. Heat transfer coefficients are extracted and put into JMAG as a heat transfer boundary condition.

1) Setup in the FEA

First a 3D model is drawn in Solidworks and imported to JMAG, as shown in Fig. 3.7. Then materials for different components are assigned. For stator and rotor, lamination steel is used, therefore, in the material properties, lamination factor and lamination direction need to be specified. And equivalent thermal conductivity also need to be assigned manually, for axial direction and radial direction. Same for the armature winding, in the model, the windings are put as a bulk of copper, the equivalent thermal conductivity for different direction need to be specified manually.

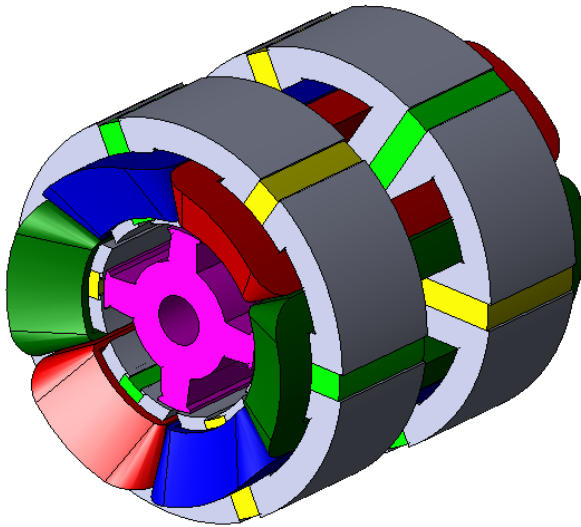


Fig.3.7. 3D structure of the dual-stator 6/4 FSPM machine

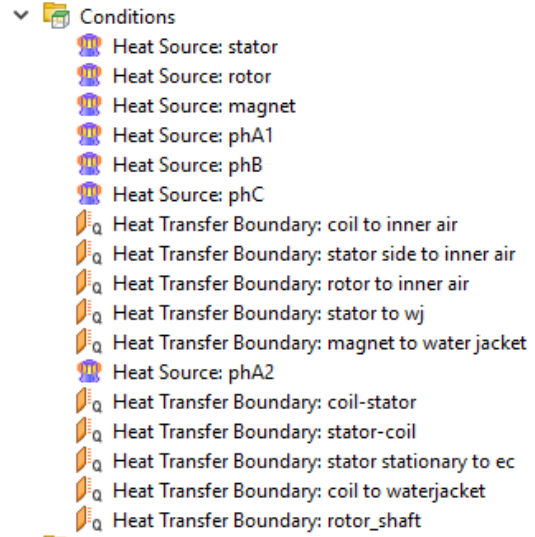


Fig.3.8. Heat transfer and heat source conditions

Heat transfer and heat source condition is then setup, as shown in Fig. 3.8. Heat source set the heat generation from different part of the machine, which is coupled with the electromagnetic simulation. The conduction heat transfer is automatically assigned, by setting the thermal conductivity of the material. However, the convection heat transfer is simulated by the boundary condition. The heat transfer boundary condition contains heat transfer coefficient and reference temperature. As mentioned previously, the FEA tool could not calculate the heat transfer coefficient, therefore, it is calculated with empirical equations or CFD tools. The reference temperature is determined by the node temperature of different part.

Unless conduction heat transfer, the convection heat transfer could not be modeled directly on the geometry. Therefore, an additional thermal circuit is needed. As shown in Fig. 3.9, the thermal network captures the heat transfer between the coil surface, rotor surface, stator surface and the inner air, heat dissipation from the water jacket, and the contact thermal resistance between the stator core and the winding.

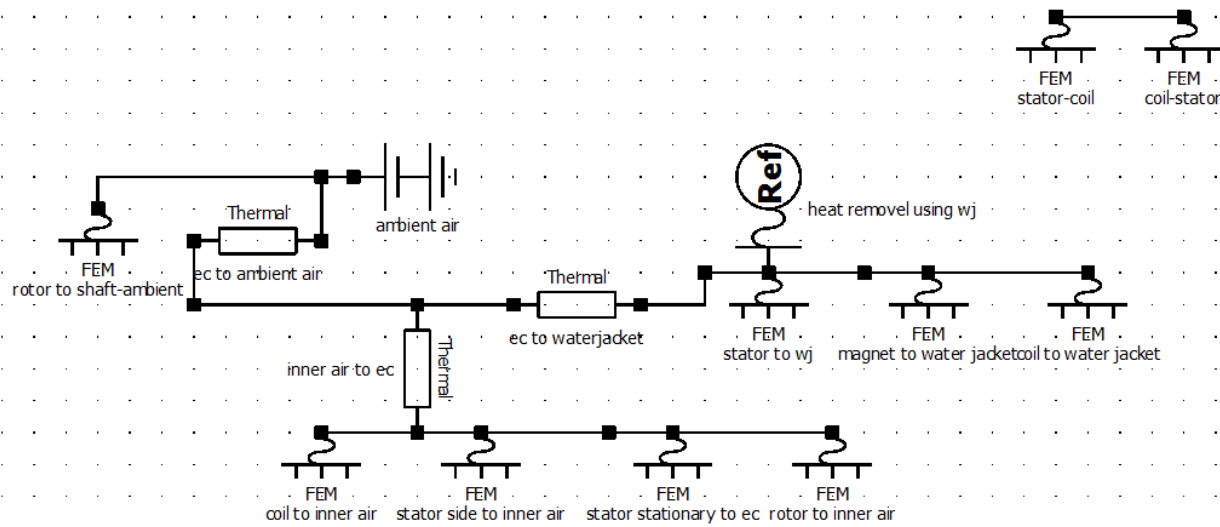


Fig.3.9. Thermal circuit for convective heat transfer

Meshes are assigned respectively for the rotor, stator, coils and permanent magnet, the heat transfer at the surface of rotor and the stator teeth are more complex, therefore, smaller surface mesh are specified. The resultant meshes for the entire model is shown in Fig. 3.10. The total number of meshes element is 238214, over 60% of the elements have quality factor of 0.5 or more. Then the FEA model is ready to run for simulation.

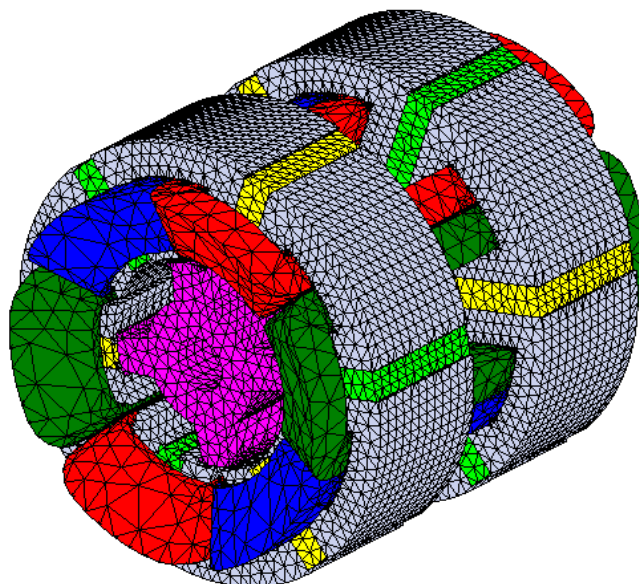


Fig.3.10. Meshes for the thermal simulation of machine

2) FEA results

The average temperatures in different parts of the machine is recapitulated in Table-3.6, together with the results from LPTN. The temperature calculated by LPTN agrees with that from FEA package, which validates the assumptions we made in the fast LPTN model. Fig. 3.11 gives the temperature contour of the machine.

As shown in Table-3.6, the discrepancy between the finite element analysis and the thermal network is not significant, but the temperature contour shown in Fig. 3.11 is absolutely more helpful for finding the hot spot inside each component.

Table-3.6 Temperatures Calculated from LPTN and FEA

Steady State Temp [C]	FEA	LPTN
Rotor	120	137.1
Stator	82	91
Windings	87.5	85.4
Magnets	91.1	88.5
Water jacket	50.5	47.9
Air gap	92.7	105.6

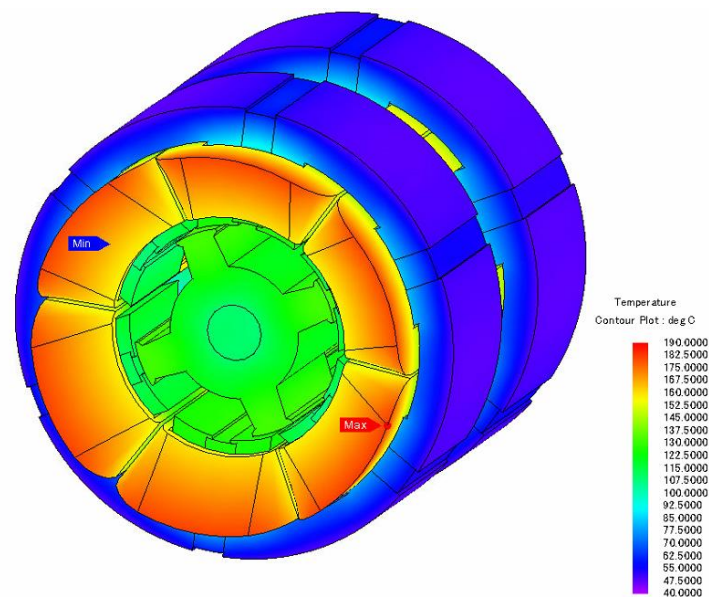


Fig.3.11. Temperature contour from steady state thermal simulation

3) Transient thermal simulation

Although both thermal network and finite element analysis could do transient simulation, but the temperature contour plot from FEA gives a more intuitive indication about the hot spot inside the machine, and the temperature surge during abrupt transient. Here we study the transient temperature distribution during the start process. Machine runs from stall to rated speed with rated torque.

Fig. 3.12 shows the temperature variation along time for different parts.

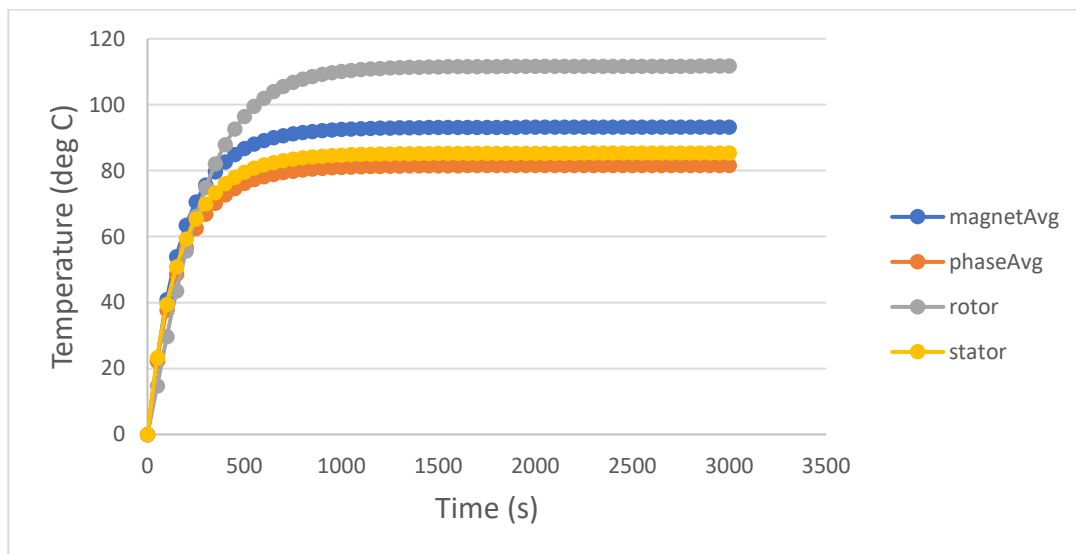


Fig.3.12 Temperature variation during machine start up

As shown in the graph, the temperature reaches equilibrium after around 1000s (17min). Since the thermal capacity of the components are close, the temperature rise almost with the same pace.

E. Coolant flow characterization in the water jacket

The water jacket used for cooling the prototype machine has spiral cooling channel, shown in Fig. 3.13. The channel employs rectangular section with 42mm^2 area. The total length of the channel is 1832mm. The flow rate and the pressure drop are calculated based on the total heat that need to be dissipated using equation (3-14).

$$P = c_p \cdot \Delta T \cdot \rho \cdot V \quad (3-14)$$

where P is the total heat that need to be dissipated, c_p is the specific heat of the coolant, ΔT is the temperature rise from inlet to outlet of the channel, ρ is the density of the coolant and V is the volume flow rate.

To leave some extra cooling margin for the design, we assume that all the 500W heat is dissipated through the water jacket. Another assumption is the temperature rise from inlet to

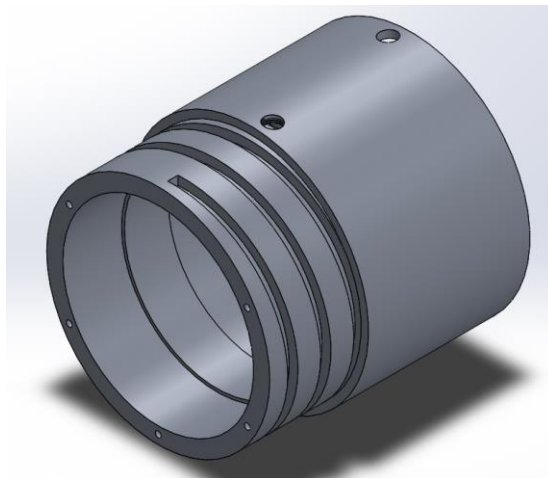


Fig.3.13 Spiral cooling channel in the water jacket

outlet is 5 degree Celsius. The volume flow rate is $2.39 \times 10^{-5} \text{ m}^3/\text{s}$, with the give cross section area, the corresponding flow velocity is 0.57 m/s.

Chapter 4 prototype machine design and manufacture

A prototype of the high-speed dual-stator 6/4 FSPM machine is built for experimental test.

The prototype machine comes together with the water jacket integrated housing describe in the previous chapter. In this chapter, more practical design aspects will be presented, for example the tolerance, fixation, thermocouples placement etc.

Fig. 4.1 shows the overall machine design, as a whole body as well as its exploded view. Each part will be presented in the following sections. There have been several iterations between the first 3D print draft and the final print, there is always small manufacturing details to pay attention when comes to the real fabrication step.

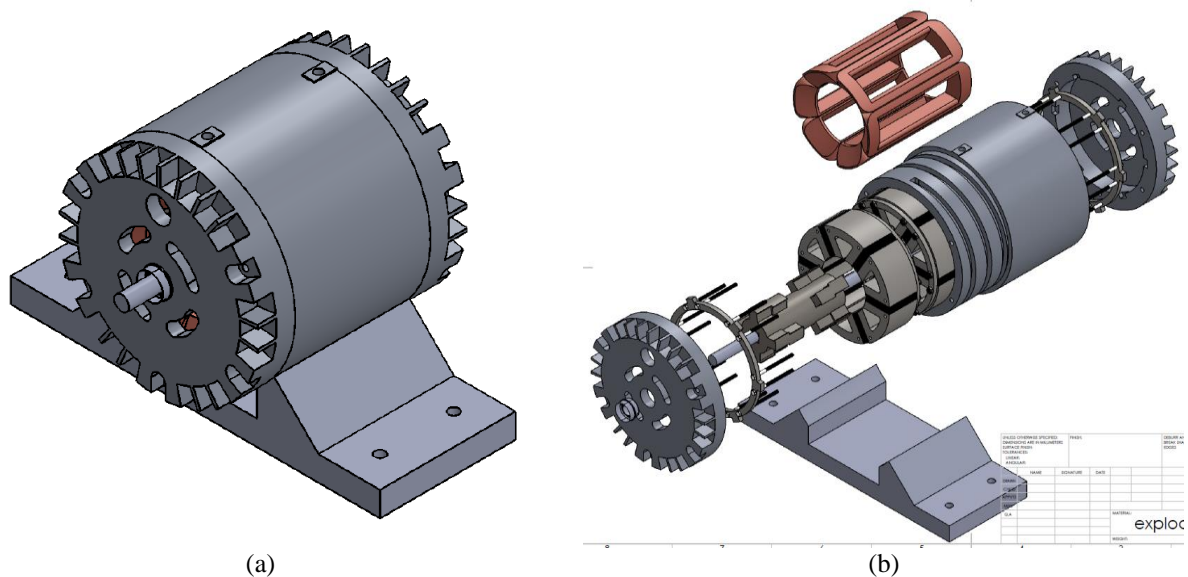


Fig. 4.1. CAD print of the overall machine design (a) assembled machine (b) exploded view

1. stator design

As can be seen in the previous chapter and Fig. 4.1, the stator of the FSPM machine is in small module, as shown in Fig. 4.2. Laminations of the unit stator is made and stacked. Then the

stator unit is put together with the permanent magnet in a sandwiched way. The geometry parameters could also be found in Fig. 4.2.

There will be 12 stator units for this machine, 6 for the front stator and 6 for the rear stator. Each group of stator unit is held together by two circular frames, shown in Fig. 4.3. The circular frames are fixed with the stator units by M4 bolts and nuts. They not only provide the fixation of the stator units but also prevent the stators from rolling inside the housing. This is realized by the keys along the circumference of the frame. The position of the fixing hole is carefully selected based on the electromagnetic simulation. The hole is punched at the place where the flux is less dense. Enough margin is needed for the sake of mechanical strength.

The stator is made up of lamination steel, since this is a machine designed for high-speed application, majority of the iron loss comes from the hysteresis loss. Therefore, thin laminations are required to minimize the loss. In this design, Arnon 5 lamination steel from Arnold Magnetic [89] is used.

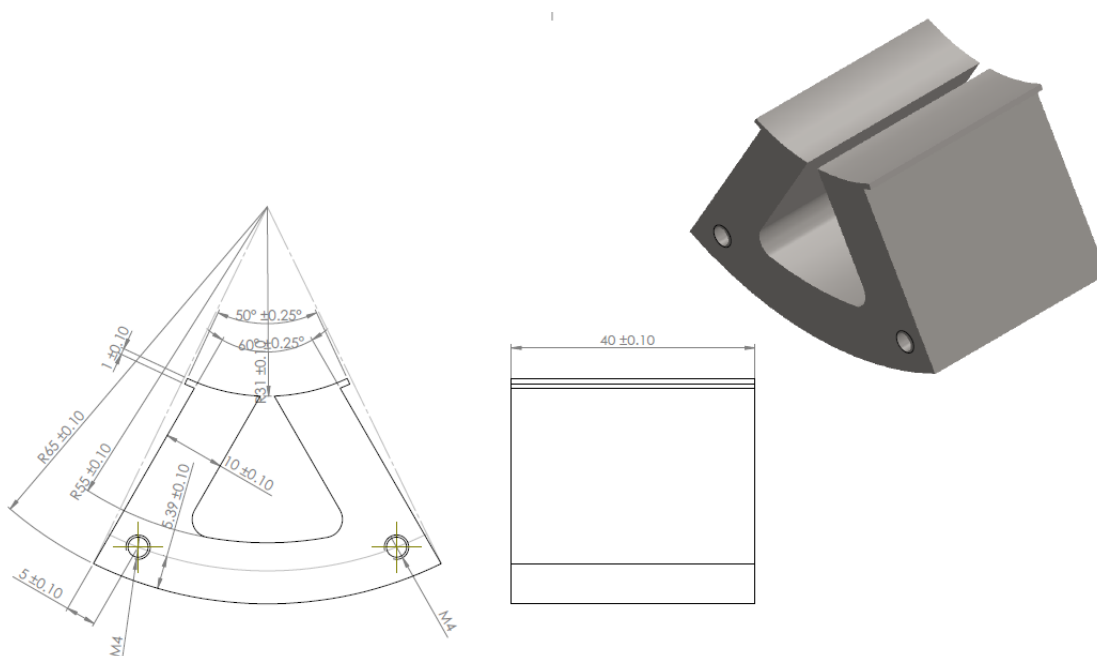


Fig. 4.2. Stator unit design and geometry parameters

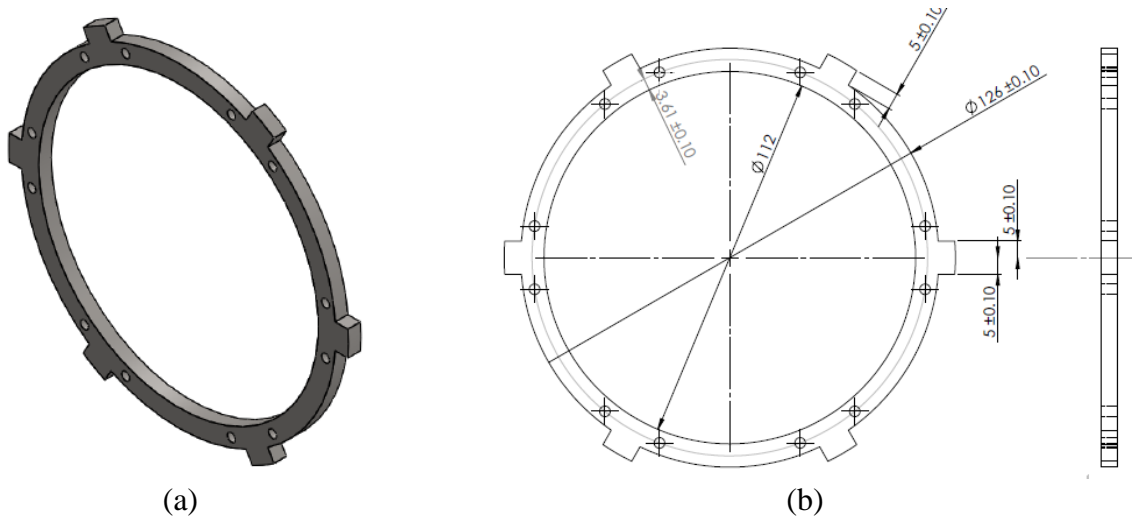


Fig. 4.3 Circular frame for stator

2. rotor design

Similar to the stator, the rotor is also made up of lamination steel. The geometry and the dimension of the rotor is given in Fig. 4.4. Although the rotor is simply a stack of lamination steel, it has five different sections, as illustrated in Fig. 4.4(c), the F1 and F2 are the front rotor that interact with the front stator. R1 and R2 are the rear rotor and M is the middle part that holds the front and rear rotor together. Since there is no axial magnetic flux flowing, therefore the middle part is only for mechanical connection and support.

To reduce the torque ripple, the front is skewed 5 degrees in two steps. Therefore, there are 5 types of lamination for the rotor in total. A square cavity is left in the rotor to place the shaft. The square blockage provides symmetric torque transmission from the rotor to the shaft. The shaft geometry and dimensions are shown in Fig. 4.5.

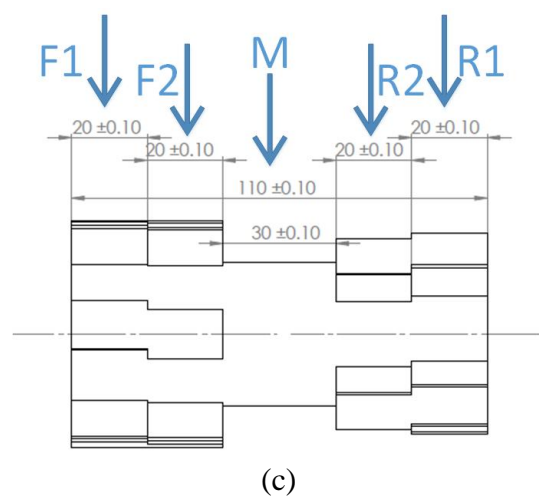
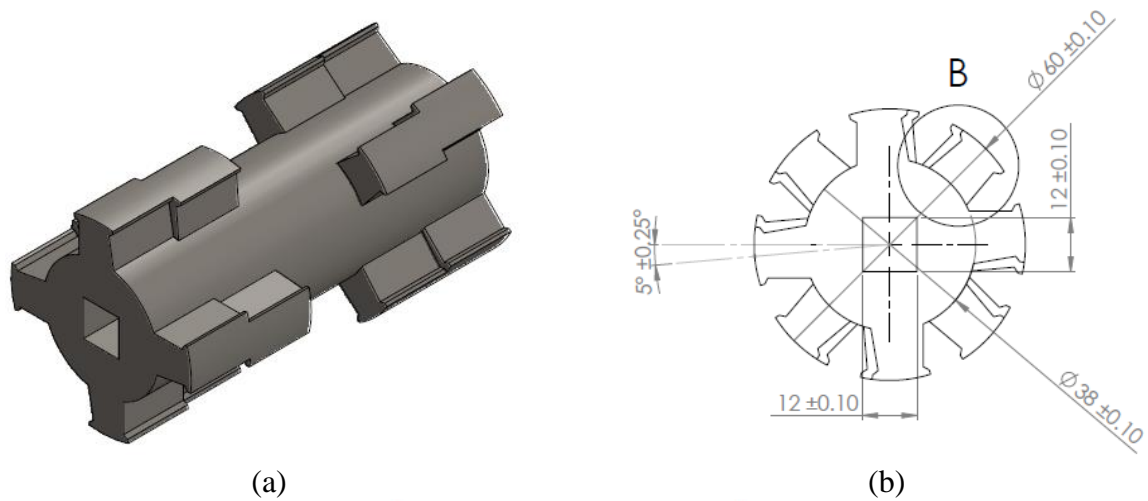


Fig. 4.4. Rotor geometry and dimensions

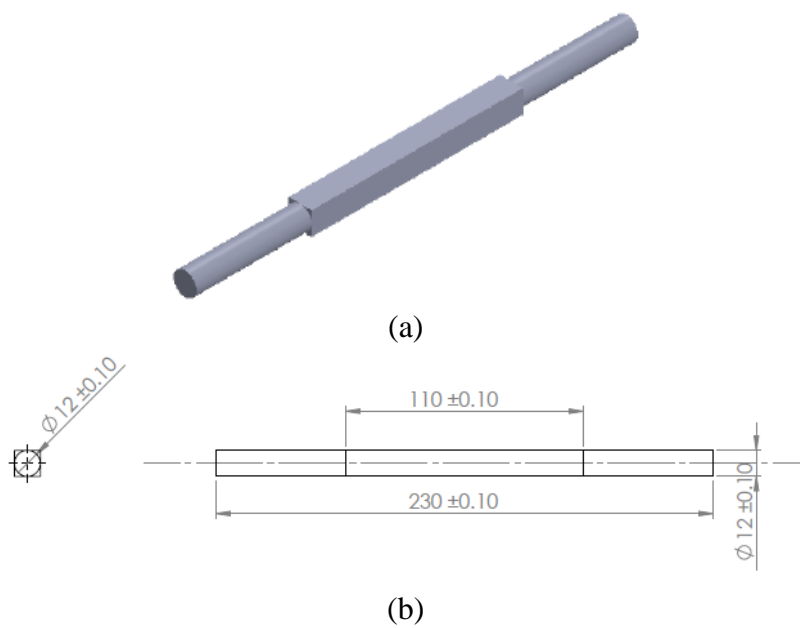


Fig. 4.5. Shaft geometry and dimension

3. winding specification

There are two coils connected in series for each phase of the machine, and each coil contains 20 turns of wire. In order to reduce the AC loss in the winding, stranded wires are used to reduce the skin effect and proximity effect. There are 7 or 8 strands per turn, the gauge for a single strand is #22. A slot filling factor of 35% to 40% is desired. A winding diagram is given in Fig. 4.6.

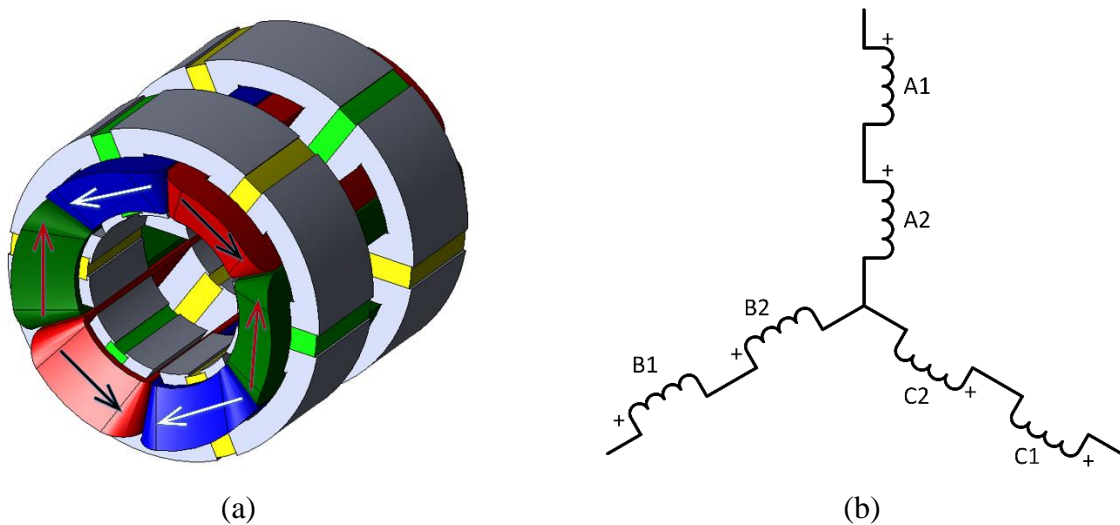


Fig. 4.6. Winding configuration of the dual-stator 6/4 FSPM machine

4. Bearing

Bearings are carefully selected for this prototype since this is for high-speed application. Ball bearing is chosen because of the low friction. And considering the size of the machine, the radial shaft stress won't be significant. The chosen AST-F63801 ball bearing has a maximum speed of 33,000 rpm, which is more than 2 times of the prototype's rated speed.

Fig. 4.7. show the geometry and the dimensions of the chosen bearing.

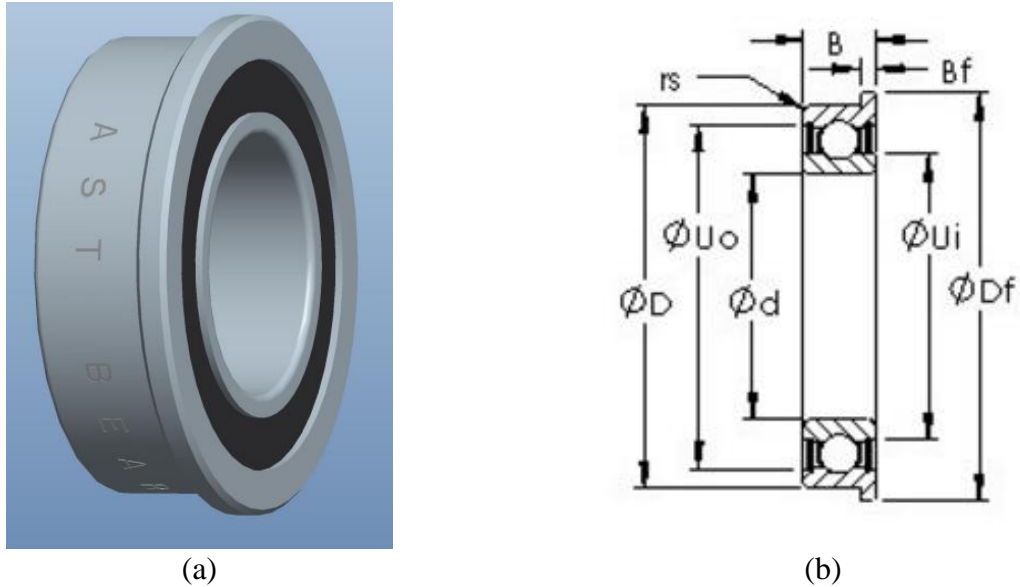
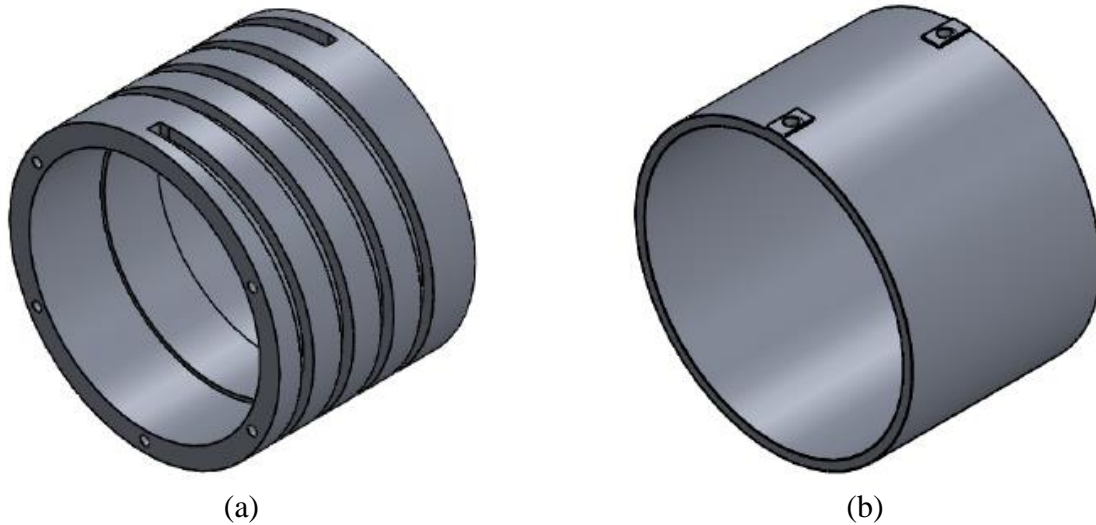


Fig. 4.7. Ball bearing chosen for the prototype machine

5. water jacket integrated housing

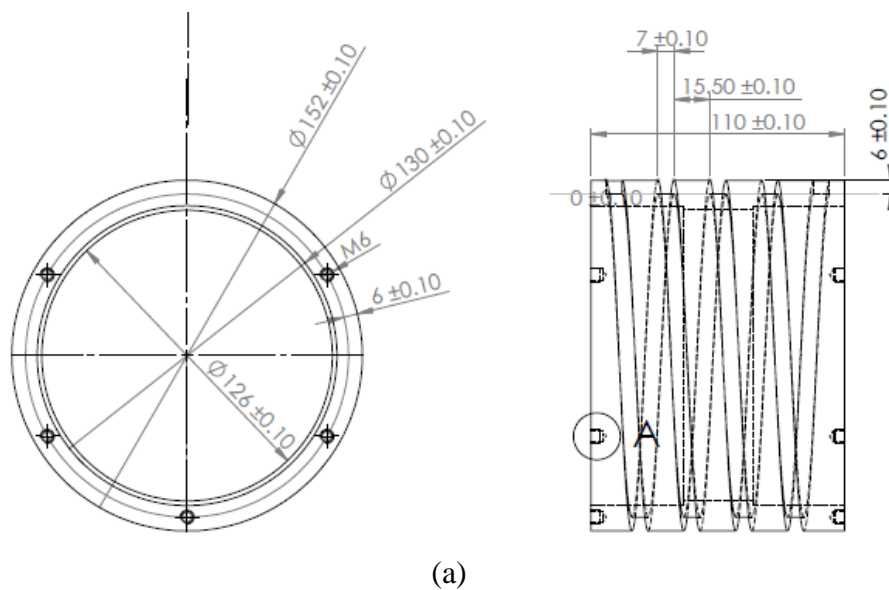
Water jacket is a commonly used cooling technique for electric machines. Due to the specified outer dimension of our machine, it is hard to purchase an off-shelf product and mount on the prototype. A water jacket is designed, manufactured and mounted directly on the prototype.

A spiral channel water jacket is constructed in this design. It is impossible to drill the whole channel directly from a whole piece of aluminum. The water jacket integrated housing is then built in two parts: an inner part with channel carved and an outer part with no channel. The inner and outer water jacket are shown in Fig. 4.8.

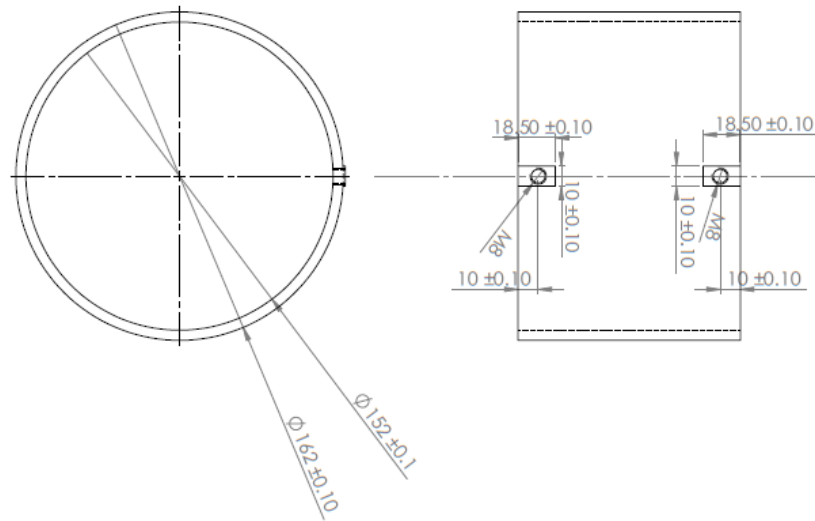


(a) (b)
Fig. 4.8. Water jacket integrated housing (a) inner part (b) outer part

The two parts are then assembled together by heat shrink. Notice that the inner part will be first put onto the stator, then the outer part will be mounted afterwards. There is a step inside the inner water jacket, this is for preventing the stator from moving axially. The dimensions of the water jacket is shown in Fig. 4.9.



(a)

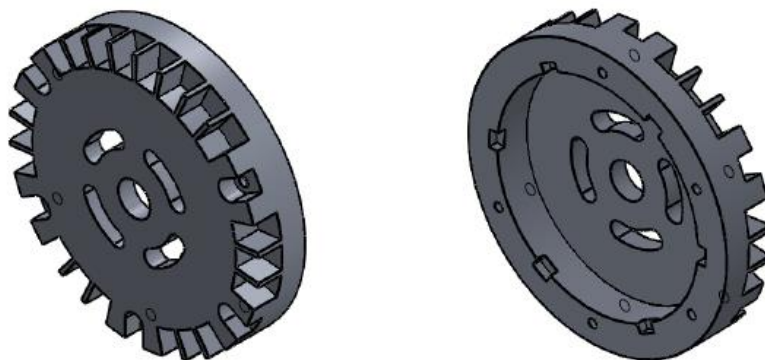


(b)

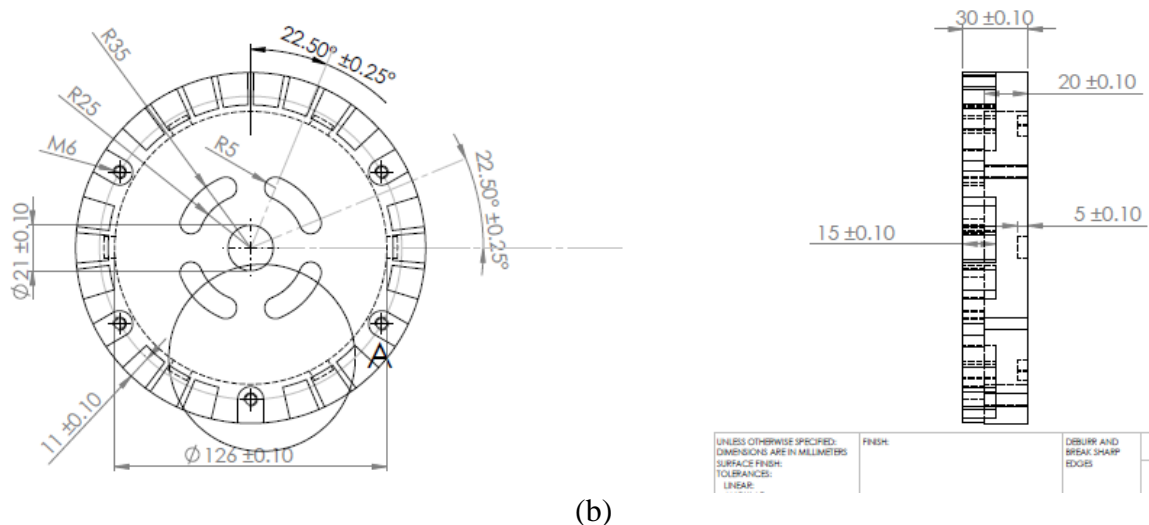
Fig. 4.9. Dimensions of the water jacket (a) inner part (b) outer part

6. end cap fin design

One innovation of this design is combining the active water jacket cooling with the passive natural convection. In addition to the water jacket, cooling fins are placed at the end cap of the housing. One major heat source of the machine will be the armature winding, since the ending is not in contact with the stator iron, the cooling of end winding is more difficult comparing to the in-slot part. The end cap fin could help to dissipate the heat from the end winding better. Fig. 4.10 shows the end cap design.



(a)



(b)
Fig. 4.10. End cap with cooling fin (a) 3D geometry of the end cap (b) dimensions of the end cap


Openings are left on the end cap, they are left for the purpose of observing the coils and for the terminals of the thermal sensing. Normally for high-speed machine, the housing is totally enclosed for the security consideration.

7. thermal sensor placement

In order to better monitor the thermal behavior of the prototype machine, 10 thermal sensors are placed in the critical parts of the machine. There are two types of thermal sensor that are commonly used: thermocouple and resistive temperature detector (RTD). Thermocouple are more often used in industrial application because of its wide temperature measuring range, fast response property and rugged structure. The thermocouples are classified into many categories based on the operating temperature. It could measure up to several thousand degree Celsius. Whereas RTD could provide a more accurate measurement and good repeatability. However, RTD is usually more fragile, it is made up of thin platinum wire that change resistivity as a function of temperature. Since the prototype is placed in a lab working condition, RTD is chosen for its long-term accuracy.

Table-4.2 gives the parameters of the RTD chosen for the prototype.

Table-4.2 Characteristics of the RTD

Model	Temperature range	Dimension	
TE connectivity GX518	-100 C to 250C	D: 1.8mm L: 10mm	

The size of the RTD is small enough to be placed inside the prototype, and it is resistant to vibration, which is an important property since FSPM machine usually has large torque ripple because of the salient structure.

In order to have a good track of the temperature variation, 10 RTDs are placed inside the machine. Fig. 4.11 shows the placement of the 10 RTDs.

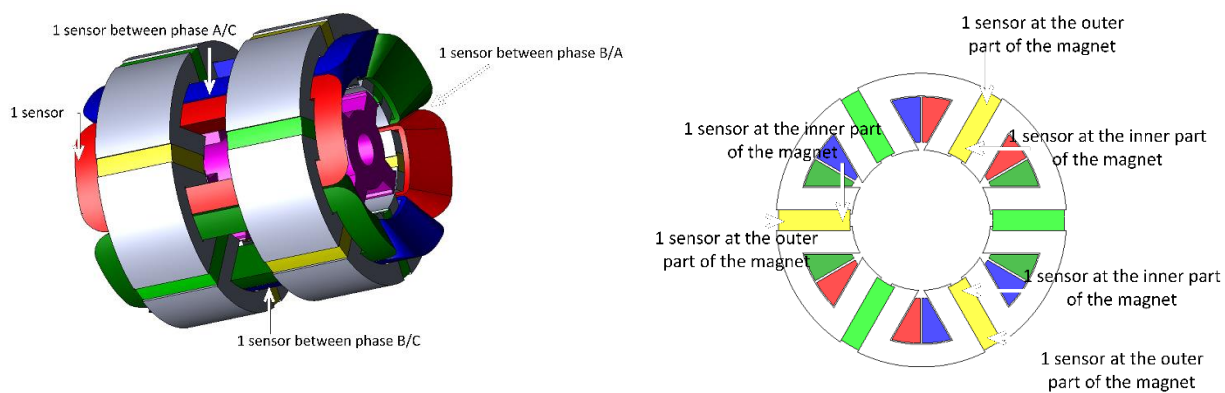


Fig. 4.11. Placement of thermal sensor

The manufacture print is attached in the annex.

Chapter 4 Conclusion and Proposed future work

1. Research conclusion

In this work, thermal analysis method for electrical machines is reviewed. Lumped-parameter thermal network (LPTN) is first introduced as a rapid method to do the preliminary thermal study. The results might be not very accurate, but is enough to predict the temperature distribution trend, i.e. to find the hot spot. The results are highly depending on the accuracy of the model. Equivalent geometry and heat transfer coefficient are usually needed.

Finite element analysis (FEA) is an alternative to LPTN. More details could be obtained from FEA. However, the calculation time is much longer than LPTN. Same as LPTN, convection heat transfer is also modeled by convective heat transfer coefficient, which is coming from the experimental result or empirical equation. Many commercial softwares could do the finite element analysis for electrical machine, most of them also have the capability doing the electromagnetic analysis. Therefore, another advantage of FEA over LPTN is that it could provide thermal-electromagnetic coupled simulation. Since the permanent magnet and iron core properties depend on temperature, coupled simulation is a critical improvement. In this study, results from a steady-state FEA

Another tool for thermal analysis is computational fluid dynamic (CFD). CFD provides the capability to get a more accurate and local convective heat transfer coefficient which is related to the fluid motion. It is also possible to couple CFD with the other thermal and electromagnetic simulation, which makes the system more complete and close to reality.

In the second part of this report, electrical machine cooling technologies are reviewed, from conventional air cooling, indirect liquid cooling to advanced direct cooling. The development of cooling technology is due to the increasing of machine power density.

Nowadays, smaller machine is widely required in transport and manufacturing industry. Therefore, efficient and high-performance cooling technology is highly needed.

The last part of this report shows the thermal analysis of a high-speed dual-stator 6-slot 4-pole FSPM machine. This type of machine has armature windings and permanent magnet on the stator side, and its rotor structure is very simple. The topological properties make this machine easy to cool from outside with water jacket. A lumped-parameter thermal network is established, steady state thermal analysis is done with the results from electromagnetic simulation. Results from these two methods shows the validity of both. In addition, a two-way coupling transient thermal analysis is done by FEA, which gives thermal information during the transient operation.

2. Future work

As mentioned in the previous section, more efficient and high-performance cooling technology is needed for higher power density machines. According to the cooling technology review in Chapter 2, direct cooling could provide the best cooling performance. However direct cooling like spray oil cooling requires extra component as spraying nozzles and coolant tank, oil pump. These components increase the volume of the system and drag down the overall efficiency. Future work of this project will mainly address to more efficient cooling technology for electrical machines.

Reference

-
- [1] J. D. McFarland, T. M. Jahns, and A. M. El, "Performance and efficiency comparisons for interior PM and flux-switching PM machines with ferrite magnets for automotive traction applications," in *2015 IEEE Energy Conversion Congress and Exposition (ECCE)*, 2015, pp. 6529–6536.
 - [2] X. Liu, Z. Q. Zhu, and D. Wu, "Evaluation of efficiency optimized variable flux reluctance machine for EVs/HEVs by comparing with interior PM machine," in *2014 17th International Conference on Electrical Machines and Systems (ICEMS)*, 2014, pp. 2648–2654.
 - [3] M. Caruso, A. O. Di Tommaso, R. Miceli, and C. Spataro, "Experimental study on efficiency enhancement in Interior Permanent Magnet Synchronous machines," in *2015 International Conference on Clean Electrical Power (ICCEP)*, 2015, pp. 518–522.
 - [4] Z. Q. Zhu and J. T. Chen, "Advanced Flux-Switching Permanent Magnet Brushless Machines," *IEEE Trans. Magn.*, vol. 46, no. 6, pp. 1447–1453, Jun. 2010.
 - [5] Wei Hua, Ming Cheng, and Gan Zhang, "A Novel Hybrid Excitation Flux-Switching Motor for Hybrid Vehicles," *IEEE Trans. Magn.*, vol. 45, no. 10, pp. 4728–4731, Oct. 2009.
 - [6] W. Hua, Z. Q. Zhu, M. Cheng, Y. Pang, and D. Howe, "Comparison of flux-switching and doubly-salient permanent magnet brushless machines," in *2005 International Conference on Electrical Machines and Systems*, 2005, p. 165–170 Vol. 1.
 - [7] T. Raminosoa, A. M. El-Refaie, D. Pan, K.-K. Huh, J. P. Alexander, K. Grace, S. Grubic, S. Galioto, P. B. Reddy, and X. Shen, "Reduced Rare-Earth Flux-Switching Machines for Traction Applications," *IEEE Trans. Ind. Appl.*, vol. 51, no. 4, pp. 2959–2971, Jul. 2015.
 - [8] C. Sanabria-Walter, H. Polinder, and J. A. Ferreira, "High-Torque-Density High-Efficiency Flux-Switching PM Machine for Aerospace Applications," *IEEE J. Emerg. Sel. Top. Power Electron.*, vol. 1, no. 4, pp. 327–336, Dec. 2013.
 - [9] N. Schofield and C. Giraud-Audine, "Design procedure for brushless PM traction machines for electric vehicle applications," in *IEEE International Conference on Electric Machines and Drives, 2005.*, 2005, pp. 1788–1792.
 - [10] Li Qi, Fan Tao, Wen Xuhui, Tai Xiang, Li Ye, and Zhang Guangzhen, "Modeling of the efficiency MAP of surface permanent magnet machine for electrical vehicles," in *2013 International Conference on Electrical Machines and Systems (ICEMS)*, 2013, pp. 1222–1225.
 - [11] D. G. Dorrell, A. M. Knight, and M. Popescu, "Performance Improvement in High-Performance Brushless Rare-Earth Magnet Motors for Hybrid Vehicles by Use of High Flux-Density Steel," *IEEE Trans. Magn.*, vol. 47, no. 10, pp. 3016–3019, Oct. 2011.
 - [12] X. Chen, J. Wang, V. I. Patel, and P. Lazari, "A Nine-Phase 18-Slot 14-Pole Interior Permanent Magnet Machine With Low Space Harmonics for Electric Vehicle Applications," *IEEE Trans. Energy Convers.*, vol. 31, no. 3, pp. 860–871, Sep. 2016.
 - [13] A. Boglietti, A. Cavagnino, D. Staton, M. Shanel, M. Mueller, and C. Mejuto, "Evolution and Modern Approaches for Thermal Analysis of Electrical Machines," *IEEE Trans. Ind. Electron.*, vol. 56, no. 3, pp. 871–882, Mar. 2009.
 - [14] G. (University of Wi.-M. Nellis and K. S. (University of Wisconsin-Madison), *Heat Transfer*. Cambridge University Press, 2008.
 - [15] M. M. Yovanovich, "Four decades of research on thermal contact, gap, and joint resistance in microelectronics," *IEEE Trans. Components Packag. Technol.*, vol. 28, no. 2,

- pp. 182–206, Jun. 2005.
- [16] M. G. Cooper, B. B. Mikic, and M. M. Yovanovich, “Thermal contact conductance,” *Int. J. Heat Mass Transf.*, vol. 12, no. 3, pp. 279–300, Mar. 1969.
- [17] D. P. Kulkarni, G. Rupertus, and E. Chen, “Experimental Investigation of Contact Resistance for Water Cooled Jacket for Electric Motors and Generators,” *IEEE Trans. Energy Convers.*, vol. 27, no. 1, pp. 204–210, Mar. 2012.
- [18] R. Camilleri, M. D. McCulloch, and D. A. Howey, “Experimental investigation of the thermal contact resistance in shrink fit assemblies with relevance to electrical machines,” in *7th IET International Conference on Power Electronics, Machines and Drives (PEMD 2014)*, 2014, pp. 0444–0444.
- [19] P. H. Mellor, D. Roberts, and D. R. Turner, “Lumped parameter thermal model for electrical machines of TEFC design,” *IEE Proc. B Electr. Power Appl.*, vol. 138, no. 5, p. 205, 1991.
- [20] A. Boglietti, A. Cavagnino, M. Lazzari, and M. Pastorelli, “A simplified thermal model for variable-speed self-cooled industrial induction motor,” *IEEE Trans. Ind. Appl.*, vol. 39, no. 4, pp. 945–952, Jul. 2003.
- [21] D. G. Dorrell, “Combined Thermal and Electromagnetic Analysis of Permanent-Magnet and Induction Machines to Aid Calculation,” *IEEE Trans. Ind. Electron.*, vol. 55, no. 10, pp. 3566–3574, Oct. 2008.
- [22] A. Boglietti, A. Cavagnino, and D. Staton, “Determination of Critical Parameters in Electrical Machine Thermal Models,” *IEEE Trans. Ind. Appl.*, vol. 44, no. 4, pp. 1150–1159, 2008.
- [23] W. Jiang and T. M. Jahns, “Development of efficient electromagnetic-thermal coupled model of electric machines based on finite element analysis,” in *2013 International Electric Machines & Drives Conference*, 2013, pp. 816–823.
- [24] X. Cai, M. Cheng, S. Zhu, and J. Zhang, “Thermal Modeling of Flux-Switching Permanent-Magnet Machines Considering Anisotropic Conductivity and Thermal Contact Resistance,” *IEEE Trans. Ind. Electron.*, vol. 63, no. 6, pp. 3355–3365, Jun. 2016.
- [25] S. Nategh, Z. Huang, A. Krings, O. Wallmark, and M. Leksell, “Thermal Modeling of Directly Cooled Electric Machines Using Lumped Parameter and Limited CFD Analysis,” *IEEE Trans. Energy Convers.*, vol. 28, no. 4, pp. 979–990, Dec. 2013.
- [26] S. Nategh, O. Wallmark, M. Leksell, and S. Zhao, “Thermal Analysis of a PMaSRM Using Partial FEA and Lumped Parameter Modeling,” *IEEE Trans. Energy Convers.*, vol. 27, no. 2, pp. 477–488, Jun. 2012.
- [27] D. T. Lussier, S. J. Ormiston, and R. M. Marko, “THEORETICAL DETERMINATION OF ANISOTROPIC EFFECTIVE THERMAL CONDUCTIVITY IN TRANSFORMER WINDINGS,” *Int. Commun. Heat Mass Transf.*, vol. 30, no. 3, pp. 313–322, Apr. 2003.
- [28] G. Huang, Z. Li, Y. Yu, and Z. Bu, “Finite element calculation and analysis on thermal field in flat permanent magnet linear synchronous motor,” in *World Automation Congress*, 2012, pp. 323–326.
- [29] A. Boglietti, A. Cavagnino, and D. Staton, “Determination of Critical Parameters in Electrical Machine Thermal Models,” *IEEE Trans. Ind. Appl.*, vol. 44, no. 4, pp. 1150–1159, 2008.
- [30] C. Ortiz, A. W. Skorek, M. Lavoie, and P. Benard, “Parallel CFD Analysis of Conjugate Heat Transfer in a Dry-Type Transformer,” *IEEE Trans. Ind. Appl.*, vol. 45, no. 4, pp. 1530–1534, Jul. 2009.

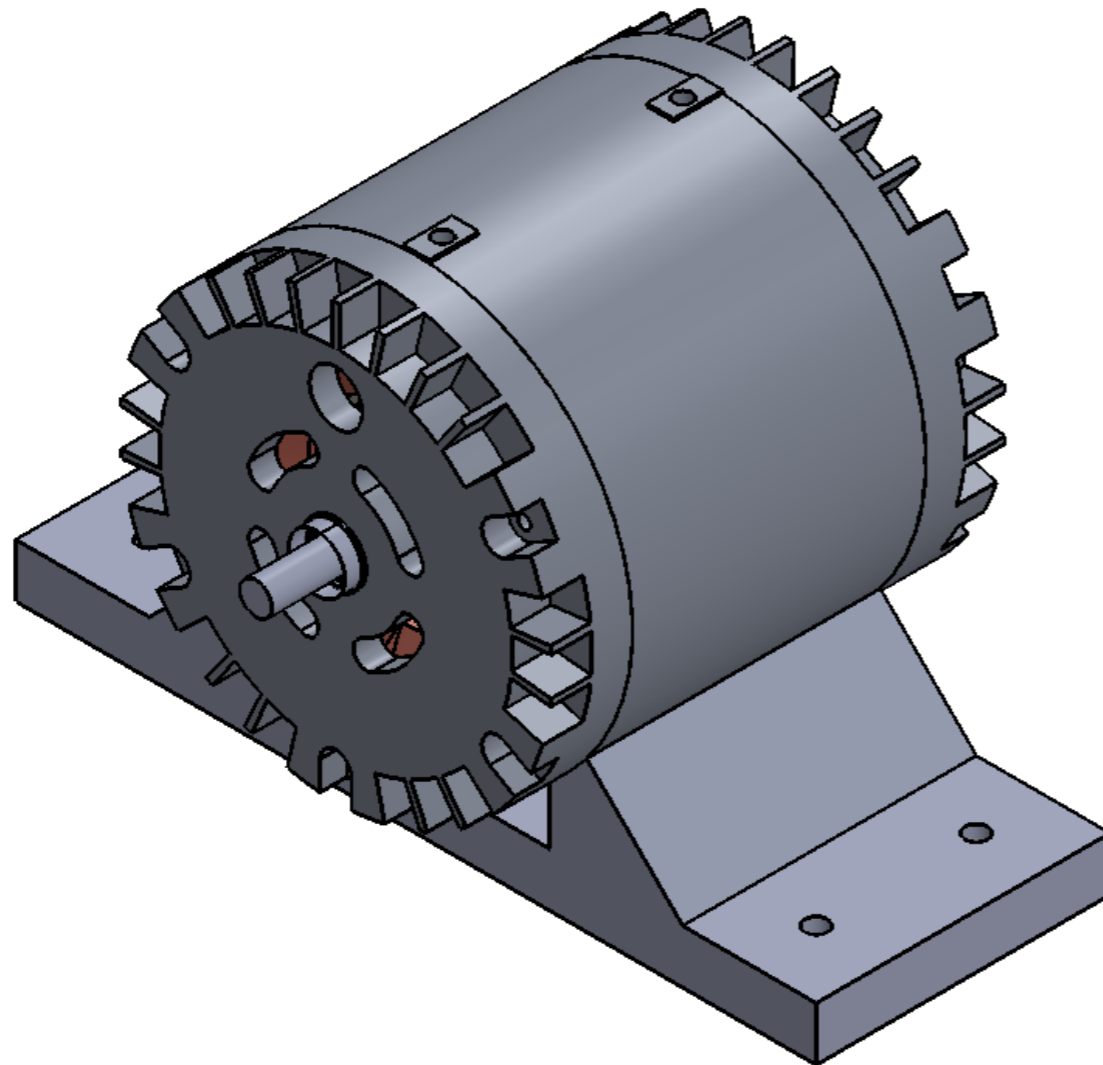
- [31] M. Doppelbauer, "The invention of the electric motor 1800-1854," 2014.
- [32] D. Staton, S. Pickering, and D. Lampard, "Recent Advancement in the Thermal Design of Electric Motors," in *Emerging technology for electric motion industry*, 2001.
- [33] A. Boglietti and A. Cavagnino, "Analysis of the Endwinding Cooling Effects in TEFC Induction Motors," *IEEE Trans. Ind. Appl.*, vol. 43, no. 5, pp. 1214–1222, 2007.
- [34] A. S. Fawzal, R. M. Cirstea, K. N. Gyftakis, T. J. Woolmer, M. Dickison, and M. Blundell, "Fan Performance Analysis for Rotor Cooling of Axial Flux Permanent Magnet Machines," *IEEE Trans. Ind. Appl.*, pp. 1–1, 2017.
- [35] B. Guo, "Investigation of the heat transfer coefficient on the fins for total enclosed fan cooled permanent-magnet motor," in *2014 17th International Conference on Electrical Machines and Systems (ICEMS)*, 2014, pp. 3264–3267.
- [36] G. M. Gilson, S. J. Pickering, D. B. Hann, and C. Gerada, "Piezoelectric Fan Cooling: A Novel High Reliability Electric Machine Thermal Management Solution," *IEEE Trans. Ind. Electron.*, vol. 60, no. 11, pp. 4841–4851, Nov. 2013.
- [37] E. Knowlton, C. W. Rice, and E. H. Freiburghouse, "Hydrogen as a cooling medium for electrical machinery," *J. A.I.E.E.*, vol. 44, no. 7, pp. 724–734, Jul. 1925.
- [38] D. S. Snell, "The hydrogen-cooled turbine generator," *Electr. Eng.*, vol. 59, no. 1, pp. 35–50, Jan. 1940.
- [39] D. Fodorean, D. C. Popa, P. Minciunescu, C. Irimia, and L. Szabo, "Study of a high-speed motorization for electric vehicle based on PMSM, IM and VRSM," in *2014 International Conference on Electrical Machines (ICEM)*, 2014, pp. 2577–2582.
- [40] G. Pellegrino, A. Vagati, B. Boazzo, and P. Guglielmi, "Comparison of Induction and PM Synchronous Motor Drives for EV Application Including Design Examples," *IEEE Trans. Ind. Appl.*, vol. 48, no. 6, pp. 2322–2332, Nov. 2012.
- [41] G. Pellegrino, A. Vagati, P. Guglielmi, and B. Boazzo, "Performance Comparison Between Surface-Mounted and Interior PM Motor Drives for Electric Vehicle Application," *IEEE Trans. Ind. Electron.*, vol. 59, no. 2, pp. 803–811, Feb. 2012.
- [42] A. M. EL-Refaie, J. P. Alexander, S. Galioto, M. R. Shah, K.-K. Huh, W. D. Gerstler, J. Tangudu, and T. M. Jahns, "Scalable, low-cost, high performance IPM Motor for Hybrid Vehicles," in *The XIX International Conference on Electrical Machines - ICEM 2010*, 2010, pp. 1–6.
- [43] J. Cros, J. R. Figueroa, and P. Viarouge, "BLDC motors with surface mounted PM rotor for wide constant power operation," in *38th IAS Annual Meeting on Conference Record of the Industry Applications Conference, 2003.*, vol. 3, pp. 1933–1940.
- [44] Wei Hua, Gan Zhang, and Ming Cheng, "Investigation and Design of a High-Power Flux-Switching Permanent Magnet Machine for Hybrid Electric Vehicles," *IEEE Trans. Magn.*, vol. 51, no. 3, pp. 1–5, Mar. 2015.
- [45] H. Zhou, L. Quan, X. Zhu, and Y. Du, "Thermal analysis of a V-shape sandwiched flux switching permanent magnet machine for electric vehicles," in *2015 18th International Conference on Electrical Machines and Systems (ICEMS)*, 2015, pp. 790–794.
- [46] P. Lindh, M. G. Tehrani, T. Lindh, J.-H. Montonen, J. Pyrhonen, J. T. Sopenan, M. Niemela, Y. Alexandrova, P. Immonen, L. Aarniovuori, and M. Polikarpova, "Multidisciplinary Design of a Permanent-Magnet Traction Motor for a Hybrid Bus Taking the Load Cycle into Account," *IEEE Trans. Ind. Electron.*, vol. 63, no. 6, pp. 3397–3408, Jun. 2016.
- [47] A. M. EL-Refaie, "Fractional-Slot Concentrated-Windings Synchronous Permanent

- Magnet Machines: Opportunities and Challenges,” *IEEE Trans. Ind. Electron.*, vol. 57, no. 1, pp. 107–121, Jan. 2010.
- [48] M. Lehr, D. Woog, and A. Binder, “Design, construction and measurements of a permanent magnet axial flux machine,” in *2016 XXII International Conference on Electrical Machines (ICEM)*, 2016, pp. 1604–1610.
- [49] J. Lin, P. Suntharalingam, F. Peng, N. Schofield, and A. Emadi, “High-speed switched reluctance machine design with toroidal-windings,” in *2015 IEEE Energy Conversion Congress and Exposition (ECCE)*, 2015, pp. 1789–1794.
- [50] E. Spooner and B. J. Chalmers, “‘TORUS’: a slotless, toroidal-stator, permanent-magnet generator,” *IEE Proc. B Electr. Power Appl.*, vol. 139, no. 6, p. 497, 1992.
- [51] J. Lin, P. Suntharalingam, N. Schofield, and A. Emadi, “Comparison of high-speed switched reluctance machines with conventional and toroidal windings,” in *2016 IEEE Transportation Electrification Conference and Expo (ITEC)*, 2016, pp. 1–7.
- [52] D.-S. Jung, Y.-H. Kim, U.-H. Lee, and H.-D. Lee, “Optimum Design of the Electric Vehicle Traction Motor Using the Hairpin Winding,” in *2012 IEEE 75th Vehicular Technology Conference (VTC Spring)*, 2012, pp. 1–4.
- [53] E. A. Boulter and G. C. Stone, “Historical development of rotor and stator winding insulation materials and systems,” *IEEE Electr. Insul. Mag.*, vol. 20, no. 3, pp. 25–39, May 2004.
- [54] S. Nategh, A. Krings, O. Wallmark, and M. Leksell, “Evaluation of impregnation materials for thermal management of liquid-cooled electric machines,” *IEEE Trans. Ind. Electron.*, vol. 61, no. 11, 2014.
- [55] T. Tomaskova, L. Harvanek, P. Trnka, V. Mentlik, M. Sebok, and M. Gutten, “New epoxy composite insulating material with nano fillers and micro fillers of silica with higher thermal conductivity,” in *2016 Diagnostic of Electrical Machines and Insulating Systems in Electrical Engineering (DEMISEE)*, 2016, pp. 89–93.
- [56] M. Polikarpova, P. M. Lindh, J. A. Tapia, and J. J. Pyrhonen, “Application of potting material for a 100 kW radial flux PMSM,” in *2014 International Conference on Electrical Machines (ICEM)*, 2014, pp. 2146–2151.
- [57] J. H. Davis, D. W. Rees, and I. H. Riley, “Silicone encapsulating and potting materials,” *Proc. IEE - Part B Electron. Commun. Eng.*, vol. 109, no. 21S, pp. 266–270, 1962.
- [58] D. Tracy, L. Nguyen, R. Giberti, A. Gallo, C. Bischof, J. N. Sweet, and A. W. Hsia, “Reliability of aluminum-nitride filled mold compound,” in *1997 Proceedings 47th Electronic Components and Technology Conference*, pp. 72–77.
- [59] J. F. Maddox, R. W. Knight, and S. H. Bhavnani, “Non-uniform thermal properties of an alumina granule/epoxy potting compound,” in *2010 12th IEEE Intersociety Conference on Thermal and Thermomechanical Phenomena in Electronic Systems*, 2010, pp. 1–6.
- [60] R. Wrobel, S. J. Williamson, J. D. Booker, and P. H. Mellor, “Characterising the performance of selected electrical machine insulation systems,” in *2015 IEEE Energy Conversion Congress and Exposition (ECCE)*, 2015, pp. 4857–4864.
- [61] A. Tuysuz, M. Steichen, C. Zwysig, and J. W. Kolar, “Advanced cooling concepts for ultra-high-speed machines,” in *2015 9th International Conference on Power Electronics and ECCE Asia (ICPE-ECCE Asia)*, 2015, pp. 2194–2202.
- [62] G. B. Sugden, “Oil-cooled a.c. generators for aircraft —present trends,” *Students Q. J.*, vol. 40, no. 160, p. 128, 1970.
- [63] T. Davin, J. Pellé, S. Harmand, and R. Yu, “Experimental study of oil cooling systems for

- electric motors,” *Appl. Therm. Eng.*, vol. 75, pp. 1–13, 2015.
- [64] J. Jia, Y. Guo, W. Wang, and S. Zhou, “Modeling and Experimental Research on Spray Cooling,” in *2008 Twenty-fourth Annual IEEE Semiconductor Thermal Measurement and Management Symposium*, 2008, pp. 118–123.
- [65] L. Zhenguang, R. Lin, and T. Longyao, “Heat transfer characteristics of spray evaporative cooling system for large electrical machines,” in *2015 18th International Conference on Electrical Machines and Systems (ICEMS)*, 2015, pp. 1740–1743.
- [66] S. A. Semidey and J. R. Mayor, “Experimentation of an Electric Machine Technology Demonstrator Incorporating Direct Winding Heat Exchangers,” *IEEE Trans. Ind. Electron.*, vol. 61, no. 10, pp. 5771–5778, Oct. 2014.
- [67] M. Schiefer and M. Doppelbauer, “Indirect slot cooling for high-power-density machines with concentrated winding,” in *2015 IEEE International Electric Machines & Drives Conference (IEMDC)*, 2015, pp. 1820–1825.
- [68] P. Lindh, I. Petrov, R. Semken, M. Niemela, J. Pyrhonen, L. Aarniovuori, T. Vaimann, and A. Kallaste, “Direct Liquid Cooling in Low-Power Electrical Machines – Proof-of-Concept,” *IEEE Trans. Energy Convers.*, pp. 1–1, 2016.
- [69] A. Reinap, F. J. Marquez-Fernandez, R. Andersson, C. Hogmark, M. Alakula, and A. Goransson, “Heat transfer analysis of a traction machine with directly cooled laminated windings,” in *2014 4th International Electric Drives Production Conference (EDPC)*, 2014, pp. 1–7.
- [70] Y. Xuan and W. Lian, “Electronic cooling using an automatic energy transport device based on thermomagnetic effect,” *Appl. Therm. Eng.*, vol. 31, no. 8, pp. 1487–1494, 2011.
- [71] H. Garg, J. S. Mehta, and R. Kumar, “Performance study of magnetic cooling system using kerosene based ferrofluid under magnetic field effect,” in *2015 2nd International Conference on Recent Advances in Engineering & Computational Sciences (RAECS)*, 2015, pp. 1–5.
- [72] G. Karimi-Moghaddam, R. D. Gould, S. Bhattacharya, and D. D. Tremelling, “Thermomagnetic liquid cooling: A novel electric machine thermal management solution,” in *2014 IEEE Energy Conversion Congress and Exposition (ECCE)*, 2014, pp. 1482–1489.
- [73] S. E. Rauch and L. J. Johnson, “Design principles of flux-switch alternators,” *Trans. Am. Inst. Electr. Eng. Part III Power Appar. Syst.*, vol. 74, no. 3, Jan. 1955.
- [74] W. Li, M. Cheng, and W. Hua, “Thermal analysis and cooling system design of flux switching permanent magnet machine,” in *2015 18th International Conference on Electrical Machines and Systems (ICEMS)*, 2015, pp. 1224–1229.
- [75] E. Ilhan, M. F. J. Kremers, T. E. Motoasca, J. J. H. Paulides, and E. Lomonova, “Transient thermal analysis of flux switching PM machines,” in *2013 Eighth International Conference and Exhibition on Ecological Vehicles and Renewable Energies (EVER)*, 2013, pp. 1–7.
- [76] X. Cai, M. Cheng, S. Zhu, and J. Zhang, “Thermal Modeling of Flux-Switching Permanent-Magnet Machines Considering Anisotropic Conductivity and Thermal Contact Resistance,” *IEEE Trans. Ind. Electron.*, vol. 63, no. 6, pp. 3355–3365, Jun. 2016.
- [77] Z. Q. Zhu, Y. Pang, D. Howe, S. Iwasaki, R. Deodhar, and A. Pride, “Analysis of electromagnetic performance of flux-switching permanent-magnet Machines by nonlinear adaptive lumped parameter magnetic circuit model,” *IEEE Trans. Magn.*, vol. 41, no. 11, pp. 4277–4287, Nov. 2005.

- [78] Wei Hua, Ming Cheng, and Gan Zhang, "A novel hybrid excitation flux-switching motor for hybrid vehicles," *IEEE Trans. Magn.*, vol. 45, no. 10, pp. 4728–4731, Oct. 2009.
- [79] Y. Li, J. H. Kim, R. Leuzzi, M. Liu, and B. Sarlioglu, "Novel 6-slot 4-pole dual-stator flux-switching permanent magnet machine comparison studies for high-speed applications," in *Energy conversion congress & EXPO*, 2016.
- [80] P. H. Mellor, D. Roberts, and D. R. Turner, "Lumped parameter thermal model for electrical machines of TEFC design," *IEE Proc. B Electr. Power Appl.*, vol. 138, no. 5, p. 205, 1991.
- [81] A. Boglietti, A. Cavagnino, D. Staton, M. Shanel, M. Mueller, and C. Mejuto, "Evolution and modern approaches for thermal analysis of electrical machines," *IEEE Trans. Ind. Electron.*, vol. 56, no. 3, pp. 871–882, Mar. 2009.
- [82] A. Boglietti, A. Cavagnino, M. Lazzari, and M. Pastorelli, "A simplified thermal model for variable-speed self-cooled industrial induction motor," *IEEE Trans. Ind. Appl.*, vol. 39, no. 4, pp. 945–952, Jul. 2003.
- [83] D. G. Dorrell, "Combined thermal and electromagnetic analysis of permanent-magnet and induction machines to aid calculation," *IEEE Trans. Ind. Electron.*, vol. 55, no. 10, pp. 3566–3574, Oct. 2008.
- [84] S. Nategh, O. Wallmark, M. Leksell, and S. Zhao, "Thermal analysis of a PMaSRM using partial FEA and lumped parameter modeling," *IEEE Trans. Energy Convers.*, vol. 27, no. 2, pp. 477–488, Jun. 2012.
- [85] S. I. Mueller, "Model and design of an air-cooled thermal management system for an integrated motor/controller," University of Wisconsin-madison, 2005.
- [86] D. Staton, A. Boglietti, and A. Cavagnino, "Solving the more difficult aspects of electric motor thermal analysis in small and medium size industrial induction motors," *IEEE Trans. Energy Convers.*, vol. 20, no. 3, pp. 620–628, Sep. 2005.
- [87] A. F. Mills, *Heat transfer*. Prentice Hall, 1999.
- [88] P. E. PHELAN, K. ITO, K. HIJIKATA, and T. OHMORI, "Thermal resistance of metallic point contacts," in *EXPERIMENTAL HEAT TRANSFER, FLUID MECHANICS AND THERMODYNAMICS, 1993, VOLS 1 AND 2*, 1993, pp. 1688–1695.
- [89] "<http://www.arnoldmagnetics.com/en-us/Products/Arnon-Electrical-Steel>."
- [90] M. Popescu, D. A. Staton, A. Boglietti, A. Cavagnino, D. Hawkins, and J. Goss, "Modern Heat Extraction Systems for Power Traction Machines—A Review," *IEEE Trans. Ind. Appl.*, vol. 52, no. 3, pp. 2167–2175, May 2016.
- [91] "NISSAN." [Online]. Available: <http://www.proteanelectric.com>.
- [92] J. Juergens, A. Fricasse, L. Marengo, J. Gragger, M. De Gennaro, and B. Ponick, "Innovative design of an air cooled ferrite permanent magnet assisted synchronous reluctance machine for automotive traction application," in *2016 XXII International Conference on Electrical Machines (ICEM)*, 2016, pp. 803–810.

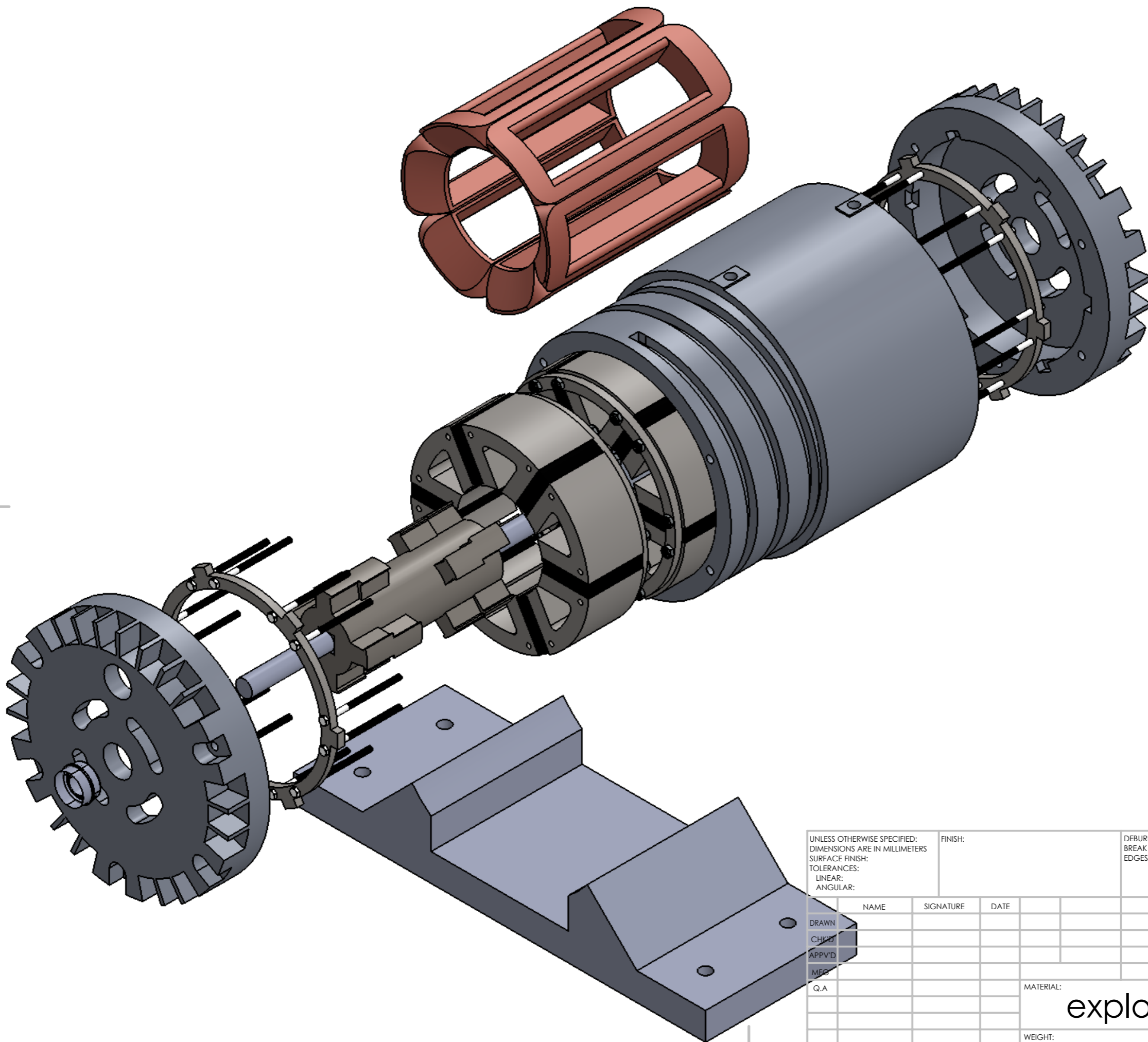
Annex 1



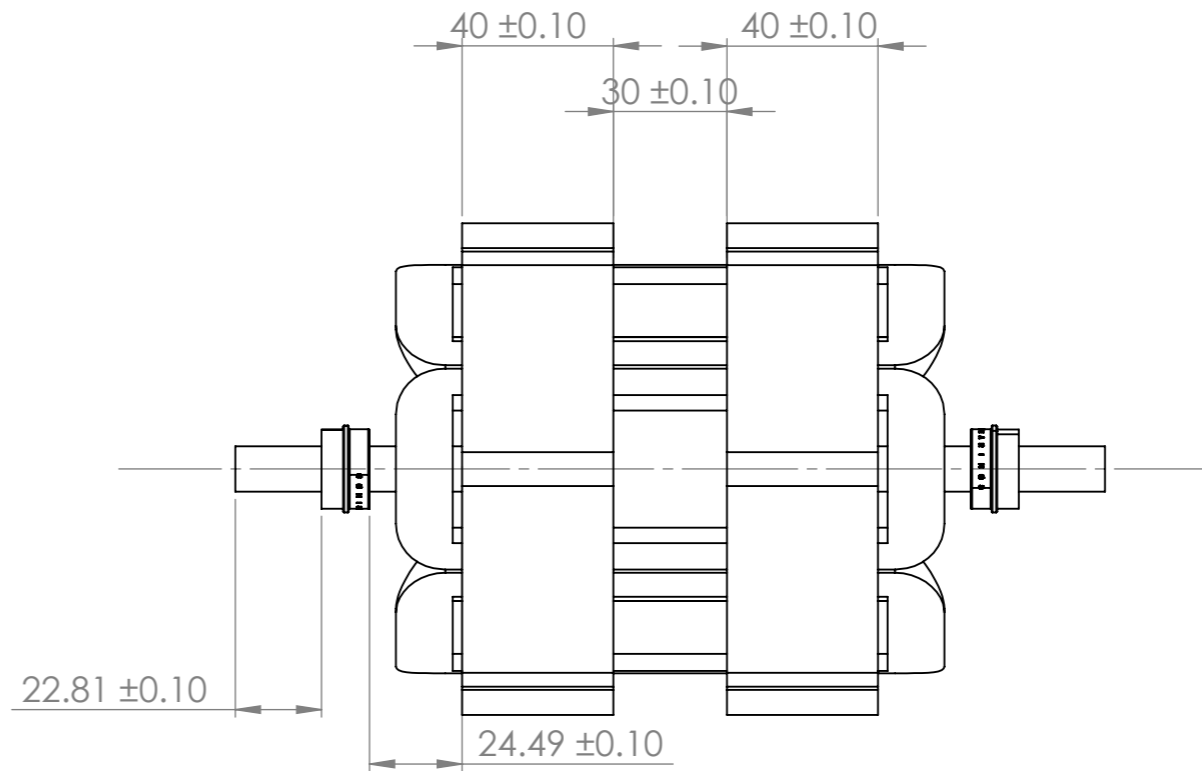
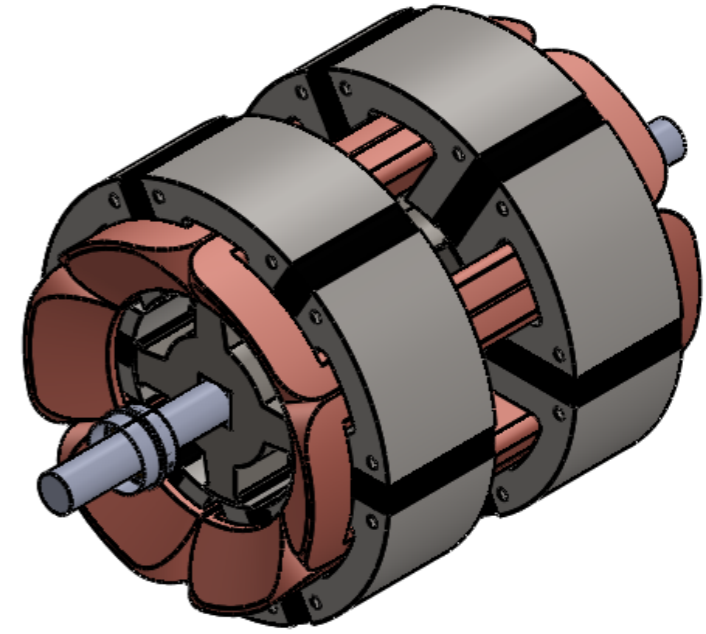
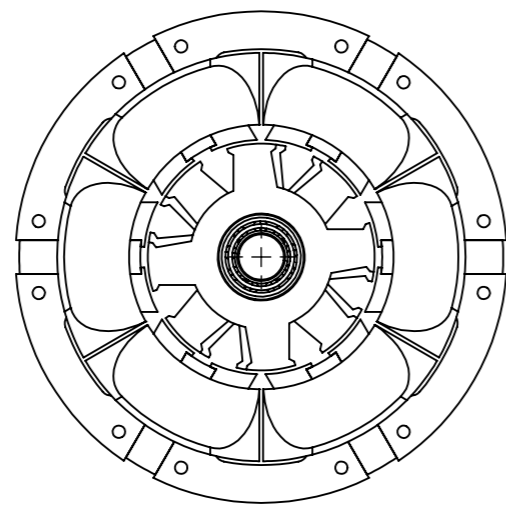
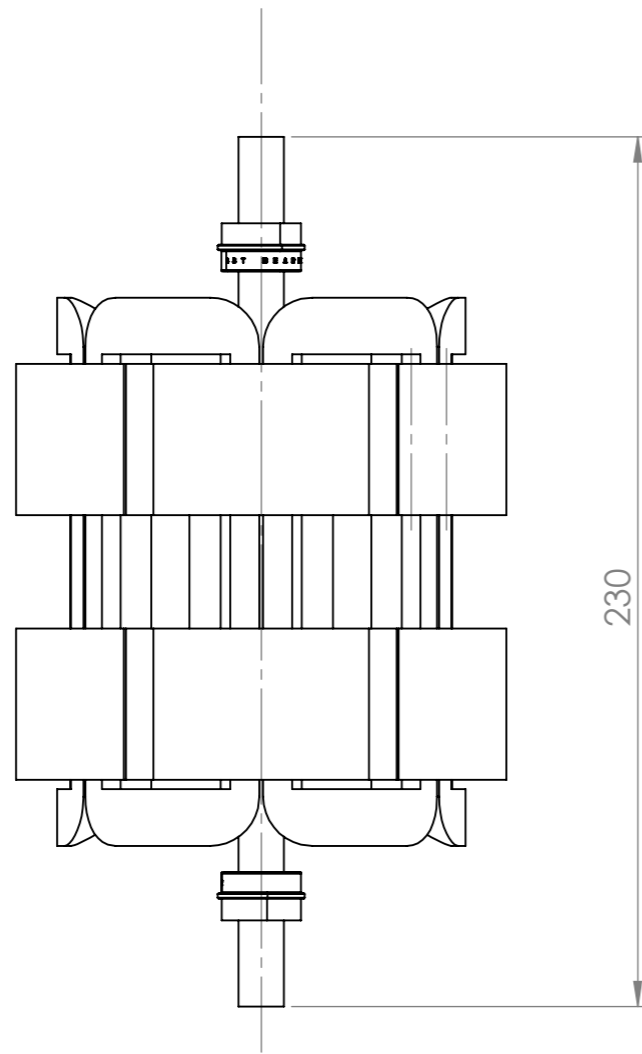
UNLESS OTHERWISE SPECIFIED: DIMENSIONS ARE IN MILLIMETERS SURFACE FINISH: TOLERANCES: LINEAR: ANGULAR:				FINISH:		DEBURR AND BREAK SHARP EDGES		DO NOT SCALE DRAWING		REVISION	
										TITLE:	
DRAWN				NAME		SIGNATURE		DATE			
CHK'D											
APPV'D											
MFG											
Q.A								MATERIAL:		DWG NO.	
										FSPM_wj_housing_integ	
								WEIGHT:		SCALE:1:5	
										SHEET 1 OF 1	

FSPM_wj_housing_integ

A3

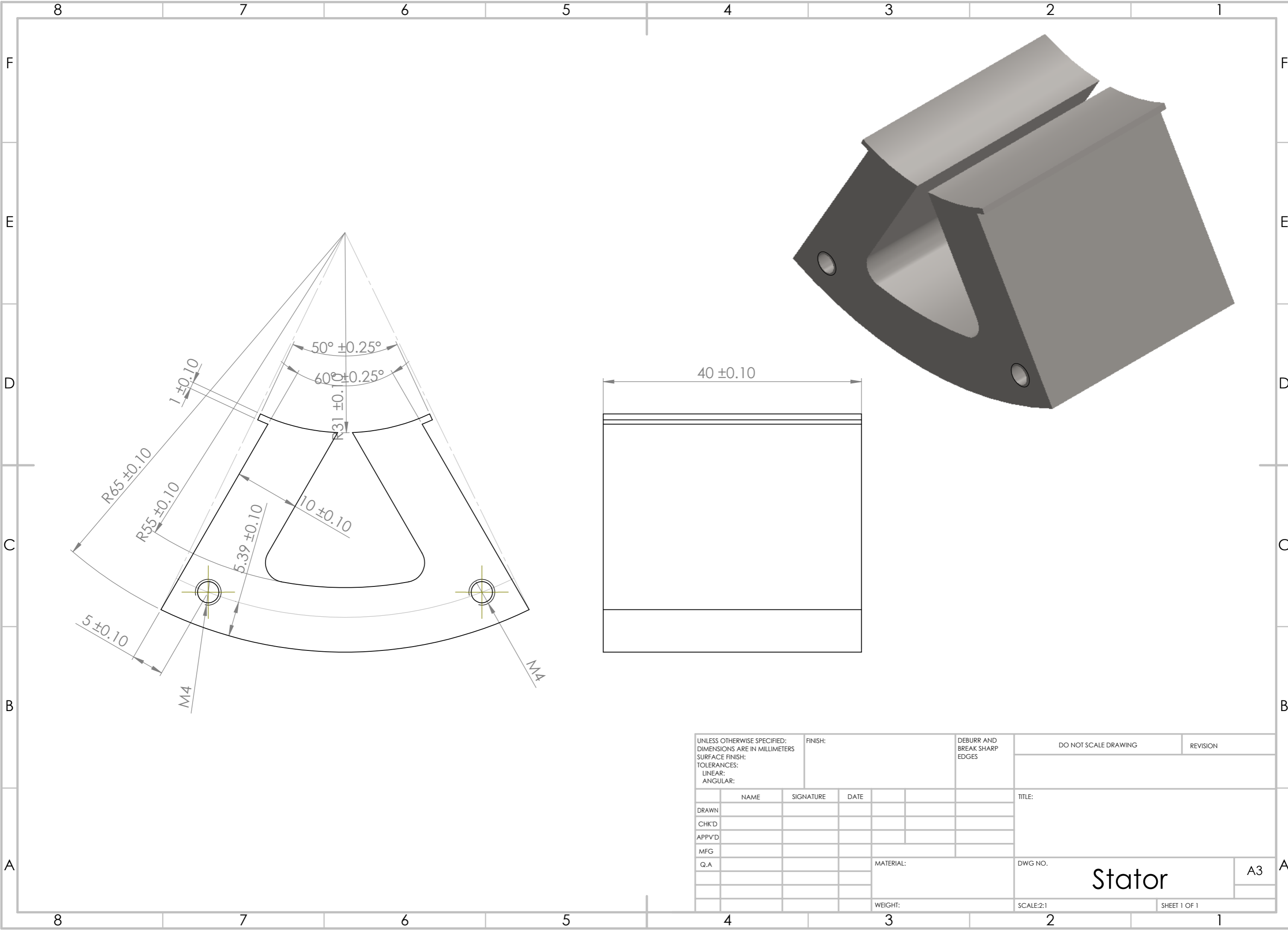


UNLESS OTHERWISE SPECIFIED: DIMENSIONS ARE IN MILLIMETERS		FINISH:		DEBURR AND BREAK SHARP EDGES		DO NOT SCALE DRAWING		REVISION	
SURFACE FINISH:									
TOLERANCES:									
LINEAR:									
ANGULAR:									
DRAWN		NAME	SIGNATURE	DATE		TITLE:			
CHKD									
APPVD									
MFG									
Q.A									
		MATERIAL:				DWG NO.		A3	
						exploded_FSPM_wj_housing_in			
		WEIGHT:				SCALE:1:10		SHEET 1 OF 1	

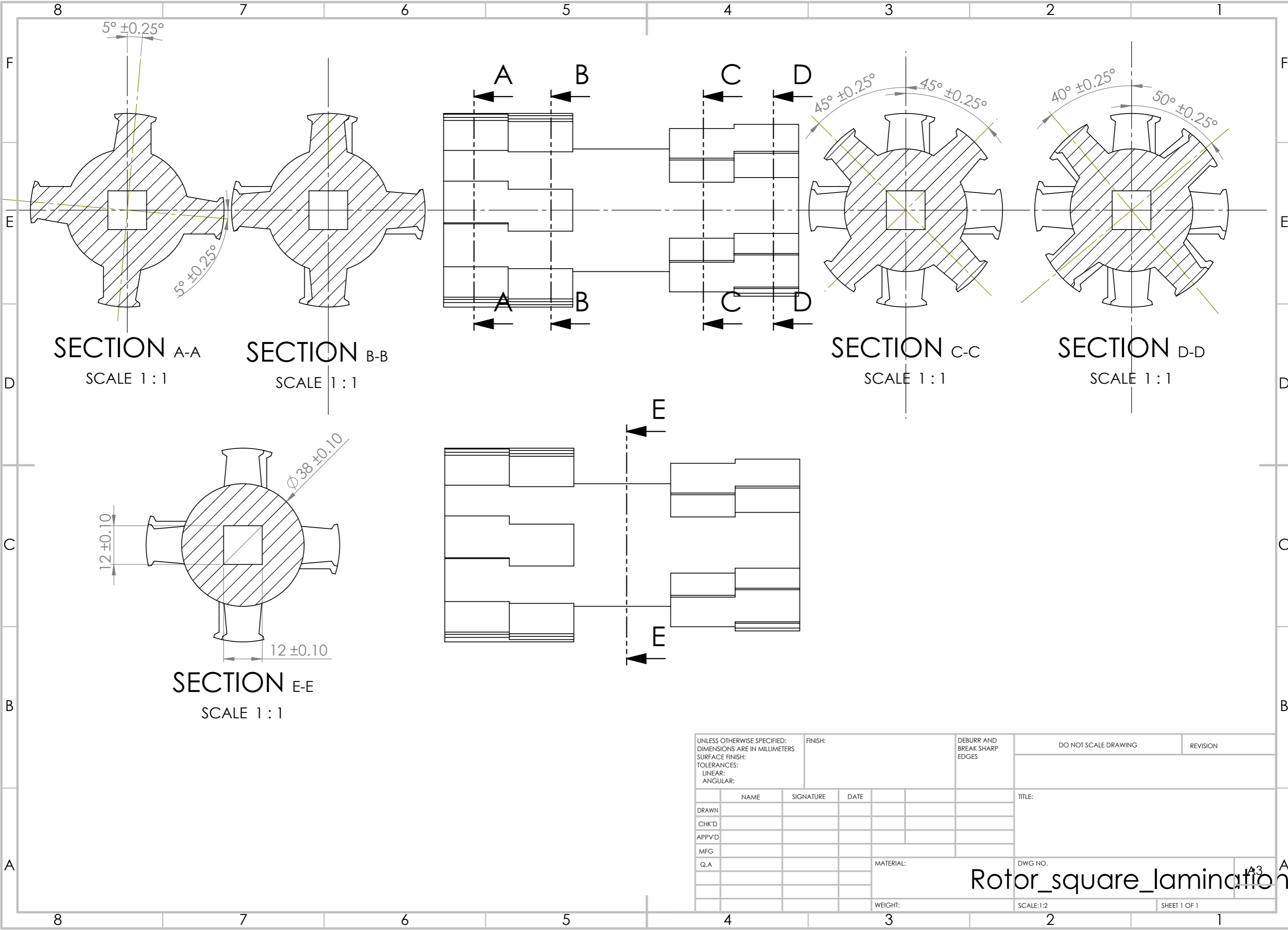


UNLESS OTHERWISE SPECIFIED: DIMENSIONS ARE IN MILLIMETERS		FINISH:		DEBURR AND BREAK SHARP EDGES		DO NOT SCALE DRAWING		REVISION	
SURFACE FINISH:									
TOLERANCES:									
LINEAR:									
ANGULAR:									
DRAWN		NAME	SIGNATURE	DATE			TITLE:		
CHK'D									
APPV'D									
MFG									
Q.A					MATERIAL:	DWG NO.		A3	
					WEIGHT:	SCALE:1:5		SHEET 1 OF 1	

Prototype_assembly_innerPar



UNLESS OTHERWISE SPECIFIED: DIMENSIONS ARE IN MILLIMETERS SURFACE FINISH: TOLERANCES: LINEAR: ANGULAR:			FINISH:		DEBURR AND BREAK SHARP EDGES		DO NOT SCALE DRAWING		REVISION		
DRAWN			NAME		SIGNATURE		DATE		TITLE:		
CHK'D											
APPV'D											
MFG											
Q.A							MATERIAL:		DWG NO.		
									Stator		
							WEIGHT:		SCALE:2:1		
									SHEET 1 OF 1		
									A3		



SECTION A-A
SCALE 1 : 1

SECTION B-B
SCALE 1 : 1

SECTION C-C
SCALE 1 : 1

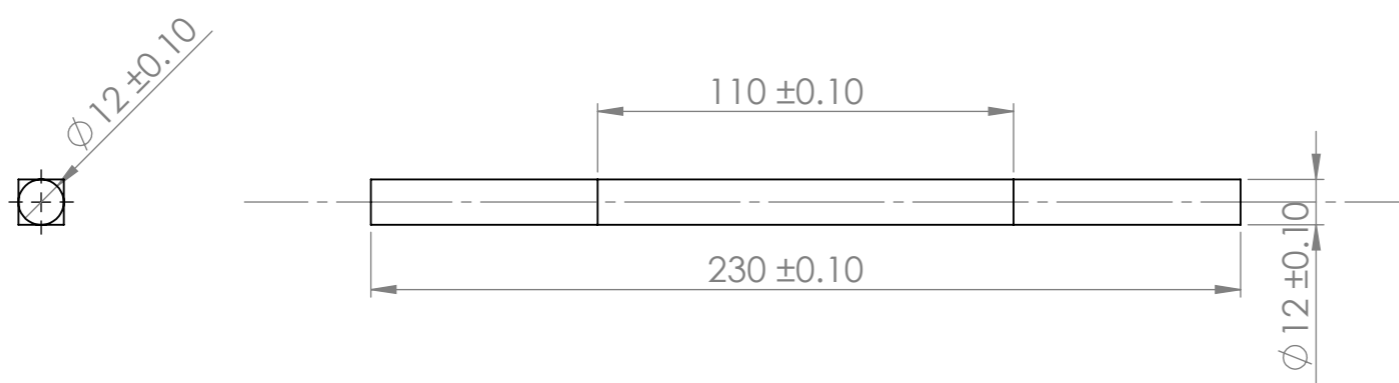
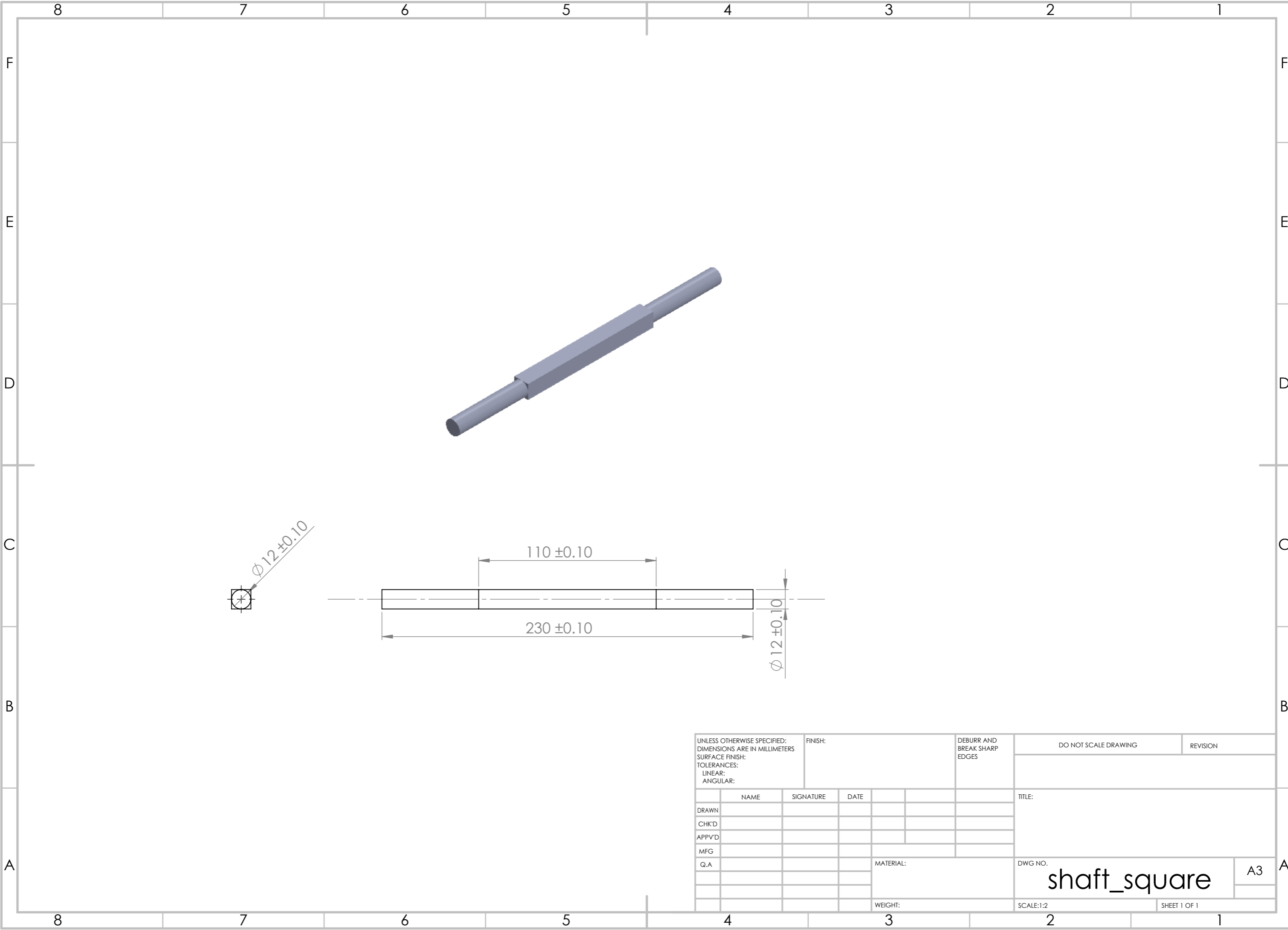
SECTION D-D
SCALE 1 : 1

SECTION E-E
SCALE 1 : 1

UNLESS OTHERWISE SPECIFIED: DIMENSIONS ARE IN MILLIMETERS SURFACE FINISH: TOLERANCES: LINEAR: ANGULAR:				FINISH:		DEBURR AND BREAK SHARP EDGES		DO NOT SCALE DRAWING		REVISION	
DRAWN				NAME		SIGNATURE		DATE		TITLE:	
CHK'D											
APPV'D											
MFG											
Q.A								MATERIAL:		DWG NO.	
								WEIGHT:		SCALE:1:2	
										SHEET 1 OF 1	

Rotor_square_lamination

A3



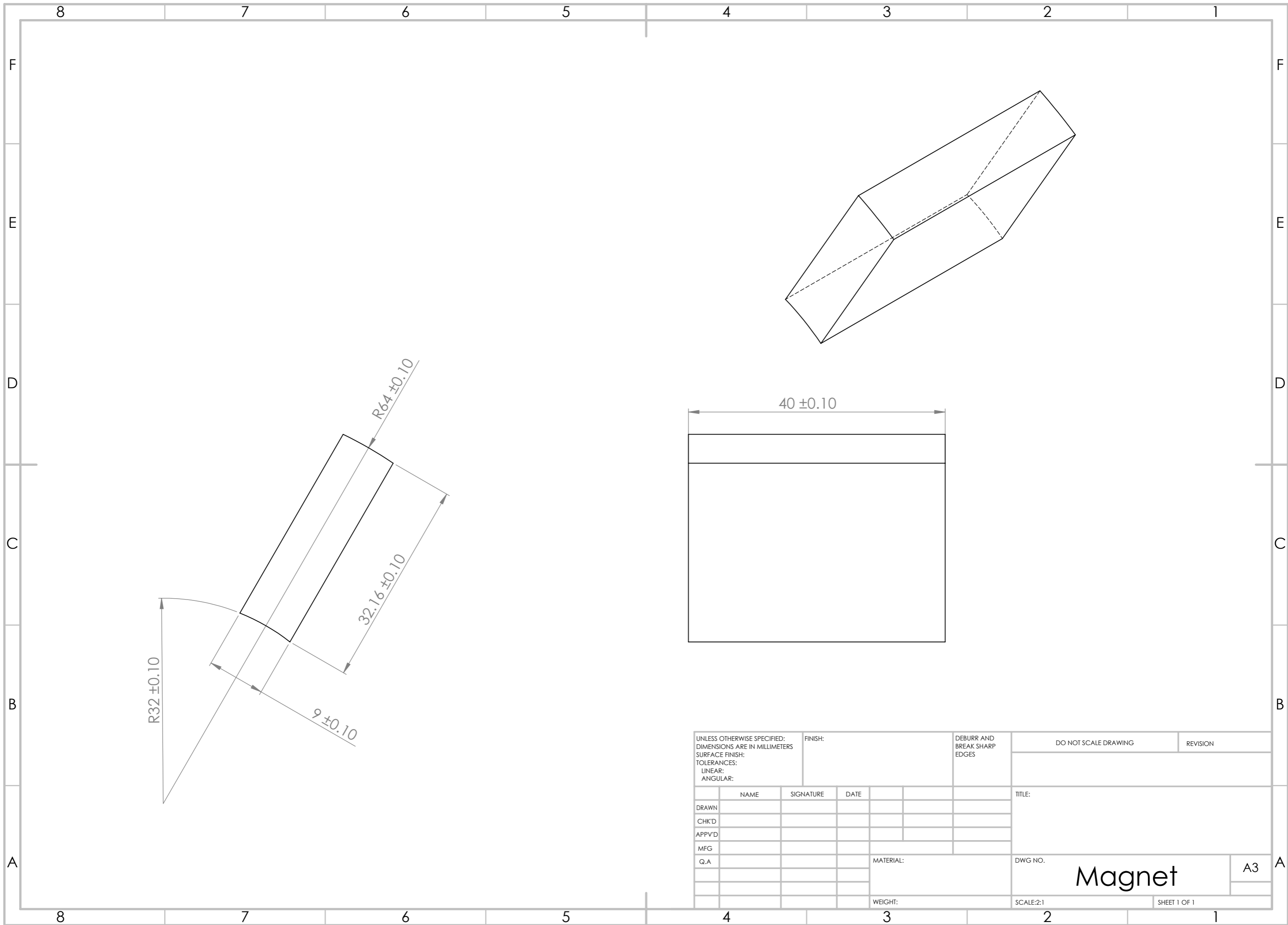
UNLESS OTHERWISE SPECIFIED: DIMENSIONS ARE IN MILLIMETERS SURFACE FINISH: TOLERANCES: LINEAR: ANGULAR:				FINISH:		DEBURR AND BREAK SHARP EDGES		DO NOT SCALE DRAWING		REVISION	
DRAWN				NAME		SIGNATURE		DATE		TITLE:	
CHK'D											
APPV'D											
MFG											
Q.A								MATERIAL:		DWG NO.	
										shaft_square	
								WEIGHT:		SCALE:1:2	
										SHEET 1 OF 1	

shaft_square

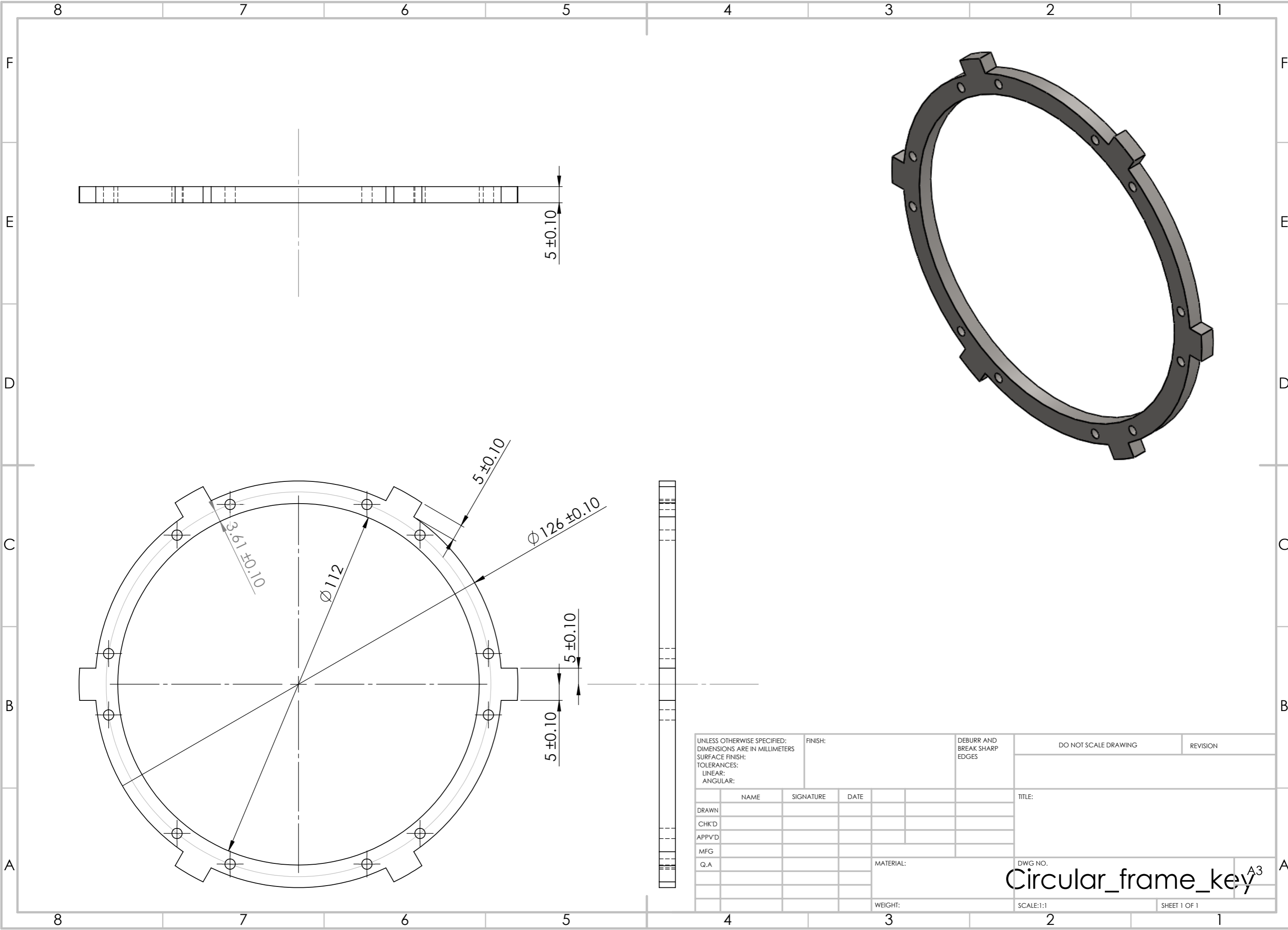
A3

SCALE:1:2

SHEET 1 OF 1

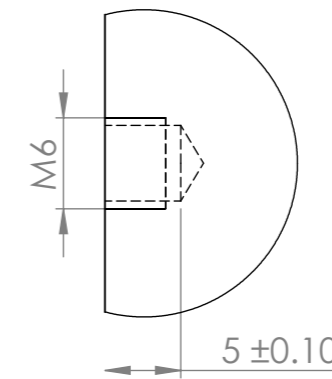
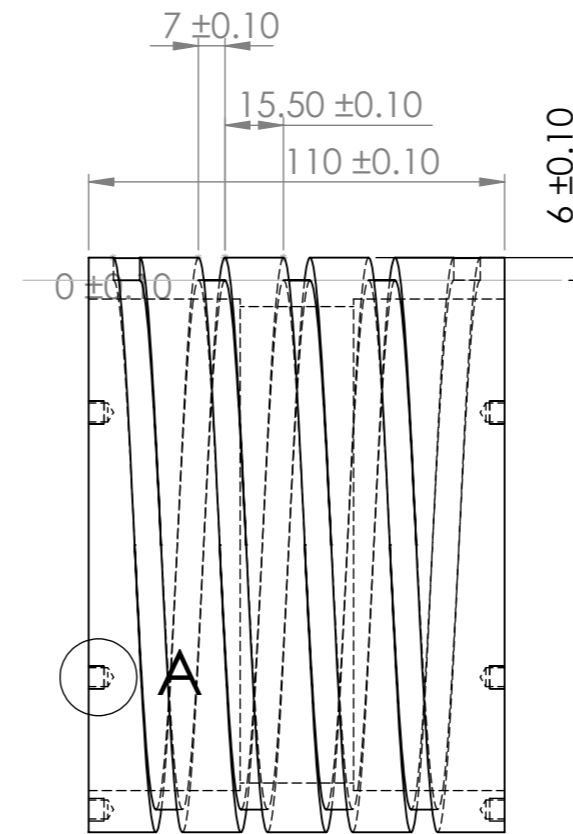
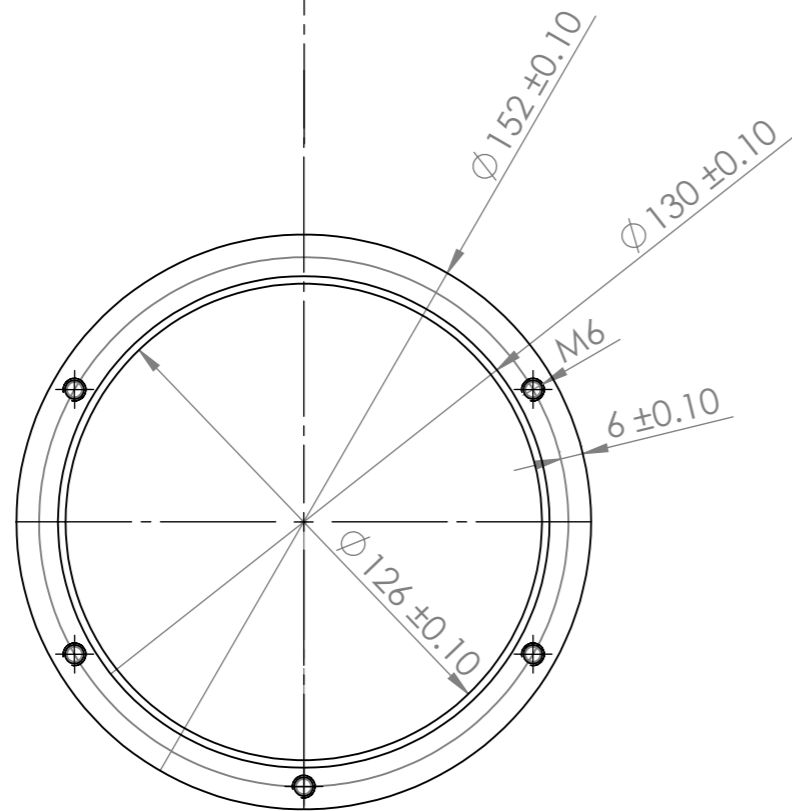
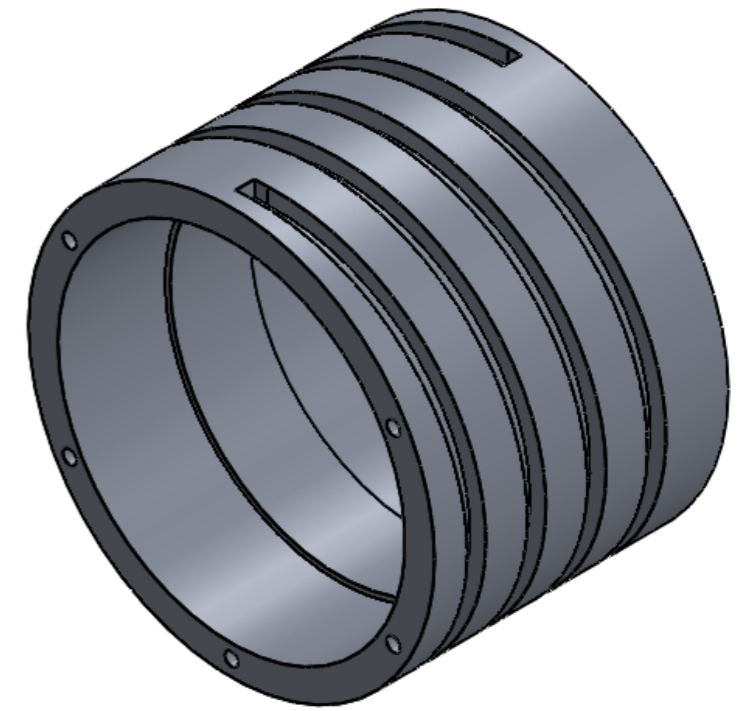
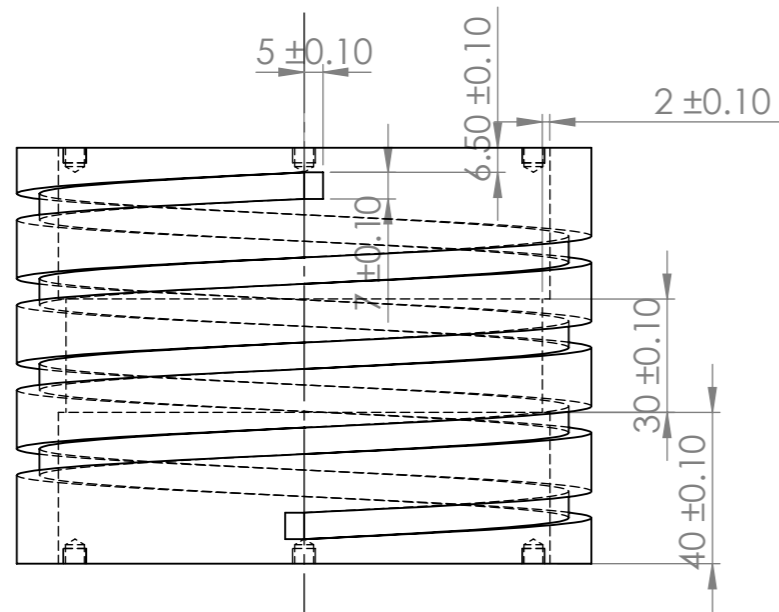


UNLESS OTHERWISE SPECIFIED: DIMENSIONS ARE IN MILLIMETERS SURFACE FINISH: TOLERANCES: LINEAR: ANGULAR:				FINISH:		DEBURR AND BREAK SHARP EDGES		DO NOT SCALE DRAWING		REVISION	
DRAWN				SIGNATURE		DATE		TITLE:			
CHK'D											
APPV'D											
MFG											
Q.A								MATERIAL:		DWG NO.	
								WEIGHT:		SCALE:2:1	
								Magnet		A3	
								SHEET 1 OF 1			



UNLESS OTHERWISE SPECIFIED: DIMENSIONS ARE IN MILLIMETERS SURFACE FINISH: TOLERANCES: LINEAR: ANGULAR:			FINISH:		DEBURR AND BREAK SHARP EDGES		DO NOT SCALE DRAWING		REVISION		
DRAWN						TITLE:					
CHK'D											
APPV'D											
MFG											
Q.A						MATERIAL:		DWG NO.		A3	
						WEIGHT:		SCALE:1:1		SHEET 1 OF 1	

Circular_frame_key



DETAIL A

UNLESS OTHERWISE SPECIFIED:
DIMENSIONS ARE IN MILLIMETERS
SURFACE FINISH:
TOLERANCES:
LINEAR:
ANGULAR:

FINISH:

DEBURR AND
BREAK SHARP
EDGES

DO NOT SCALE DRAWING

REVISION

SCALE 2 : 1

	NAME	SIGNATURE	DATE		TITLE:
DRAWN					
CHK'D					
APPV'D					
MFG					
Q.A					

mid_housing_inner_full_channel_h

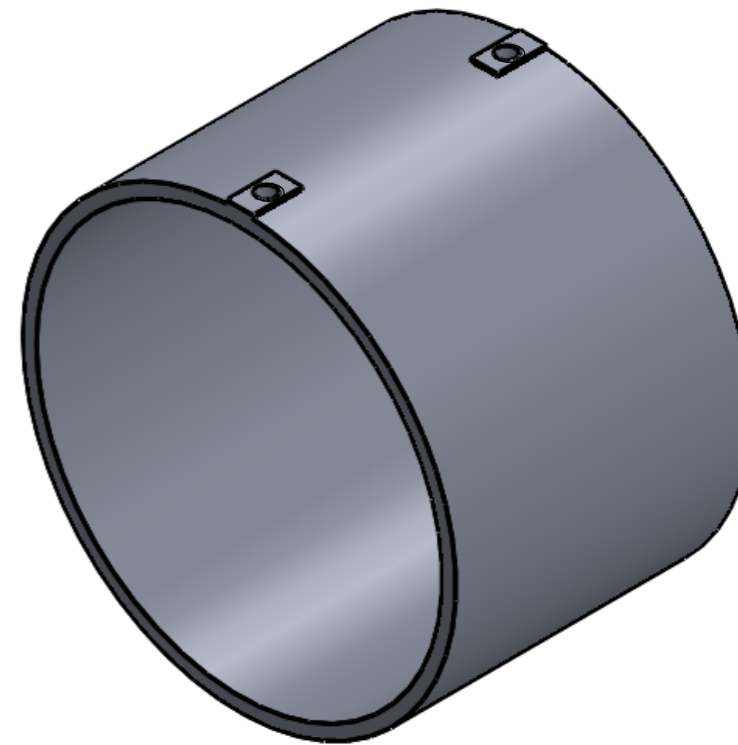
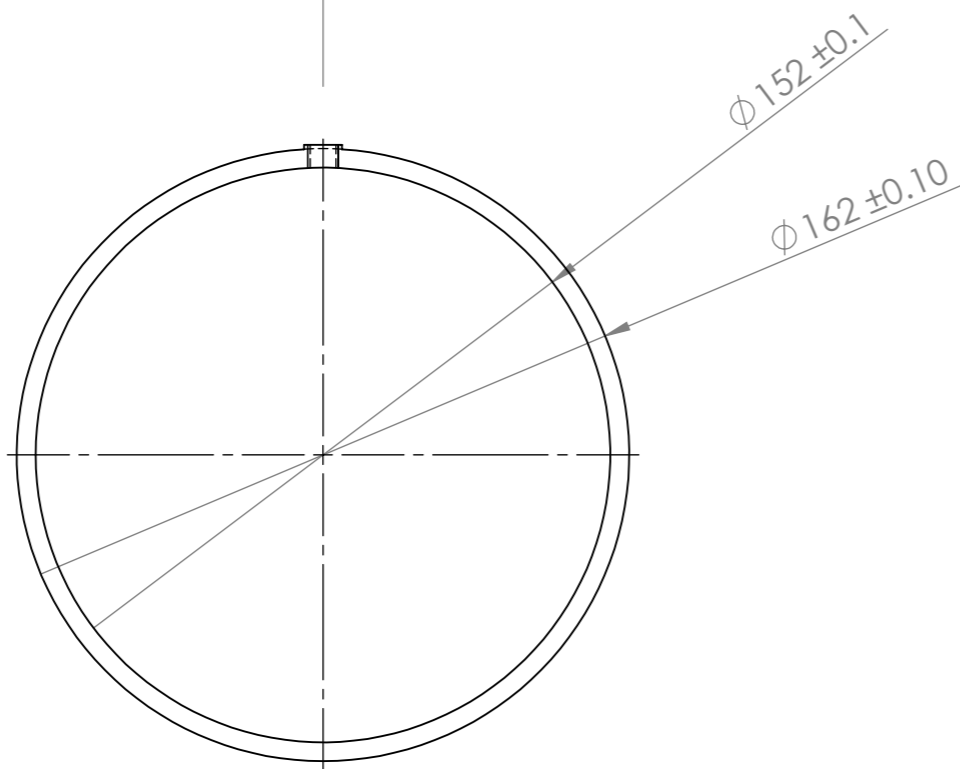
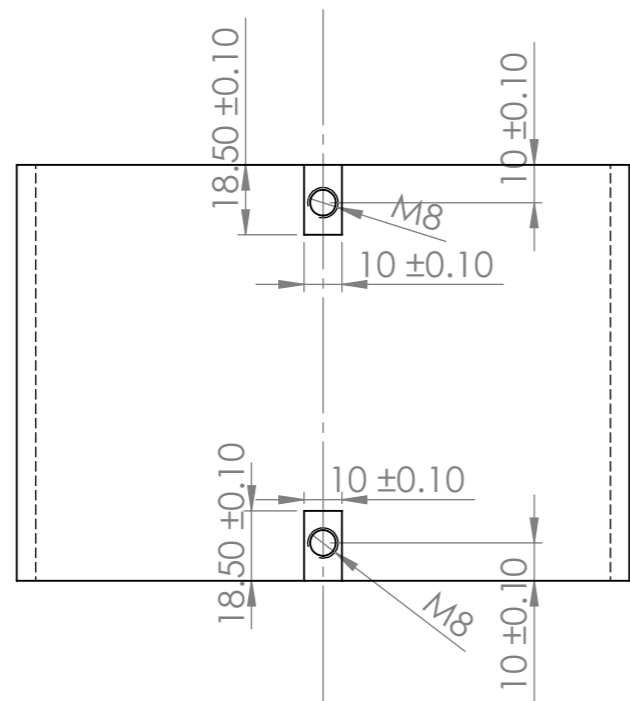
WEIGHT:

DWG NO.

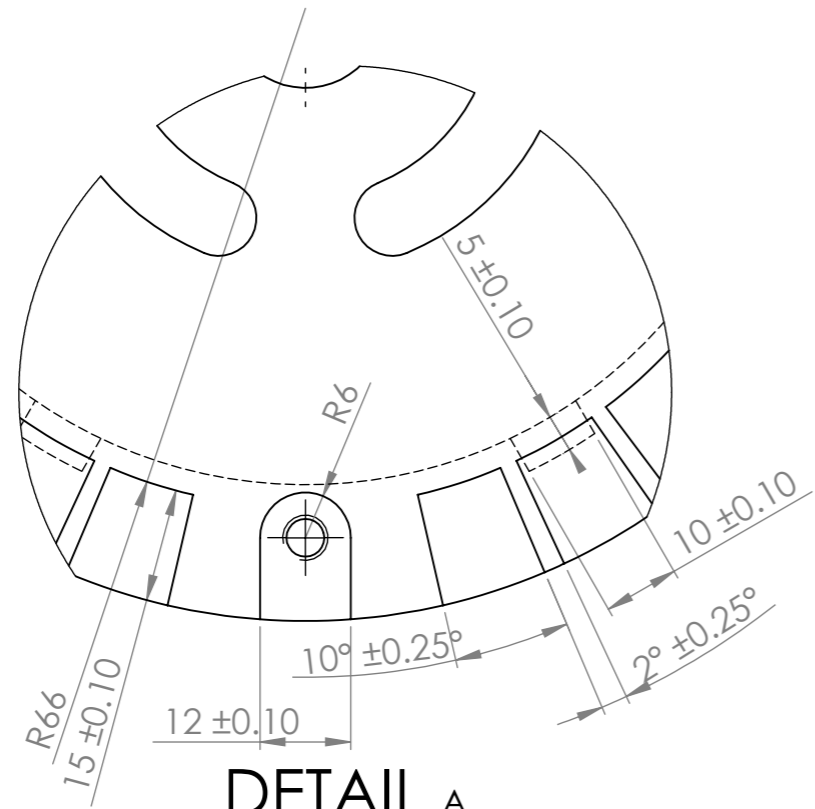
SCALE:1:2

SHEET 1 OF 1

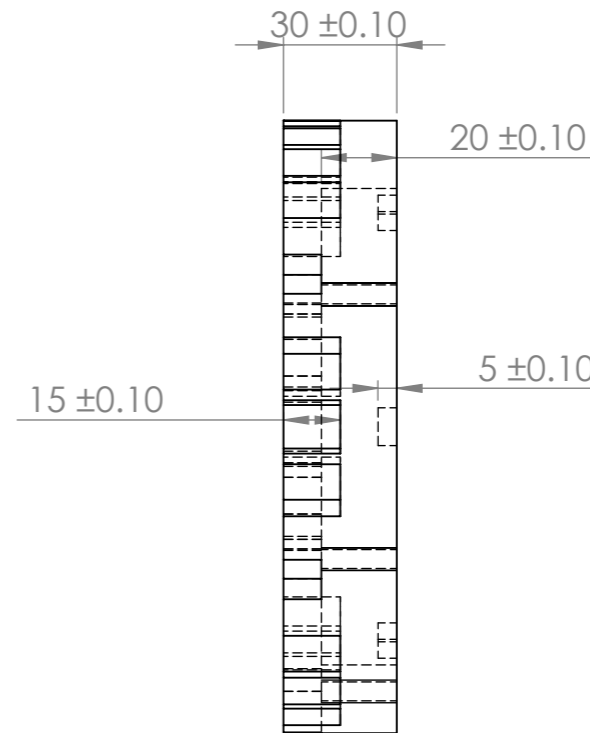
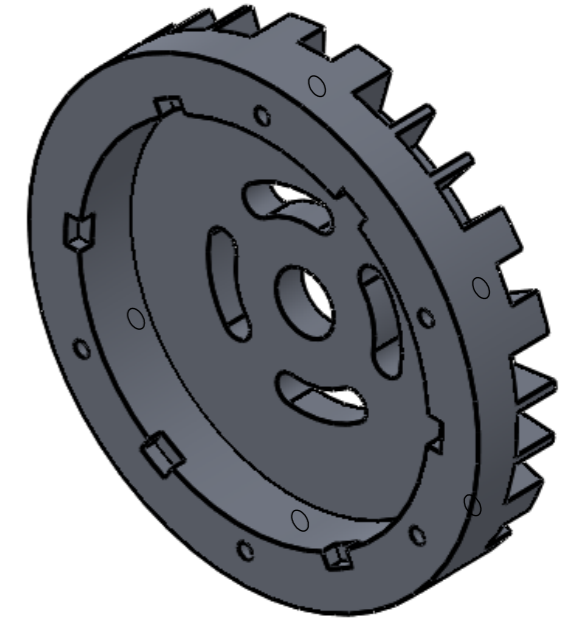
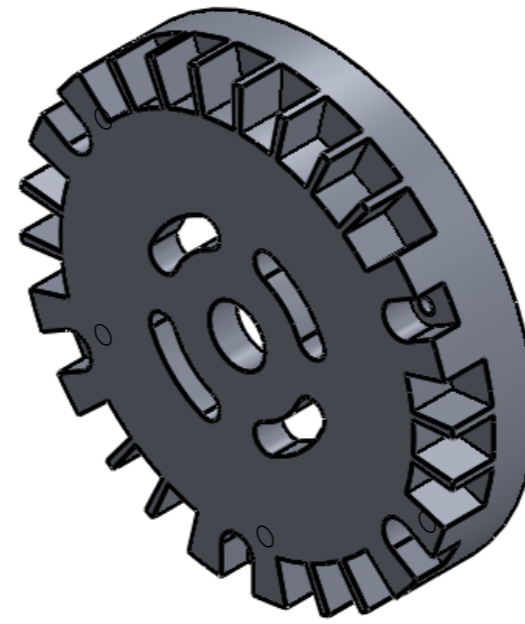
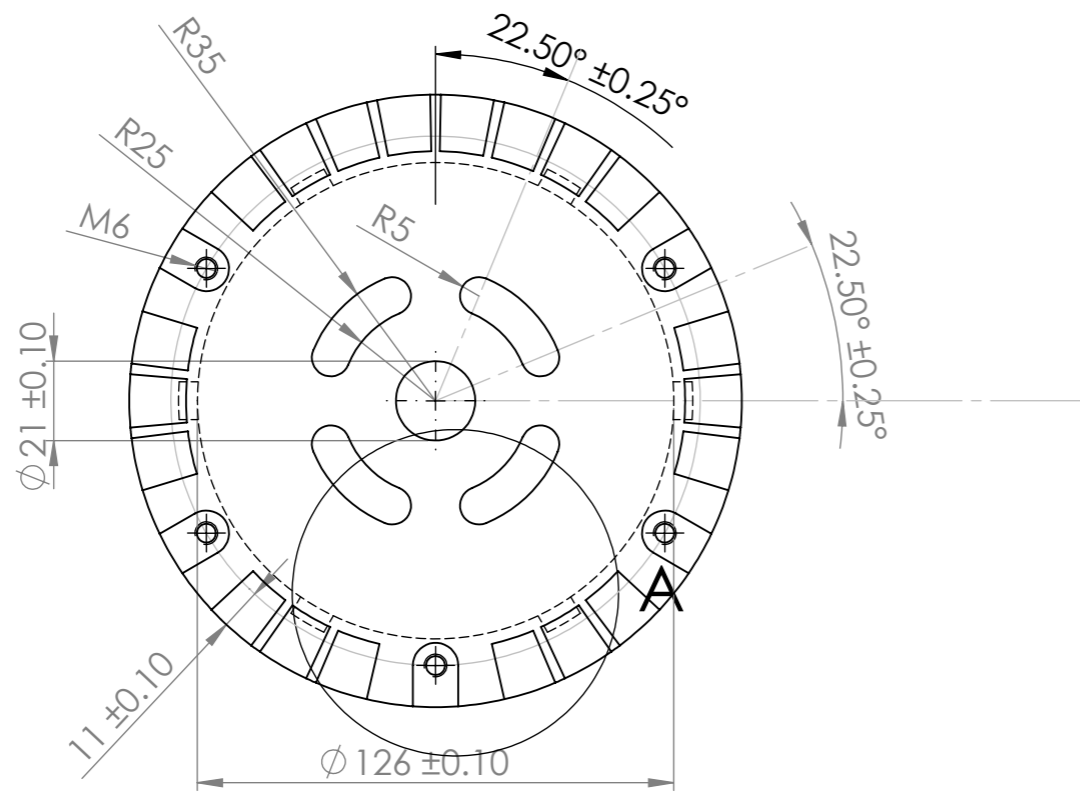
A3



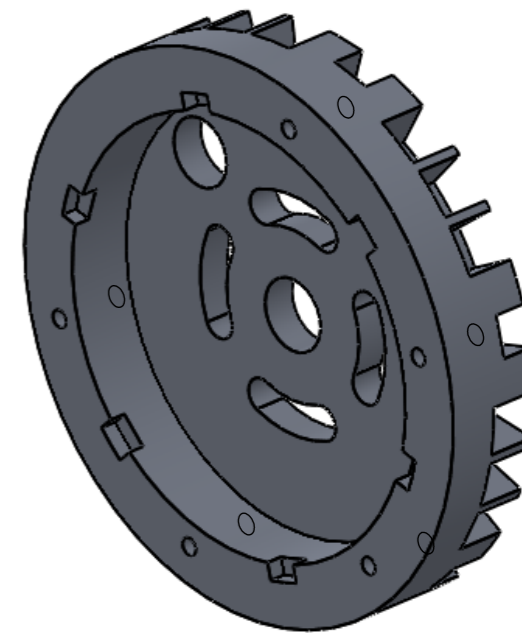
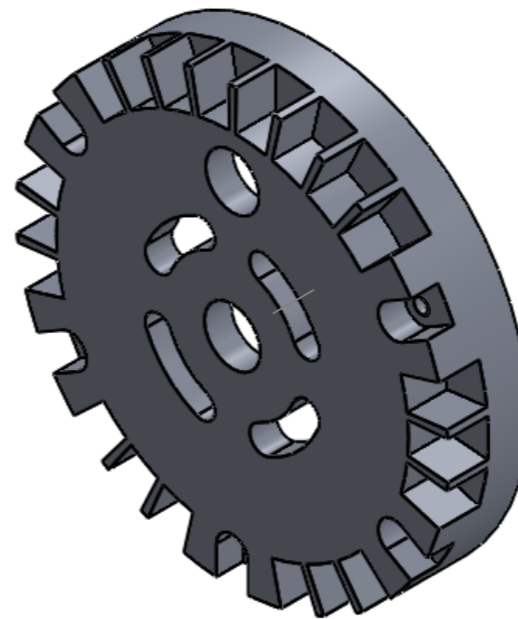
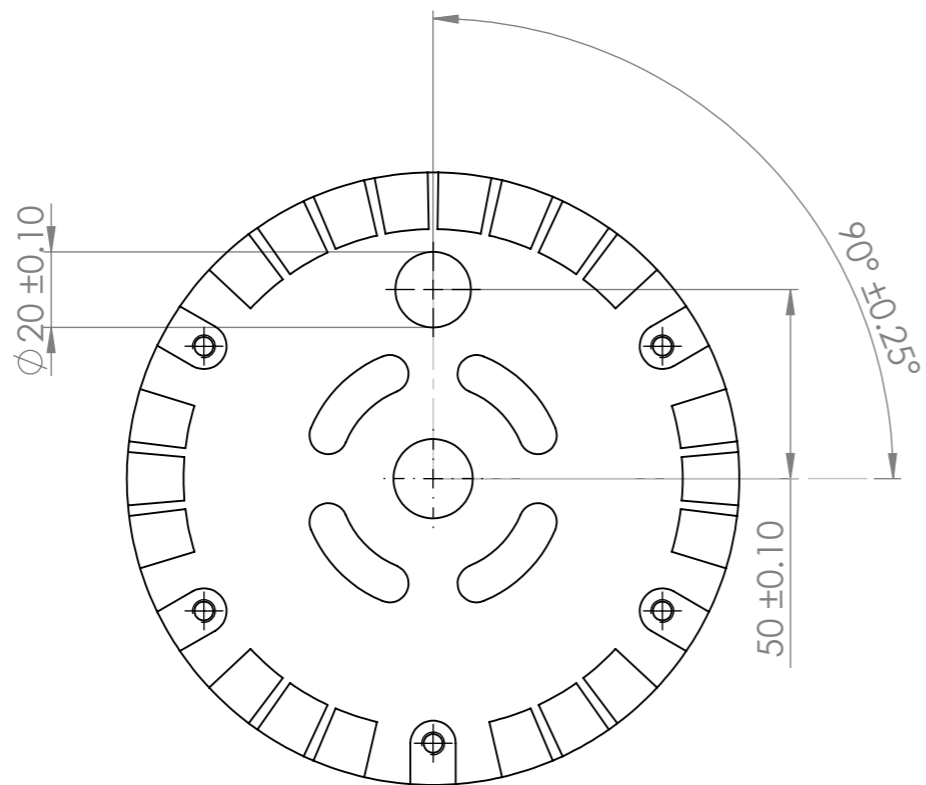
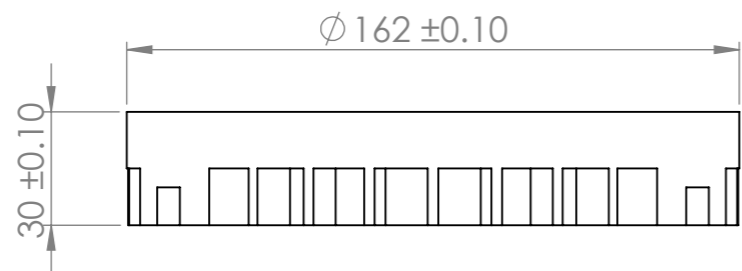
UNLESS OTHERWISE SPECIFIED: DIMENSIONS ARE IN MILLIMETERS SURFACE FINISH: TOLERANCES: LINEAR: ANGULAR:			FINISH:		DEBURR AND BREAK SHARP EDGES		DO NOT SCALE DRAWING		REVISION		
DRAWN			NAME		SIGNATURE		DATE		TITLE:		
CHK'D											
APPV'D											
MFG											
Q.A									MATERIAL:		DWG NO.
									mid_housing_outer_noChannel_ho		A3
									WEIGHT:		SCALE:1:2
											SHEET 1 OF 1



DETAIL A
SCALE 1:1



UNLESS OTHERWISE SPECIFIED: DIMENSIONS ARE IN MILLIMETERS SURFACE FINISH: TOLERANCES: LINEAR: ANGULAR:			FINISH:		DEBURR AND BREAK SHARP EDGES		DO NOT SCALE DRAWING		REVISION		
DRAWN			NAME		SIGNATURE		DATE		TITLE:		
CHK'D											
APPV'D											
MFG											
Q.A							MATERIAL:		DWG NO.		
							WEIGHT:		side_housing_closed		
							SCALE:1:2		SHEET 1 OF 1		



UNLESS OTHERWISE SPECIFIED: DIMENSIONS ARE IN MILLIMETERS SURFACE FINISH: TOLERANCES: LINEAR: ANGULAR:			FINISH:		DEBURR AND BREAK SHARP EDGES		DO NOT SCALE DRAWING		REVISION		
DRAWN			NAME		SIGNATURE		DATE		TITLE:		
CHK'D											
APPV'D											
MFG											
Q.A							MATERIAL:		DWG NO.		
									side_housing_open ^{A3}		
							WEIGHT:		SCALE:1:2		
									SHEET 1 OF 1		

8 7 6 5 4 3 2 1

F

F

E

E

D

D

C

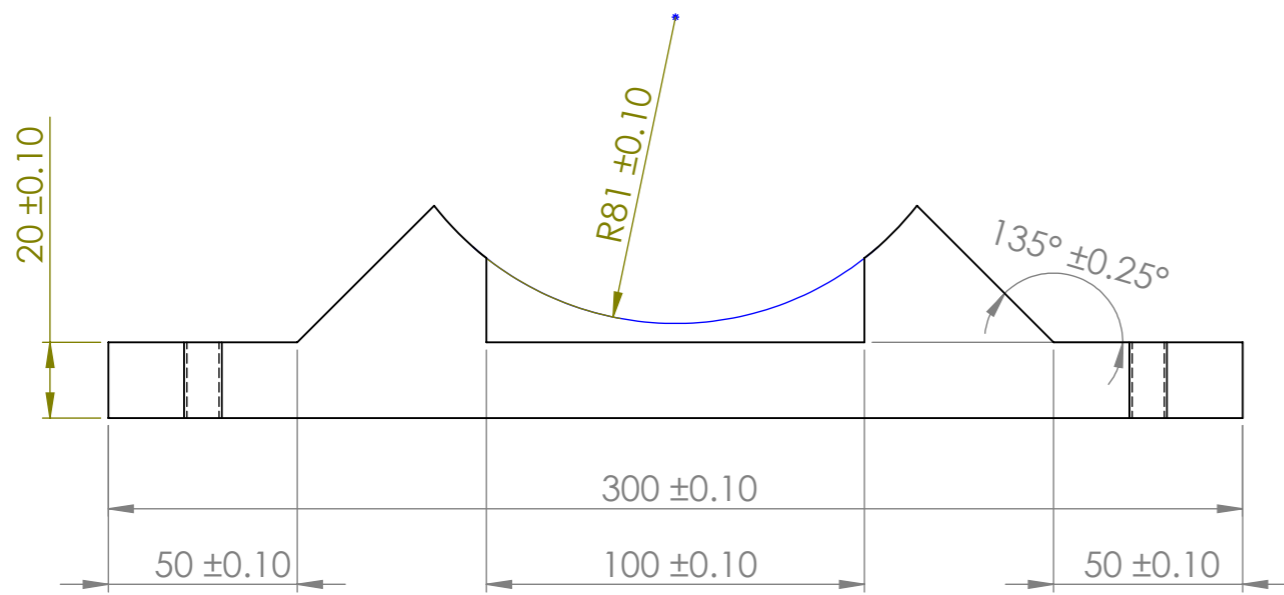
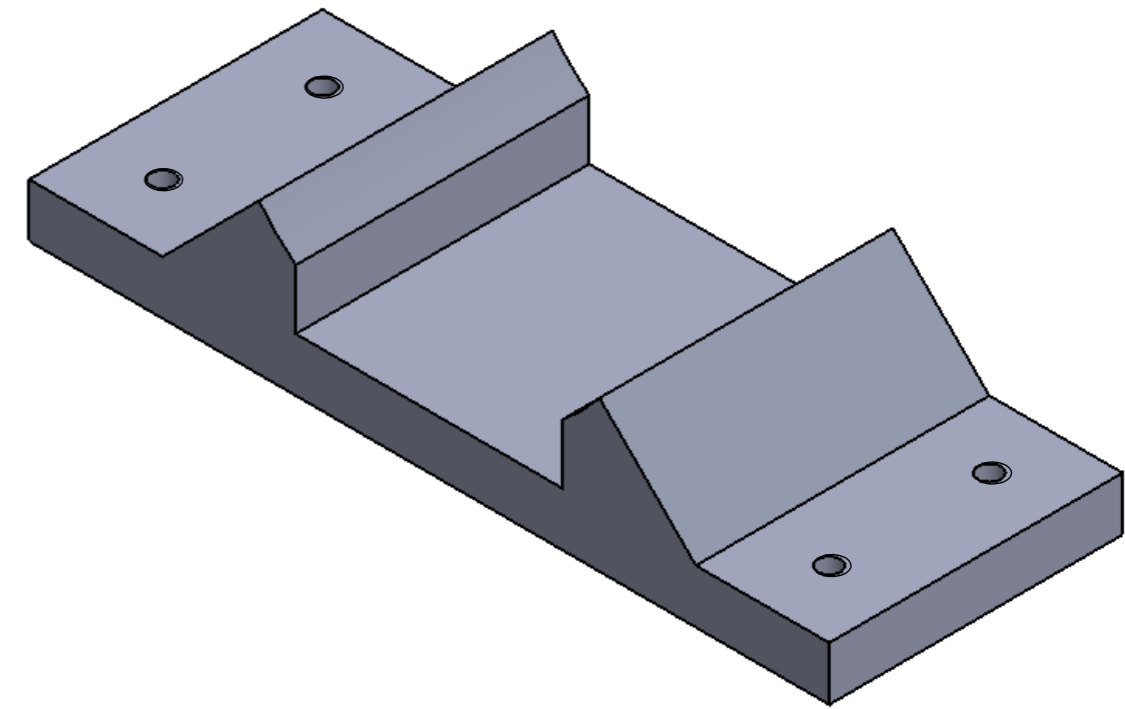
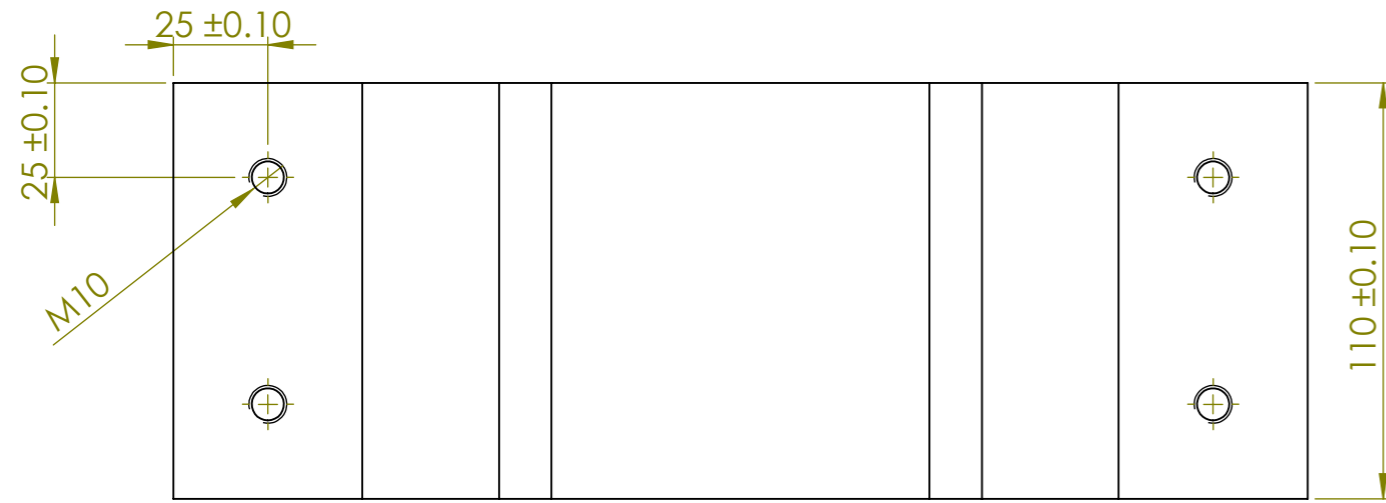
C

B

B

A

A



UNLESS OTHERWISE SPECIFIED: DIMENSIONS ARE IN MILLIMETERS SURFACE FINISH: TOLERANCES: LINEAR: ANGULAR:			FINISH:		DEBURR AND BREAK SHARP EDGES		DO NOT SCALE DRAWING		REVISION				
							TITLE:						
DRAWN													
CHK'D													
APPV'D													
MFG													
Q.A							MATERIAL:		DWG NO.			A3	
							WEIGHT:		SCALE:1:2			SHEET 1 OF 1	
							machine_base						

8 7 6 5 4 3 2 1